AD_____

Award Number: W81XWH-10-2-0162

TITLE: Spectroscopic Biomarkers for Monitoring Wound Healing and Infection in Combat Wounds”

PRINCIPAL INVESTIGATOR: Eric Elster

CONTRACTING ORGANIZATION: The Geneva Foundation
Tacoma, WA 98402

REPORT DATE: October 2012

TYPE OF REPORT: Annual

PREPARED FOR: U.S. Army Medical Research and Materiel Command
Fort Detrick, Maryland 21702-5012

DISTRIBUTION STATEMENT: Approved for Public Release;
Distribution Unlimited

REPORT DOCUMENTATION PAGE

Form Approved
OMB No. 0704-0188

1. REPORT DATE	**2. REPORT TYPE**	**3. DATES COVERED**
29 October 2012	Annual	30 September 2011- 29 September 2012

4. TITLE AND SUBTITLE
Spectroscopic Biomarkers for Monitoring Wound Healing and Infection in Combat Wounds

5a. CONTRACT NUMBER

5b. GRANT NUMBER
W81XWH-10-2-0162

5c. PROGRAM ELEMENT NUMBER

6. AUTHOR(S)
Dr. Eric Elster, Dr. Nicole Crane

E-Mail: eric.elster1@med.navy.mil

5d. PROJECT NUMBER

5e. TASK NUMBER

5f. WORK UNIT NUMBER

7. PERFORMING ORGANIZATION NAME(S) AND ADDRESS(ES)

The Geneva Foundation
Tacoma, WA 98402

8. PERFORMING ORGANIZATION REPORT NUMBER

9. SPONSORING / MONITORING AGENCY NAME(S) AND ADDRESS(ES)
U.S. Army Medical Research and Materiel Command
Fort Detrick, Maryland 21702-5012

10. SPONSOR/MONITOR'S ACRONYM(S)

11. SPONSOR/MONITOR'S REPORT NUMBER(S)

12. DISTRIBUTION / AVAILABILITY STATEMENT
Approved for Public Release; Distribution Unlimited

13. SUPPLEMENTARY NOTES

14. ABSTRACT

.
This proposal focuses on the use of multimodal imaging and spectroscopy of post-traumatic soft tissue and bone to assess wound healing. Combining infrared (IR) imaging, near-infrared spectroscopic (NIRS) imaging, and visible reflectance spectroscopic (VRS) imaging with Raman Spectroscopy (RS) will enable the surgeon to probe the tissue with a two-dimensional, real-time approach. This assessment allows optimal determination of the viability of damaged tissue, the suitability of the tissue environment for healing, the potential for wound infection and ectopic bone formation based on the degree of tissue compromise, and development of potential objective indicators for early limb salvage versus amputation. These imaging systems are currently available and readily applicable for clinical use. Combining these technologies in a multimodal system holds great promise in permitting the surgeon to make a better objective assessment of the viability of tissues in ways that have not previously been possible.

15. SUBJECT TERMS- none provided

16. SECURITY CLASSIFICATION OF:			**17. LIMITATION OF ABSTRACT**	**18. NUMBER OF PAGES**	**19a. NAME OF RESPONSIBLE PERSON**
					USAMRMC
a. REPORT	**b. ABSTRACT**	**c. THIS PAGE**			**19b. TELEPHONE NUMBER** *(include area code)*
U	U	U	UU	159	

Table of Contents

INTRODUCTION

Casualties in Operation Iraqi Freedom (OIF) and Operation Enduring Freedom (OEF) have experienced a high rate of extremity injuries with nearly ubiquitous diffuse tissue damage and compromised local circulation often associated with overt vascular injury. These injuries include traumatic amputations, open fractures, crush injuries, burns, acute vascular disruption, blastwave-associated pressure injuries, air, thrombotic, and fat embolism, and compartment syndrome. In the treatment of such complex traumatic injuries, improved assessment of global and regional perfusion, extent of infection, location and development of necrotic tissue, as well as location and development of early heterotopic ossification would facilitate the resuscitation and definitive treatment of these patients. Noninvasive spectroscopic methods may fulfill such a role, particularly Raman spectroscopy, infrared imaging, near-infrared spectroscopic imaging, and visible reflectance spectroscopic imaging. These technologies are capable of monitoring tissue temperature[1], perfusion[2] and associated hypoxia[3-6], collagen deposition[7, 8], and development of calcified tissue[9-18].

BODY

Aim 2 is comprised of five tasks:

a) Correlate the presence of necrotic tissue with spectroscopic markers.

b) Correlate spectroscopic markers with wound infection.

c) Correlate spectroscopic markers with the development of heterotopic ossification (HO).

d) Correlate spectral parameters and their response with physician and pathologist observations.

Since submission of the proposal, we have received tissue biopsies from wounds for an additional 24 patients and Raman spectra have been collected for these patients. We have also enrolled 50 patients into the 3-CCD study, collecting 3-CCD images of wounds for all of these patients. Briefly, the majority of the patients enrolled in the 3-CCD study to date have been normal healers, so correlation of outcome to 3-CCD data has not yet been possible. We have, however, determined the optimum conditions for obtained quality 3-CCD images and this practice has been implemented by the clinical team.

We are continuing to build our Raman spectral database of bacterial isolates. Preliminary findings were presented at an international conference in January 2012 (Photonics West – see Reportable Outcomes). In addition to the 30 strains of Acinetobacter baumanii, we are adding another 12 species of bacteria with multiple strains of each commonly observed in wounds (*including Pseudomonas, Bacillus, Arcanobacterium, Staphylococcus, Enterococcus, Klebsiella, Citrobacter, Stenotrophomonas, Enterbacter, Morganella* and *Escherichia*). These samples have been generously donated by Biomerieux, a manufacturer of in vitro diagnostics for clinical microbiology.

Efforts to collect Raman spectra of colonized wound effluent samples and tissue from patients that develop HO advances.

We are beginning to compile the Raman data into a central database for prediction modeling. We have completed preliminary modeling of a smaller data set (25 wounds) and have presented these results at two national conferences and a workshop (MHSRS, August 2012; SCIX, October 2012; IEEE AIPR, October 2012 – see Reportable Outcomes). Specifically, we have compared various data analysis techniques for predicting wound outcome. Univariate data analysis demonstrates statistically significant differences in the 1004 cm^{-1}, 1040 cm^{-1}, and 1250 cm^{-1} band areas (Figure 1). Thresh holding spectral bands for wound classification (i.e. normal healing or dehisced), however, correctly classifies wound outcome in less than 70% of the test data set. Several multivariate data analysis techniques were probed for predicting wound outcome: naïve Bayesian belief network, support vector machine, and linear discriminant analysis. The Bayesian belief

network model was based on an initial univariate analysis and performed worst (accuracy of ~65% for both normal healing and dehisced wounds – Figure 2A). The addition of clinical data to the data set improved model prediction by almost 10% (Figure 2B). The support vector model provided 80% accuracy for predicting wound dehiscence, while the linear discriminant analysis exhibited 90% accuracy for predicting wound dehiscence. These preliminary results demonstrate great promise for the potential of Raman spectroscopy to predict wound healing.

Aim 3 revolves around the completion of a swine hind limb ischemia protocol.

a) Acquire spectroscopic images of the limb before, during and after limb ischemia using VRS, NIRS and IR imaging.

b) Measure standard systemic assessments of reperfusion injury (creatine kinase (CK), urine myoglobin) in addition to cardiac output, blood pressure, serum lactate, base deficit and hemoglobin levels before, during, and after limb ischemia.

We have collected images and biological samples from 32 pigs to date, including all sham animals as well as all control animals. As we suspected, imaging data indicates that reperfusion and subsequent oxygenation of the ischemic limb do not proceed at the same rate for severely affected tissues. Calculated 3CCD values at 30 minutes post-reperfusion, inidicative of tissue oxygenation, trend in a similar manner to Tarlov scale values (clinical evaluation of mobility) – Figure 3.

c) Optimize resuscitation methods by correlating standard and spectroscopic parameters with porcine model outcomes.

We are in the process of analyzing the data generated by the swine limb ischemia model. Preliminary results of the imaging work have been presented at two national conferences (MHSRS, August 2012 and SCIX, October 2012 – see Reportable Outcomes). Preliminary results of the data collected from clinical samples will be presented at a national conference in November 2012 (AALAS – see Reportable Outcomes).

Starting in 2013, we will begin the experimental arms of the protocol, which involves administering Lifor perfusate after limb ischemia.

KEY RESEARCH ACCOMPLISHMENTS

- In addition to the 30 strains of Acinetobacter baumanii, we are adding another 12 species of bacteria with multiple strains of each commonly observed in wounds.

- Efforts to collect Raman spectra of colonized wound effluent samples and tissue from patients that develop HO advances.

- We are beginning to compile the Raman data into a central database for prediction modeling.

- We have generated preliminary models to predict wound healing and are able to obtain 90% accuracy for prediction of wound dehiscence.

- We have collected images and biological samples from 32 pigs to date, including all sham animals as well as all control animals. We are in the process of analyzing the data generated by the swine limb ischemia model.

REPORTABLE OUTCOMES

Poster presentations:

Rajiv Luthra, Nicole J. Crane, Jonathan Forsberg, Eric A. Elster. Using Multimodal Imaging Techniques to Monitor Limb Ischemia. MHSRS. Fort Lauderdale, FL: August 2012.

Maricela Rodriguez, Rajiv Luthra, Tiffani Slaughter, Eric Elster, Nicole J. Crane. Understanding Systemic Responses to Localized Limb Ischemia/Reperfusion Injury: A Yorkshire Swine Model. AALAS: Minneapolis, MN: November 2012.

Oral Presentations:

Nicole J. Crane, Eric A. Elster. Profiling wound healing with wound effluent: Raman spectroscopic indicators of infection. Photonics West (BiOS): San Francisco, CA: January 2012.

Nicole J. Crane, Rajiv Luthra, Emily Valaik, Jonathan A. Forsberg, Eric A. Elster. Chronicling Wound Healing with Raman Spectroscopy. MHSRS. Fort Lauderdale, FL: August 2012.

Nicole J. Crane, Rajiv Luthra, Jonathan A. Forsberg, Eric Elster. Predicting Wound Outcome from Raman Spectroscopic Data: Univariate versus Multivariate Techniques. SCIX. Kansas City, MO: October 2012.

Rajiv Luthra, Nicole J. Crane, Jonathan A. Forsberg, Eric A. Elster. Using Multimodal Imaging Techniques to Monitor Limb Ischemia: A Rapid, Non-Invasive Method for Assessing Extremity Wounds. SCIX. Kansas City, MO: October 2012.

Nicole J. Crane, Rajiv Luthra, Jonathan A. Forsberg, Eric Elster. Predicting Wound Outcome from Raman Spectroscopic Data: Univariate versus Multivariate Techniques. IEEE AIPR. Washington, DC: October 2012

Manuscripts:

Nicole J. Crane, Eric A. Elster. Vibrational spectroscopy: a tool being developed for the noninvasive monitoring of wound healing. *Journal of Biomedical Optics*, 17(1), 010902 (2012).

Nicole J. Crane, Eric A. Elster. Profiling wound healing with wound effluent: Raman spectroscopic indicators of infection. *Proceedings of SPIE*, 8220-27 (2012).

CONCLUSION

In this effort we have made progress in all task areas and disseminated our findings through both national presentations and publications. With regards to three of the key outcomes in wounded warriors (the development of HO, wound failure and wound infection) our efforts have begun to demonstrate success. With regards to wound healing, we have enrolled more than 50 patients (each with multiple wounds and time points) for both Raman and 3CCD analysis and are continuing to obtain control specimens from non-injured patients and heterotopic ossification tissue from injured patients. We continue to move closer to an “optical biomarker” which can guide debridement and predict outcomes. Finally, as both HO and wound failure are related to the presence of bioburden our efforts in determining the spectra of common flora in combat patients will not only augment our understanding of the interplay between host and response to injury but help select appropriate anti-microbial approaches. In summary, this multi-faceted approach has laid the foundation for continued advances over the ensuing years. In the future, we hope to apply these efforts to civilian trauma as well as military trauma.

REFERENCES

1. Katz L, Nauriyal V, Nagaral S, et al. Infrared imaging for detection of compartment syndrome. *Academic Emergency Medicine.* 2007;14(5):S41.

2. Gorbach A, Simonton D, Hale D, Swanson S, Kirk A. Objective, real-time, intraoperative assessment of renal perfusion using infrared imaging. *American Journal of Transplantation.* 2003;3:988-993.

3. Zuzak KJ, Gladwin MT, Cannon III RO, Levin IW. Imaging hemoglobin oxygen saturation in sickle cell disease patients using noninvasive visible reflectance hyperspectral techniques: effects of nitric oxide. *American Journal of Physiology: Heart and Circulation Physiology.* 2003;285:H1183-H1189.

4. Zuzak KJ, Schaeberle MD, Gladwin MT, Cannon III RO, Levin IW. Noninvasive determination of spatially resolved and time-resolved tissue perfusion in humans during nitric oxide inhibition and inhalation by use of a visible-reflectance hyperspectral imaging technique. *Circulation.* 2001;104:2905-2910.

5. Zuzak KJ, Schaeberle MD, Lewis EN, Levin IW. Visible reflectance hyperspectral imaging: characterization of a noninvasive, in vivo system for determining tissue perfusion. *Analytical Chemistry.* 2002;74:2021-2028.

6. Khaodhiar L, Dinh T, Schomacker KT, et al. The use of medical hyperspectral technology to evaluate microcirulatory changes in diabetic foot ulcers and to predict clinical outcomes. *Diabetes Care.* 2007;30:903-910.

7. Chan KL, Zhang G, Tomic-Canic M, et al. A Coordinated Approach to Cutaneous Wound Healing: Vibrational Microscopy and Molecular Biology. *J Cell Mol Med.* Aug 9 2008.

8. Frushour BG, Koenig JL. Raman scattering of collagen, gelatin, and elastin. *Biopolymers.* 1975 1975;14:379-391.

9. Carden A, Morris MD. Application of vibrational spectroscopy to the study of mineralized tissues. *J. Biomed. Optics.* 2000 2000;5(3):259-268.

10. Kontoyannis CG, Vagenas NV. FT-Raman spectroscopy: a tool for monitoring the demineralization of bone. *Applied Spectroscopy.* 2000 2000;54(11):1605-1609.

11. Wang Y-N, Galiotis C, Bader DL. Determination of Molecular Changes in Soft Tissues Under Strain Using Laser Raman Microscopy. *Journal of Biomechanics.* 2000 2000;33:483 - 486.

12. Carden A, Morris TJA, Edwards CM, et al. Raman imaging of bone mineral and matrix: composition and function. *Proc. SPIE.* 1999 1999;3608:132-138.

13. Crane NJ, Popescu V, Morris MD, Steenhuis P, Ignelzi Jr. MA. Raman spectroscopic evidence for octacalcium phosphate and other transient mineral species deposited during intramembraneous mineralization. *Bone.* 2006;39:434-442.

14. Morris MD, Stewart S, Tarnowski C, et al. Raman spectroscopy of early mineralization of normal and pathological calvaria. *Proc. SPIE.* 2002 2002;4614:28-39.

15. Morris MD, Tarnowski C, Dreier JL, Ignelzi Jr. MA. Raman microscopy of *de novo* woven bone tissue. *Proc. SPIE.* 2001 2001;4254.

16. Tarnowski CP, Ignelzi MA, Morris MD. Mineralization of developing mouse calvaria as revealed by Raman microspectroscopy. *Journal of Bone and Mineral Research.* 2003 2003;17(6):1118-1126.

17. Timlin J, Carden A, Morris MD, Kohn DH. Raman Spectroscopic Imaging Markers for Fatigue-Related Microdamage in Bovine Bone. *Analytical Chemistry.* 2000 2000;72(10):2229 - 2236.

18. Timlin JA, Carden A, Morris MD. Chemical microstructure of cortical bone probed by Raman transects. *Applied Spectroscopy.* 1999 1999;53(11):1429-1435.

SUPPORTING DATA:

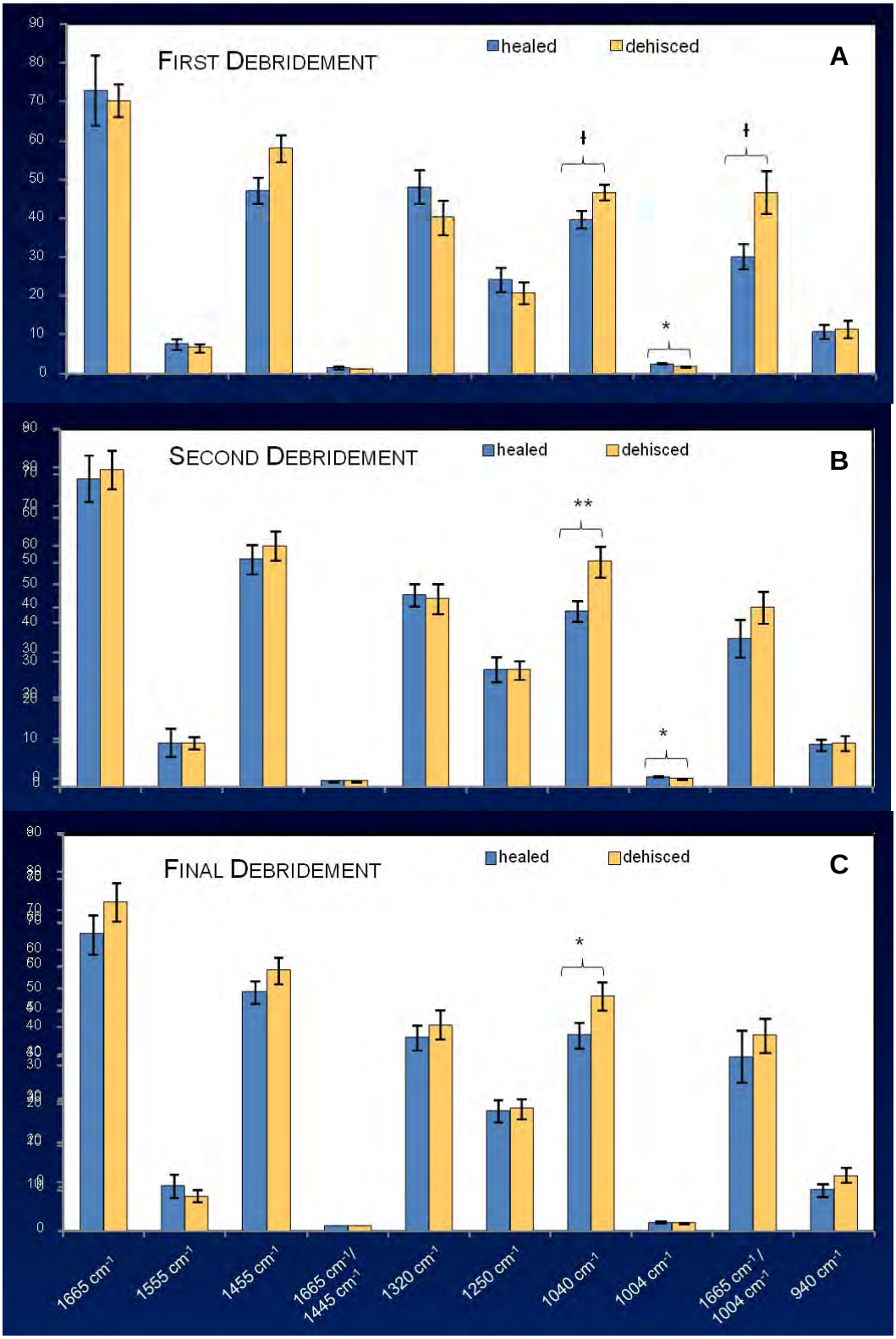

Figure 1. Band areas and band area ratios calculated for first (A), second (B), and final (C) debridements. Asterisks indicate statistically significant differences. * = $p > 0.05$; ** = $p > 0.01$.

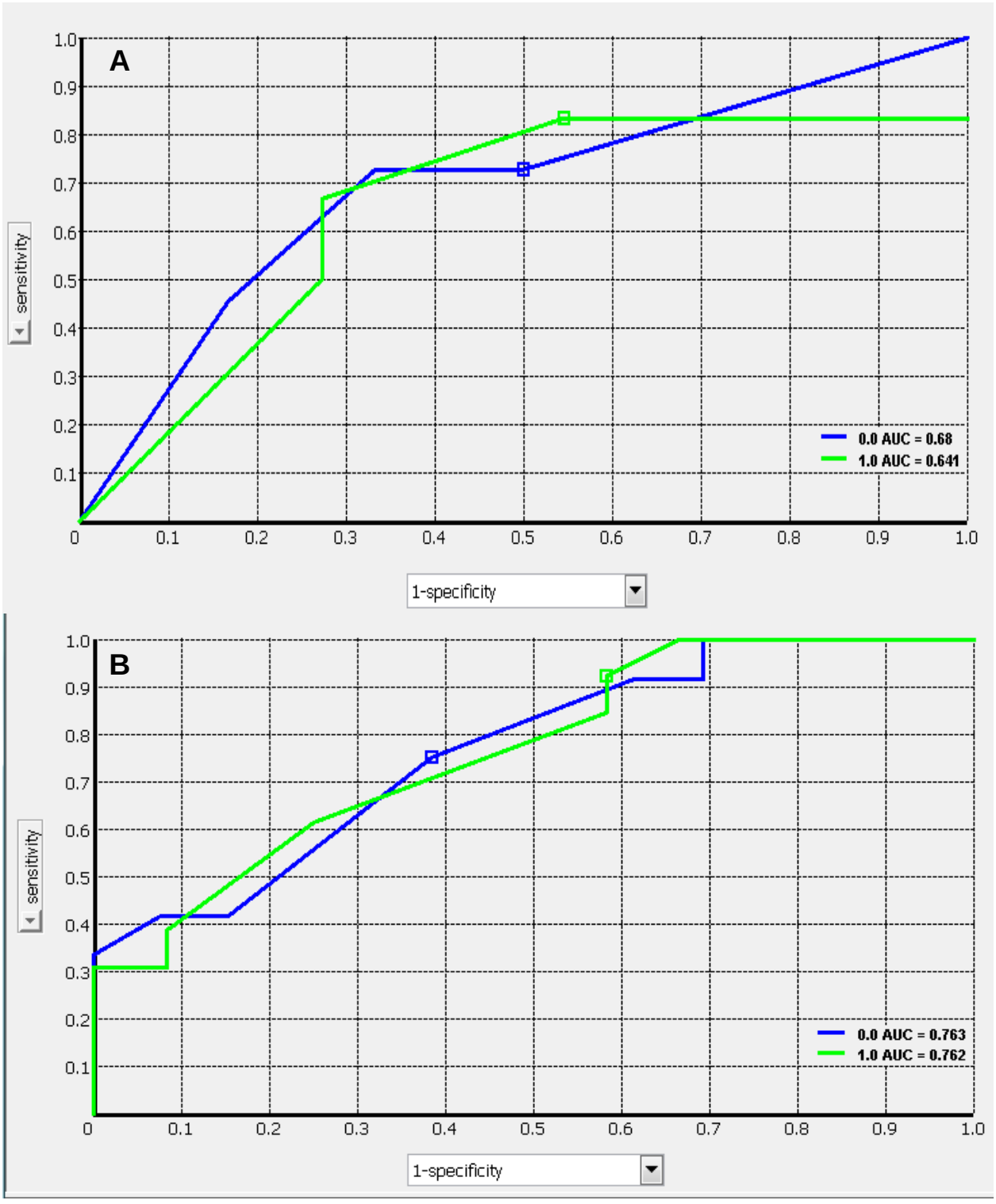

Figure 2. Reciever operating curve for wound outcome prediction (0 – normal healing wounds, 1 – dehisced wounds). Area under the curves (AUCs) are calculated for both a spectroscopic only dataset (A) and a spectroscopic and clinical dataset (B).

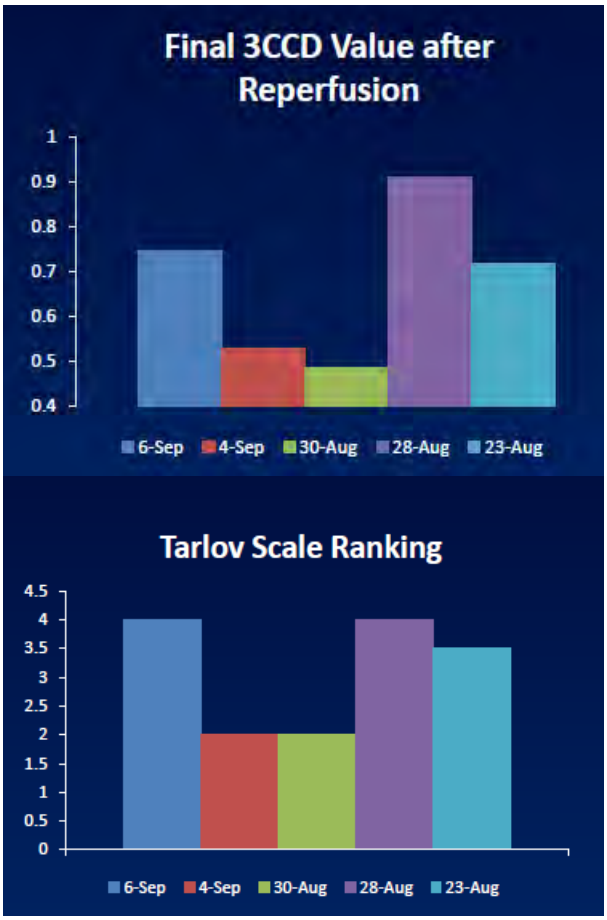

Figure 3. Comparison of calculated final 3CCD values (after 30 minutes of reperfusion) and Tarlov scale values. Note that the highest Tarlov scale values correlate with the highest calculated 3CCD values.

Using Multimodal Imaging Techniques to Monitor Limb Ischemia

Rajiv Luthra[1], Nicole J. Crane Ph.D.[1], Jonathan Forsberg, M.D[1], Eric A. Elster M.D.[1,2]

[1]Department of Regenerative Medicine, Operational and Undersea Medicine Directorate, Naval Medical Research Center, Silver Spring, MD
[2]Department of Surgery, Uniformed Services University of the Health Sciences, Bethesda, MD

INTRODUCTION

- Our goal is to develop technology for real-time monitoring of extremity oxygenation and perfusion.
- Our hypothesis is that changes in tissue oxygentation and perfusion can be accurately monitored using a multimodal imaging system with 3CCD imaging and infrared imaging.
- Thermal imaging provides better data regarding overall perfusion of the extremity.
- 3CCD imaging provides data regarding the surface oxygenation of the extremity and is based on the spectral response of hemoglobin in the visible region of the spectrum.
- By integrating multiple imaging methods, we can quantitatively identify and track regions of tissue where oxygenation and perfusion change in real-time.
- This is the first step in actualizing a clinically relevant and objective tool to aid clinicians treating critical combat care patients.

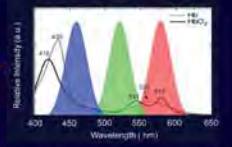

The spectra of oxygenated and de-oxygenated hemoglobin.

STUDY DESIGN

To simulate common vascular injuries sustained during blast-related extremity injuries, two methods are used:

- Direct vascular injury is modeled by occlusion/clamping of the iliac vessels.

Hind limb before (left) and after (right) two hours of ischemia by vessel occlusion.

- Crush injury is modeled by using a pneumatic tourniquet. A pressure of 250 mm Hg is used.

Hind limb before (left) and after (right) two hours of ischemia by tourniquet.

IMAGING MODALITIES

- 3CCD (Panasonic Pro AG-HMC150):

It is similar in mechanism to a common digital camera, including that is commercially and easily available, inexpensive and easy to use.

It provides enhanced color and image quality.

To achieve this it utilizes a trichroic prism to split incoming light into three channels namely red, green and blue.

Each channel has its own detector a charge-coupled device, (CCD) giving a much higher color sensitivity and dynamic range.

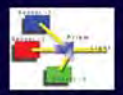

- Thermal (FLIR Tau 640):

It is comprised of a long wave infrared (IR) camera with a spectral response between 7.5 - 13.5 µm.

The detector itself is a thermoelectrically cooled microbolometer (640 x 512 pixels).

RESULTS

3CCD IMAGING

Shown below are 3CCD images at different time points during a tourniquet induced ischemia.

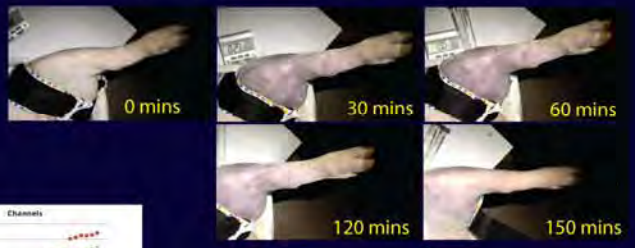

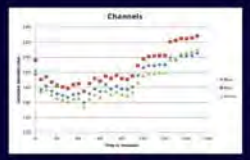

Using a custom MATLAB script, the Red, Green and Blue channels are extracted from the captured 3CCD images and plotted.

The blue channel is subtracted from the red channel and plotted.

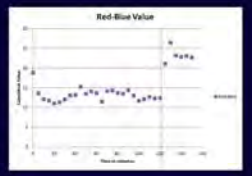

Ischemia is started at the 0 minute time point and continues until the 120 minute mark (line). Once the tourniquet is released, the limb is reperfused for 30 minutes.

The Red-Blue value intially drops until ~40 minutes, where the value holdsat a relatively constant value until reperfusion. Upon reperfusion, the valuejumps rapidly before returning to pre-ischemic values.

INFRARED IMAGING

Shown to the right are captured thermal images at different representative time points during the induced ischemia.

Note that before and after ischemia the vessel is clearly visible, but quickly dissapears while the cuff is inflated.

Similar to how the 3CCD images are processed, a thermal value can the extracted from the image using MATLAB that correlates to temperature.

The response from the IR camera is linear, and with a simple two point calibration, the actual temperature of the limb can be obtained.

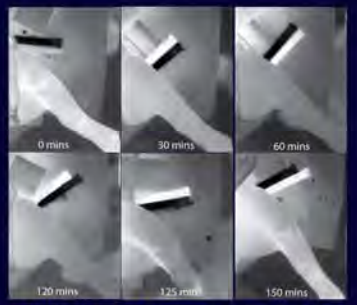

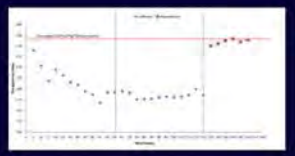

The plot of the extracted temperature values is shown as a function of time.

The average temperature of the extremity seems to closely follow overall perfusion state.

The temperature graph tracks changes observed in the 3CCD images (R-B images).

For the first 40-60 minutes during ischemia, the temperature drops almost linearly before stablizing.

At the 120 minute mark, when reperfusion occurs, the temperature rapidly rises and then slowly stabilizes to the pre-ischemic value.

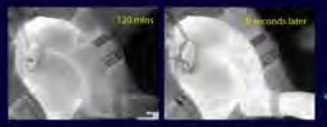

To the left is an example of how rapid and drastic the thermal change occuring during the initial reperfusion can be.

DATA INTEGRATION AND REAL TIME DISPLAY

Using a custom MATLAB program, both the 3CCD and thermal images can be continuously aquired. This is achieved using an IMPREX FrameLink Express card and CameraLink connections to both cameras.

Once the video feeds are aquired, using the 3CCD frame as reference, the IR image is registered using in-built registration code in MATLAB. This will be optimized to reduce the time burden.

A region of interest is selected, and our program will display a false color intensity map of the red-blue (R-B) calculated image.

This allows for a quick visual representation of tissue oxygenation of the region of interest.

Along side of the image, a plot of the red and blue channel values, along with their difference (R-B) is updated in real-time.

Finally, the thermal image is displayed along side of or overlayed directly onto the 3CCD image in grayscale.

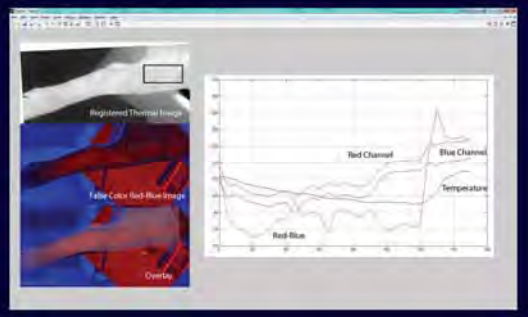

CONCLUSIONS

Here, the combined information of the localized change in limb temperature and skin surface absorption spectra are displayed in a user-friendly visual representation in real-time.

The data collected is minimally manipulated using simple matrix arithmetic methods, allowing for easy and rapid on chip processing.

Data collected from this study so far, indicates that this method could allow for a rapid, objective assessment of the severity and extent of ischemic damage.

This could provide surgeons with accurate information regarding overall limb viability as well as the appropriate timing of wound closure.

The multidisciplinary care of these patients would not have been possible without the dedicated efforts of everyone at WRAMC and NNMC. Both civilian and military personnel have rendered skilled and compassionate care for these casualties. All of our efforts are dedicated to those who have been placed in harm's way for the good of our nation. The views expressed are those of the authors and do not reflect the official policy of the Department of the Navy, Army, the Department of Defense, or the US Government. This effort was supported (in part) by the U.S. Navy Bureau of Medicine and Surgery under the Medical Development Program and Office of Naval Research work unit number (6047715.0933.001.A0604), PROMP award OR990138, and the Medical Development Program (PE 0604771N). We are a military service members (or employee of the U.S. Government). This work was prepared as part of our official duties. Title 17 U.S.C. 105 provides the "Copyright protection under this title is not available for any work of the United States Government." Title 17 U.S.C. 101 defines a U.S. Government work as a work prepared by a military service member or employee of the U.S. Government as part of that person's official duties. This study was approved by the National Naval Medical Center Institutional Review Board (protocol NNMC.2005.0061) in compliance with all Federal regulations governing the protection of human subjects. I/We certify that all individuals who qualify as authors have been listed; each has participated in the conception and design of this work, the analysis of data (when applicable), the writing of the document, and the approval of the submission of this version; that the document represents valid work; that if we used information derived from another source, we obtained all necessary approvals to use it and made appropriate acknowledgements in the document; and that each takes public responsibility for it.

Chronicling Wound Healing with Raman Spectroscopy

Nicole J. Crane Ph.D.[1,3], Rajiv Luthra[1], Emily Valaik[1], Jonathan A. Forsberg M.D.[1,2,3], Eric A. Elster M.D.[1,2,3]

[1]Naval Medical Research Center
[2]Walter Reed National Military Medical Center
[3]Uniformed Services University of the Health Sciences

MHSRS, Fort Lauderdale, FL
13 July 2012

Acute Combat Wounds

Acute Combat Wounds

- The management of modern traumatic war wounds remains a significant challenge for clinicians.
  - Extensive osseous and soft-tissue damage caused by blasts and high-energy projectiles.
- The ensuing inflammatory response ultimately dictates the pace of wound healing and tissue regeneration.
- The timing of wound closure or definitive coverage is subjectively based.
- Despite the use and application of novel wound-specific treatment modalities, some wounds fail to close, or dehisce.

Acute Combat Wounds – Current Treatment

Surgical debridements are performed every 2-3 days.

- remove devitalized tissue
- decrease bacterial load

Negative pressure wound therapy (NPWT) is applied between debridements. NPWT promotes wound closure.

Wound assessment involves:

- patient's general condition
- injury location
- adequacy of perfusion
- gross appearance of the wound

Acute Combat Wounds – The Challenge

Monitor wound healing *in vivo*, i.e. monitor wound healing during surgical debridements.

- Is it the best time to close the wound?
- Is the wound developing HO?
- Is the wound infected? With what?

Develop an objective and predictive model for wound healing.

The Toolbox

Our Toolbox

Real-time PCR

Multiplex Protein Assay

Raman Spectroscopy

FTIR Imaging

Thermography

Visible Reflectance Imaging

Bayesian Belief Network modeling

Sample Collection

Wound is surgically cleaned

Collect 1 cm³ tissue biopsy from center of wound bed

RT-PCR
Raman spectroscopy
Micro culture

NPWT is applied

Serum is collected

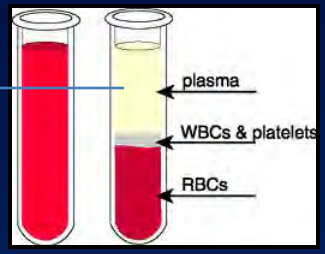

Protein assay

Effluent is collected

Protein assay

Raman spectroscopy
Micro culture

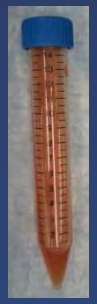

Preliminary Study – Raman Mapping Results

- Previous study demonstrated the potential of Raman spectroscopic analysis of wound biopsies for classification of wounds as normal or impaired healing from changes in the 1665 cm^{-1}/1445 cm^{-1} band area ratio.

Wound Rep Regen. 18(4): 409-416, 2010.

Ann Surg. 250(6):1002-7, 2009.

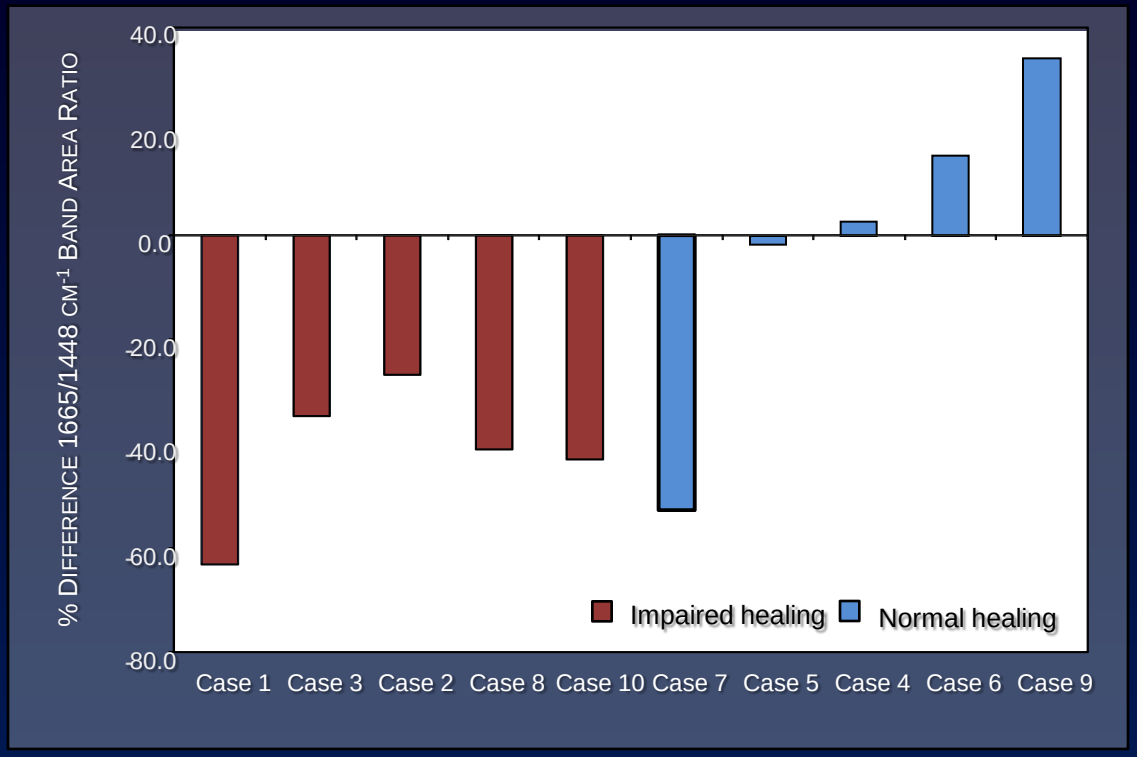

- Impaired healing wounds demonstrate a significant decrease in the 1665/1448 cm^{-1} band area ratio compared to normal healing wounds, as demonstrated by Raman spectroscopic mapping.

Preliminary Study – Real-Time PCR Analysis Results

- Results were corroborated by altered collagen/collagenase gene expression profiles of tissue biopsies.
- Gene expression profiles confirm decreased gene expression of collagen types I and III at the first debridement and collagen type III at the final debridement in impaired wounds.

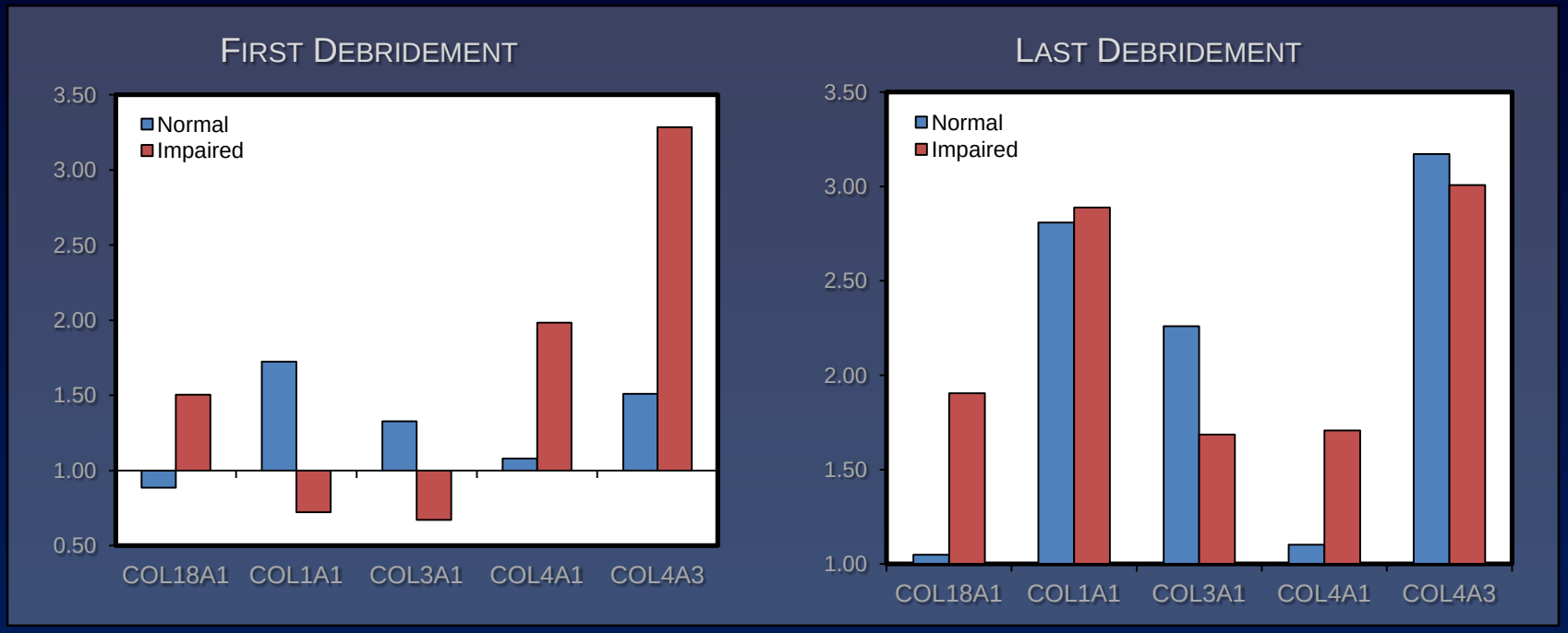

- COL18A1 mRNA expression remains elevated for impaired healing wounds at almost all time points when compared to normal healing wounds. Continued elevation of endostatin would inhibit neovascularization.

Wound Rep Regen. 18(4): 409-416, 2010.; Ann Surg. 250(6):1002-7, 2009.

Preliminary Study – Normal vs. Impaired Healing

During early wound healing, type III collagen is the most abundant collagen and is gradually replaced by type I collagen.

- *delayed deposition of type III collagen* = *delayed deposition of type I collagen* = *delayed re-epithelialization*

Could this type of analysis be extended to intact wound biopsies and ultimately obviate the need for excisional wound biopsies?

Chronicling Wound Healing with Raman Spectroscopy

Raman Fiber Probe Data Collection

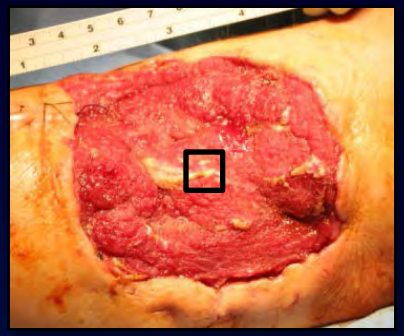

Approximately 1 cm^2 tissue biopsy is excised from the center of the wound bed.

Tissue is fixed in 10% neutral buffered formalin for storage.

Prior to spectral acquisition, samples are rinsed in 0.9% NaCl saline solution.

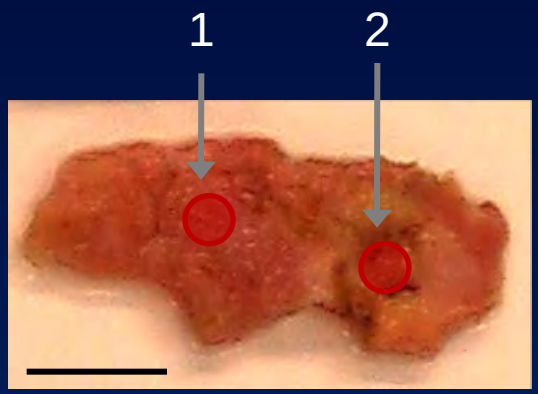

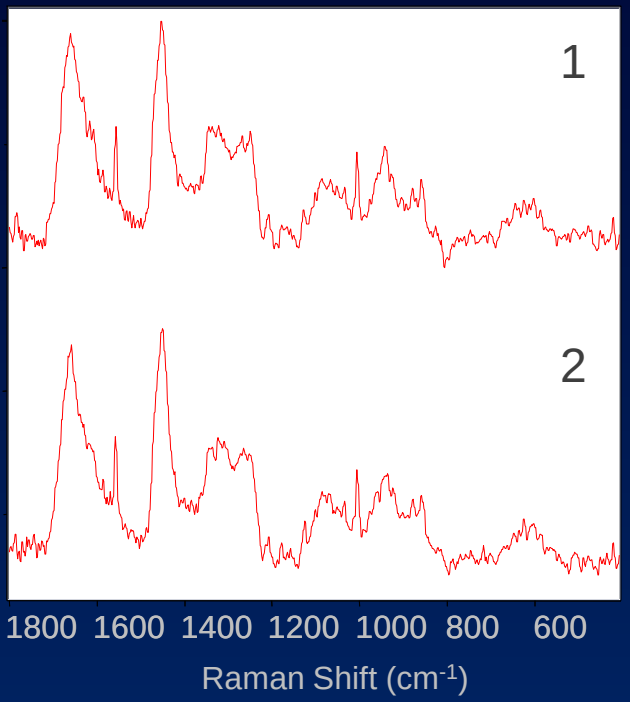

Examine multiple spots across the tissue.

40 accumulations, 5s spectrum

Monitoring a Wound Over Time

First Debridement

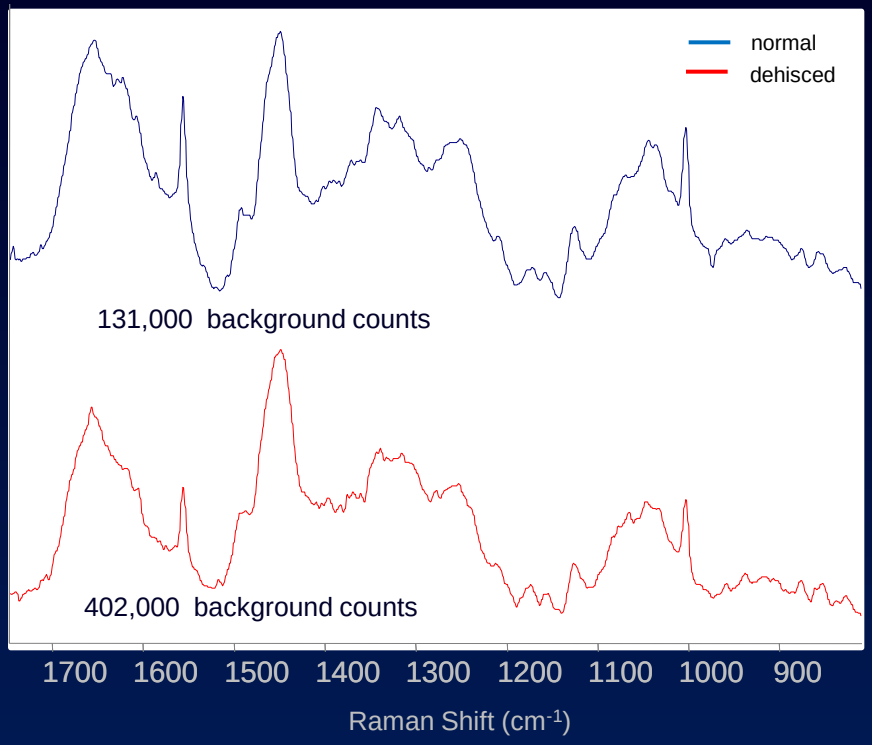

Final Debridement

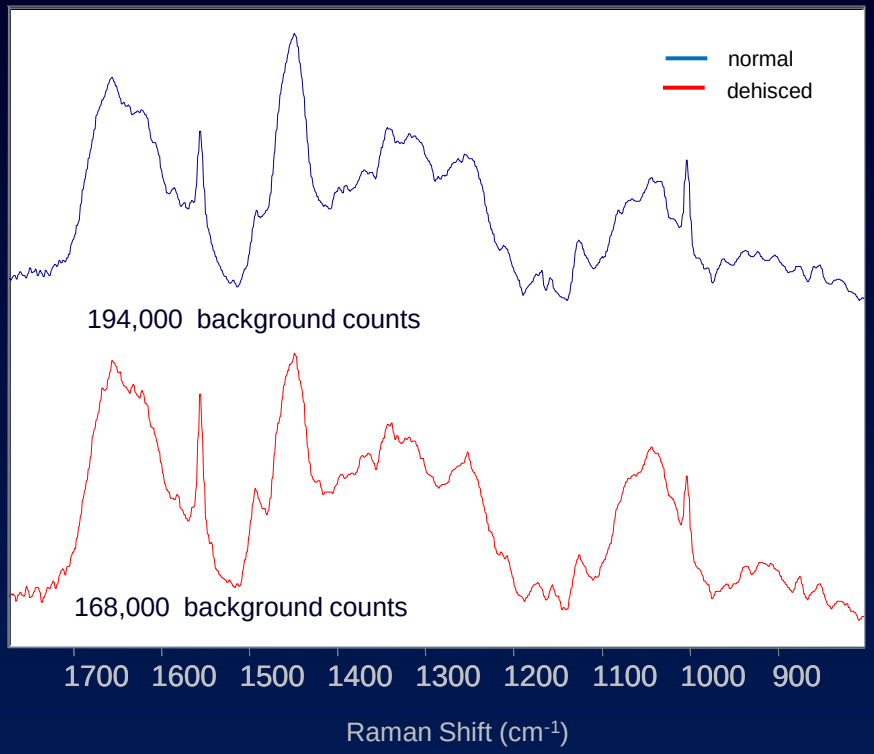

- Spectral differences between biopsies collected from normal healing wounds (n=8) and dehisced wounds (n=8) are not readily apparent.
- There is, however , a significant difference in the background intensity(mostly fluorescence) that the Raman signal rides on.

Peakfitting for Spectral Deconvolution

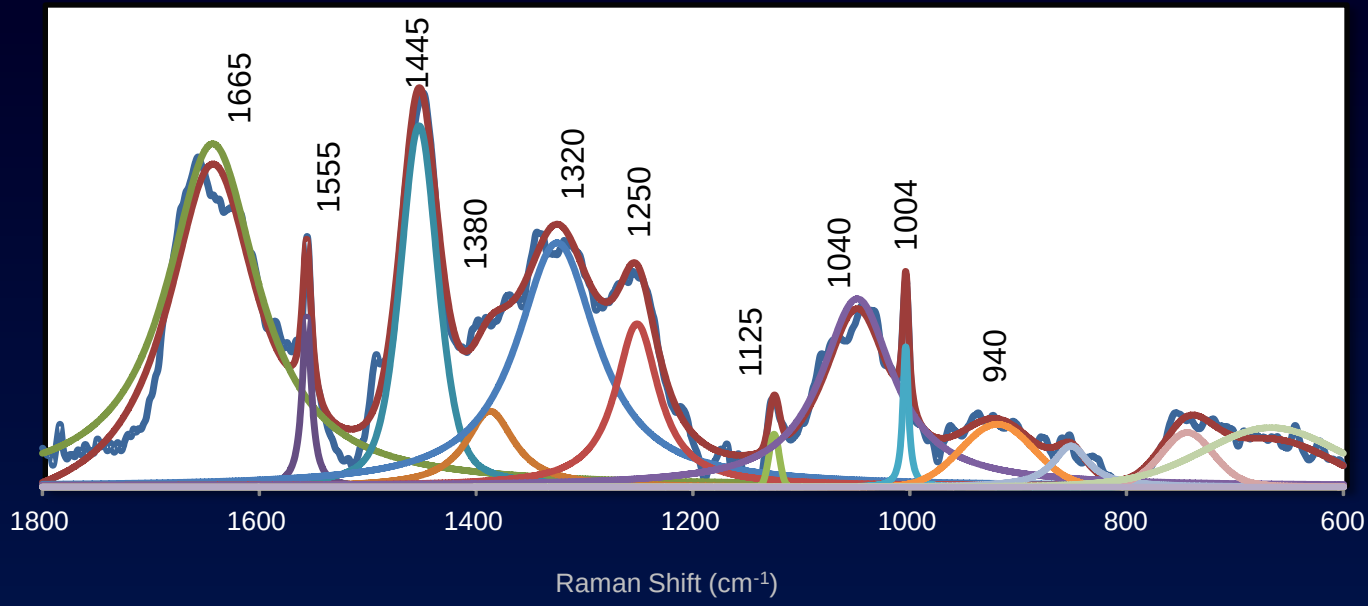

Raman Shift (cm^{-1})	Vibrational Band Assignment	Component
860	ν(C-C)	nucleic acids
920,940	ν(C-N), ν(C-C)	nucleic acids, keratin
1004	ν(C-C) ring	phenylalanine
1040	ν(C-C) skeletal	glycogen, keratin
1125	ν(C-C), ν(C-N)	nucleic acids, protein
1250	ν (C-N) and δ(N-H); Amide III	protein
1320	$\delta(CH_2)$ twisting	nucleic acids, protein
1445	$\delta(CH_3)$ and $\delta(CH_2)$ scissoring	protein
1555		aromatic amino acids, heme
1665	ν(C=O); Amide I	protein

Univariate Analysis of Band Areas

Comparison of mean band areas and band area ratios for all debridements for biopsies from normal healing wounds and dehisced wounds.

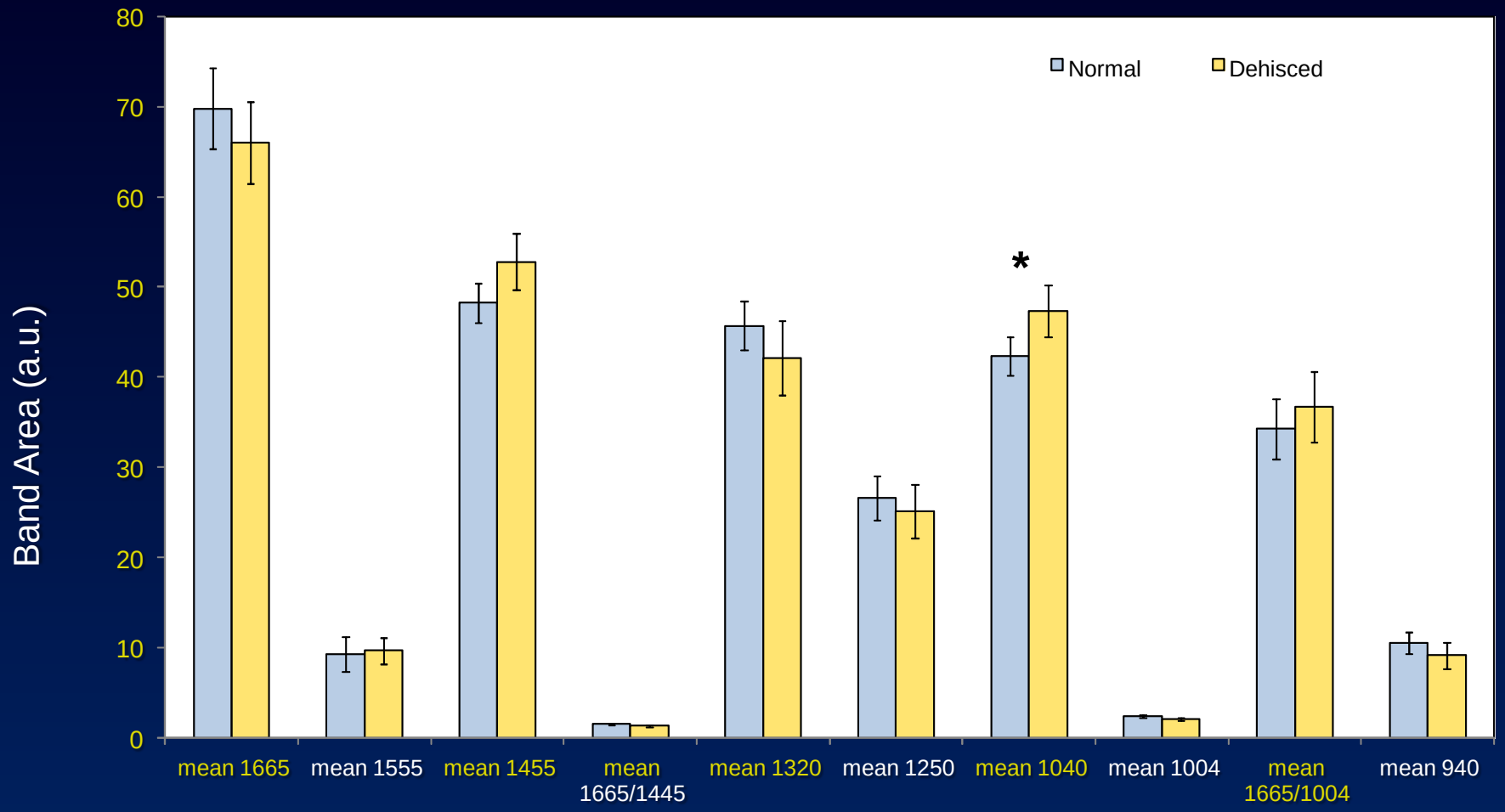

* $p < 0.02$

Univariate Analysis of Band Areas

Comparison of mean band areas and band area ratios for first debridements for biopsies from normal healing wounds and dehisced wounds.

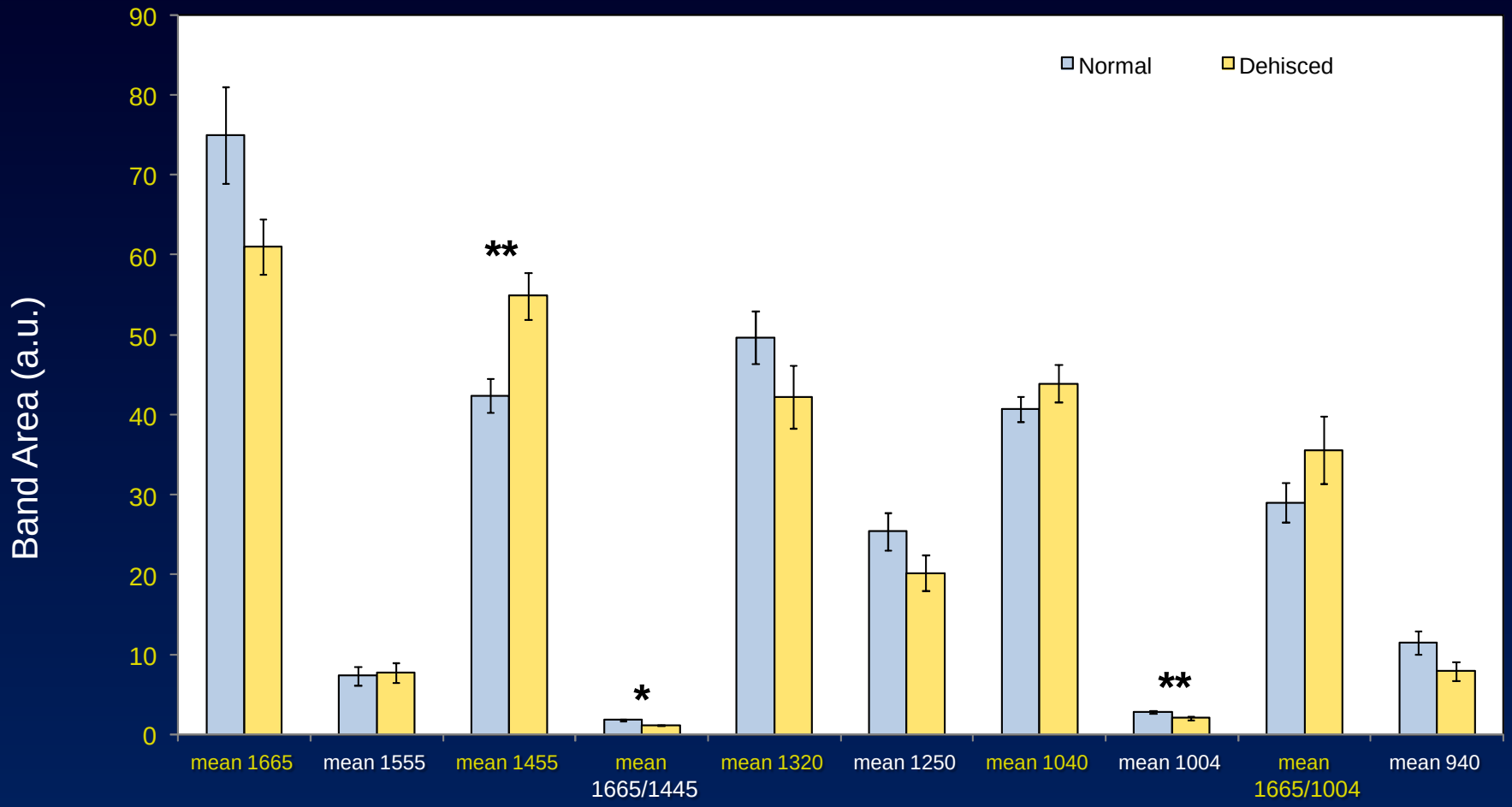

* $p < 0.02$ ** $p < 0.05$

Univariate Analysis of Band Areas

Comparison of mean band areas and band area ratios for final debridements for biopsies from normal healing wounds and dehisced wounds.

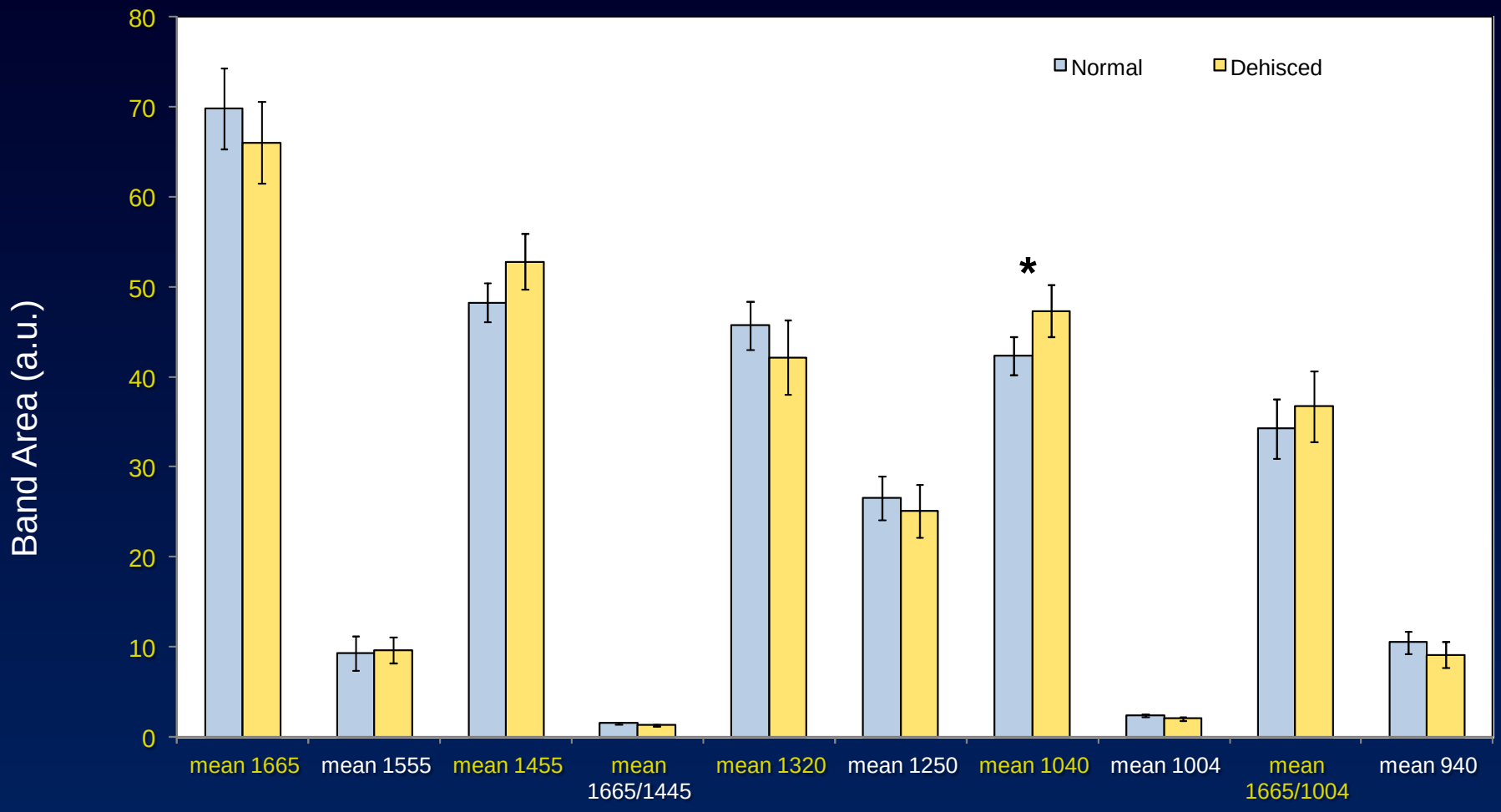

* $p < 0.02$

Monitoring a Wound Over Time – Normal Healing Wounds vs. Dehisced Wounds

- Overall, there is an increase in the mean 1040 cm^{-1} band area (BA) for all normal healing wound biopsies compared to all dehisced wound biopsies in this preliminary study.
- When just comparing the first debridement biopsies, protein related band areas and band area ratios are significantly different for normal healing wound biopsies and dehisced wound biopsies – 1445 cm^{-1} BA, 1665/1445 cm^{-1} band area ratio (BAR), and 1004 cm^{-1} BA.
- At the final debridement, the 1040 cm^{-1} BA for all normal healing wound biopsies is decreased compared to the dehisced wound biopsies.
- We have over 250 tissue biopsies from over 50 patients, most of which we have collected spectra in triplicate (over 4 years).
- Peak fitting needs to be performed over the entire spectrum to determine which vibrational bands provide optimal sensitivity and specificity. Some regions of the spectrum require a more in depth peak fitting (Amide I and III bands).
- Other aspects of the spectra, such as the fluorescence background, may also provide indications of the status of the tissue overall.

Project Goals

- Build our spectral biopsy database for Bayesian Belief Network modeling and other multivariate analysis techniques.

- Determine threshold values (band area ratios, fluorescence background, etc.) that are capable of differentiating normal healing wounds and wounds that are susceptible to dehiscence.

- Validate spectroscopic wound healing prediction models in a military and civilian population.

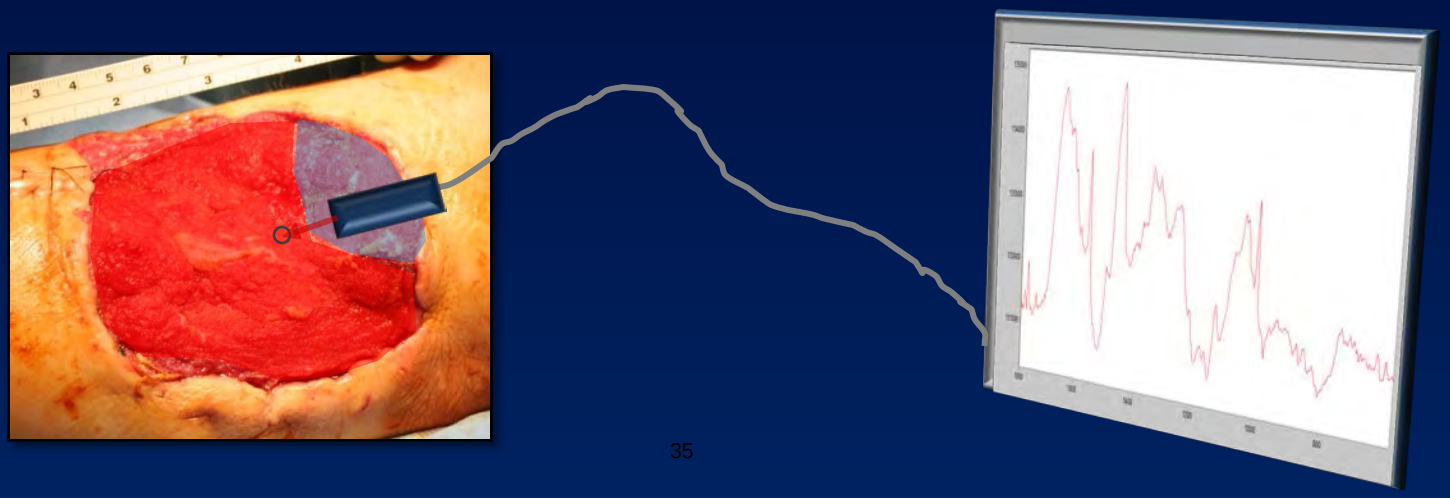

Acknowledgements

Naval Medical Research Center

Department of Regenerative Medicine

Dr. Jonathan Forsberg
Dr. Trevor Brown
Dr. Doug Tadaki
Tala Ghadimi
Dr. Felipe Lisboa
Stacia Moreno
Frederick Gage
Rajiv Luthra
Maricela Rodriguez

USUHS

Department of Surgery

Dr. Eric Elster

WRNMMC

General Surgery

http://www.med.navy.mil/sites/nmrc/Pages/ccc_regenmed.htm

Disclaimer

- The multidisciplinary care of these patients would not have been possible without the dedicated efforts of everyone at WRAMC and NNMC. Both civilian and military personnel have rendered skilled and compassionate care for these casualties. All of our efforts are dedicated to those who have been placed in harm's way for the good of our nation.

- The views expressed in this manuscript are those of the authors and do not reflect the official policy of the Department of the Army, Department of the Navy, the Department of Defense or the United States Government.

- This effort was supported (in part) by the U.S. Navy Bureau of Medicine and Surgery under the Medical Development (PE 0604771N) and Office of Naval Research work unit number (602115HP.3720.001.A1015), in part by Army DMRDP grant D10-I-AR-J2-501, and in part by CDMRP PRORP award OR090136.

- We are a military service members (or employee of the U.S. Government). This work was prepared as part of our official duties. Title 17 U.S.C. 105 provides the "Copyright protection under this title is not available for any work of the United States Government." Title 17 U.S.C. 101 defines a U.S. Government work as a work prepared by a military service member or employee of the U.S. Government as part of that person's official duties.

- This study was approved by the Walter Reed National Military Medical Center Institutional Review Board in compliance with all Federal regulations governing the protection of human subjects.

Using Multimodal Imaging Techniques to Monitor Limb Ischemia: A Rapid, Non-Invasive Method for Assessing Extremity Wounds

Rajiv Luthra[1], Nicole J. Crane Ph.D.[1,3], Jonathan A. Forsberg M.D.[1,2,3], Eric A. Elster M.D.[1,2,3]

[1]Naval Medical Research Center
[2]Walter Reed National Military Medical Center
[3]Uniformed Services University of the Health Sciences

SCIX, Kansas City, MO
3rd October 2012

Acute Combat Wounds

- Approximately 70% of military casualties from Operation Iraqi Freedom and Operation Enduring freedom were recorded as involving major limb injury.
- Roughly 90% of which were caused by blast injuries from improvised explosive devices (IEDs) .
- The management of modern traumatic war wounds remains a significant challenge for clinicians.

Acute Combat Wounds – Current Treatment

- The timing of wound closure is subjectively based.
- Surgical debridements are performed every 2-3 days to assess wound condition and remove devitalized tissue.
- Wound assessment involves combination of :
  - patient's general condition
  - injury location
  - adequacy of perfusion
  - gross appearance of the wound

Acute Combat Wounds - Challenge

- Need for an objective method to measure limb viability.
- Aim to develop technology for real-time monitoring of extremity oxygenation and perfusion.
- Ideally the technology would be:
  - Low-cost
  - Non-invasive
  - Rapid and Reliable

Potential Solution

- Multimodal imaging system with 3CCD and infrared imaging.
- Accurately monitors changes in tissue oxygenation and perfusion.
  - Real-time
  - Non-invasive
  - Uses existing commercially available cameras

Imaging Modalities

- 3CCD:
  - Provides data for surface oxygenation.
  - Based on the spectral response of hemoglobin in the visible region of the spectrum.

- IR:
  - LWIR: 7.5 - 13.5 µm.
  - Provides data for overall tissue perfusion.
  - Based on relationship of tissue temperature with perfusion.

Understanding 3CCD Cameras

- Advantages:
  - Technology similar to common digital camera.
  - Commercially and easily available.
  - Inexpensive & easy to use.
  - Provides enhanced color and image quality.
- Mechanism:
  - Utilizes a trichroic prism to split incoming light into three channels (Red, Green and Blue).
  - Each channel has its own detector a charge-coupled device (CCD).
  - Higher color sensitivity and dynamic range.

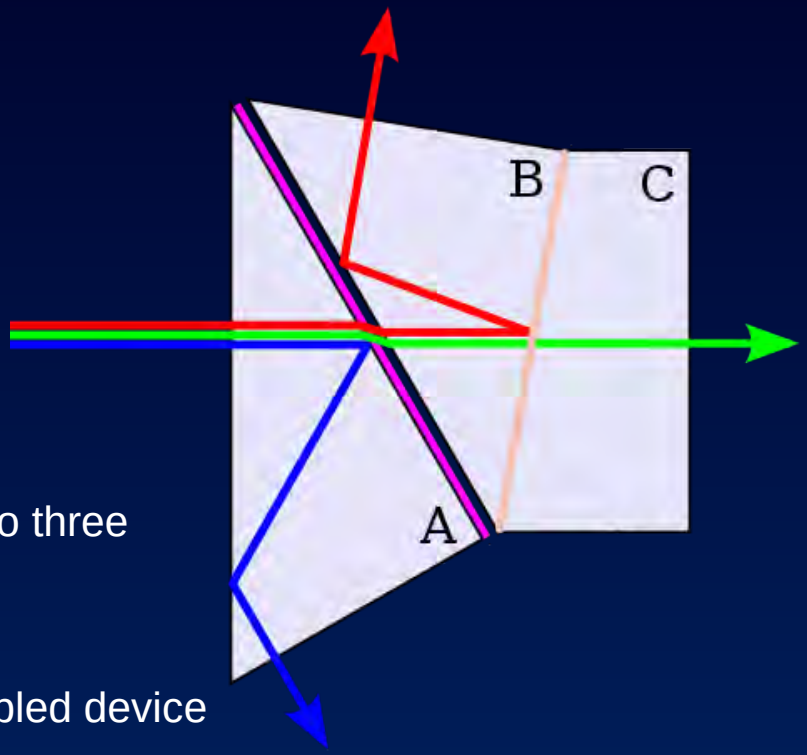

Absorption Spectra of Hb_{O_2} and Hb

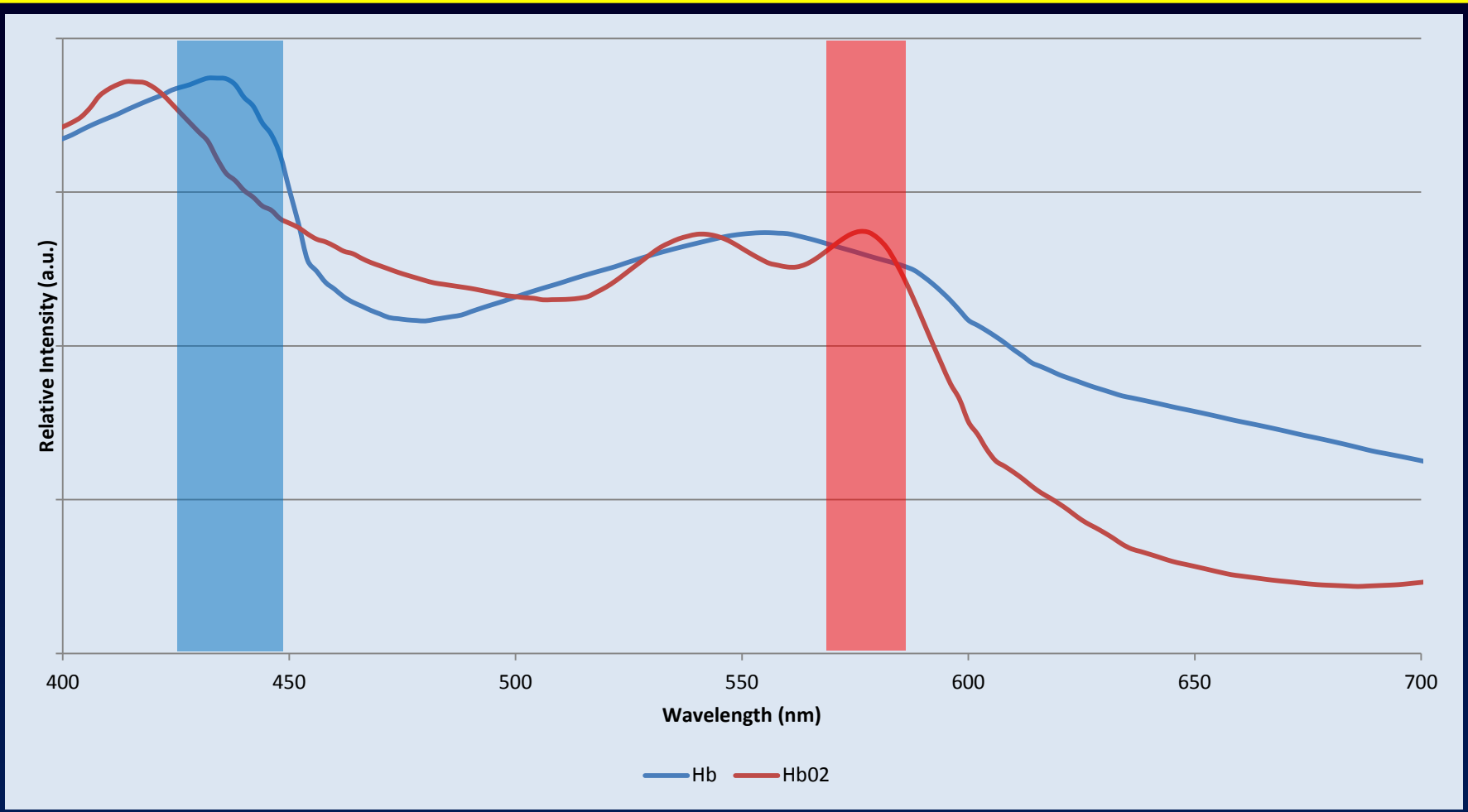

Peak Differences between HbO_2 and Hb

Relating P_{O2} values with 3CCD

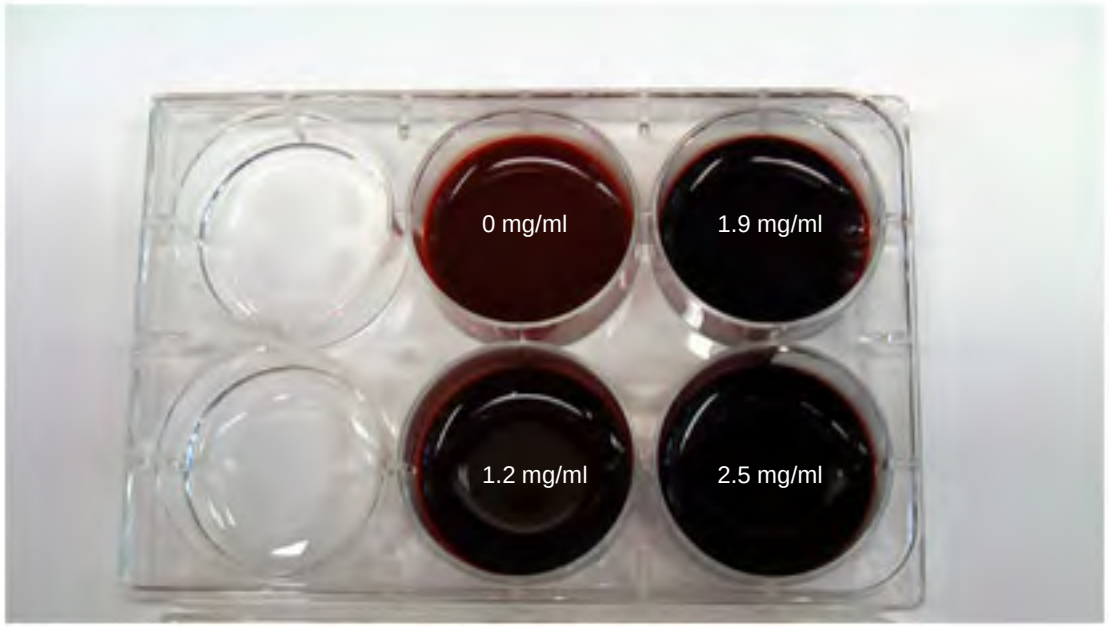

Each well initially contains the same, oxygenated blood.

Varying amounts of sodium dithionite, a reducing agent that scavenges the available O_2, are added to change the final P_{O2}.

Relating P_{O2} values with 3CCD

3CCD Image

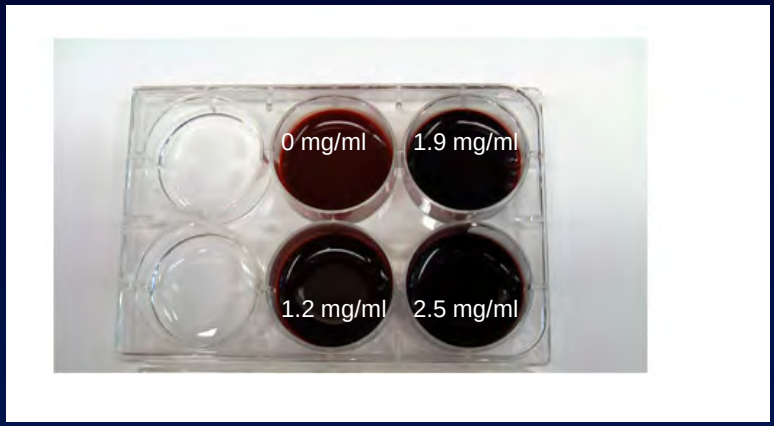

1. Image imported into Matlab.
2. Split into its component channels.

Red Channel

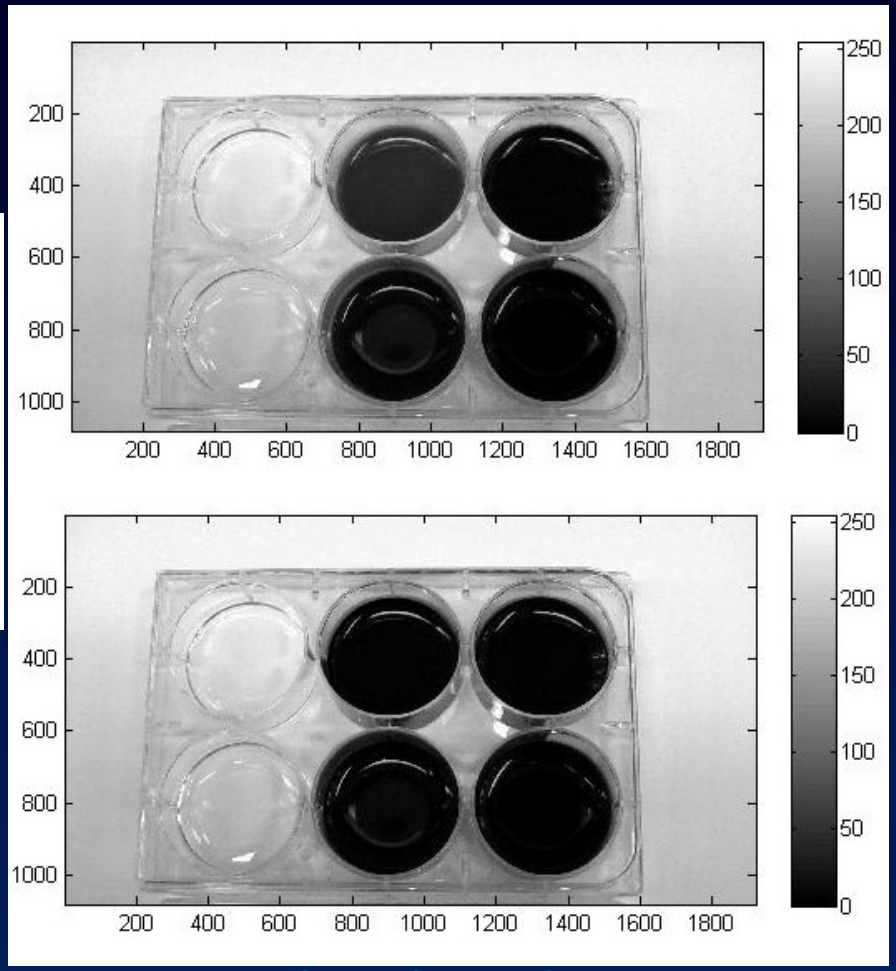

Blue Channel

Relating P_{O2} values with 3CCD

3CCD Image

Red Channel

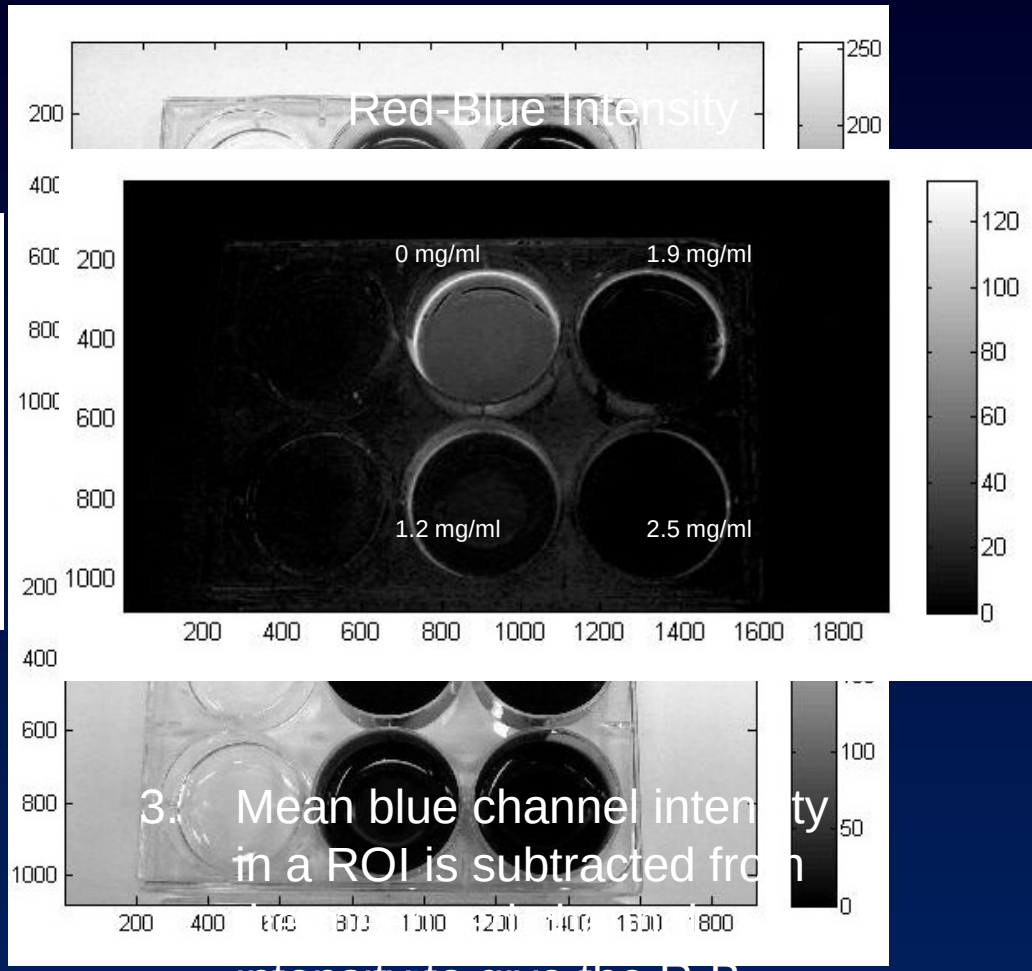

3. Mean blue channel intensity in a ROI is subtracted from the red intensity to give the R-B 3CCD value.

Relating P_{O2} values with 3CCD

Measured P_{O2} values against the 3-CCD values for each well show a very clear correlation.

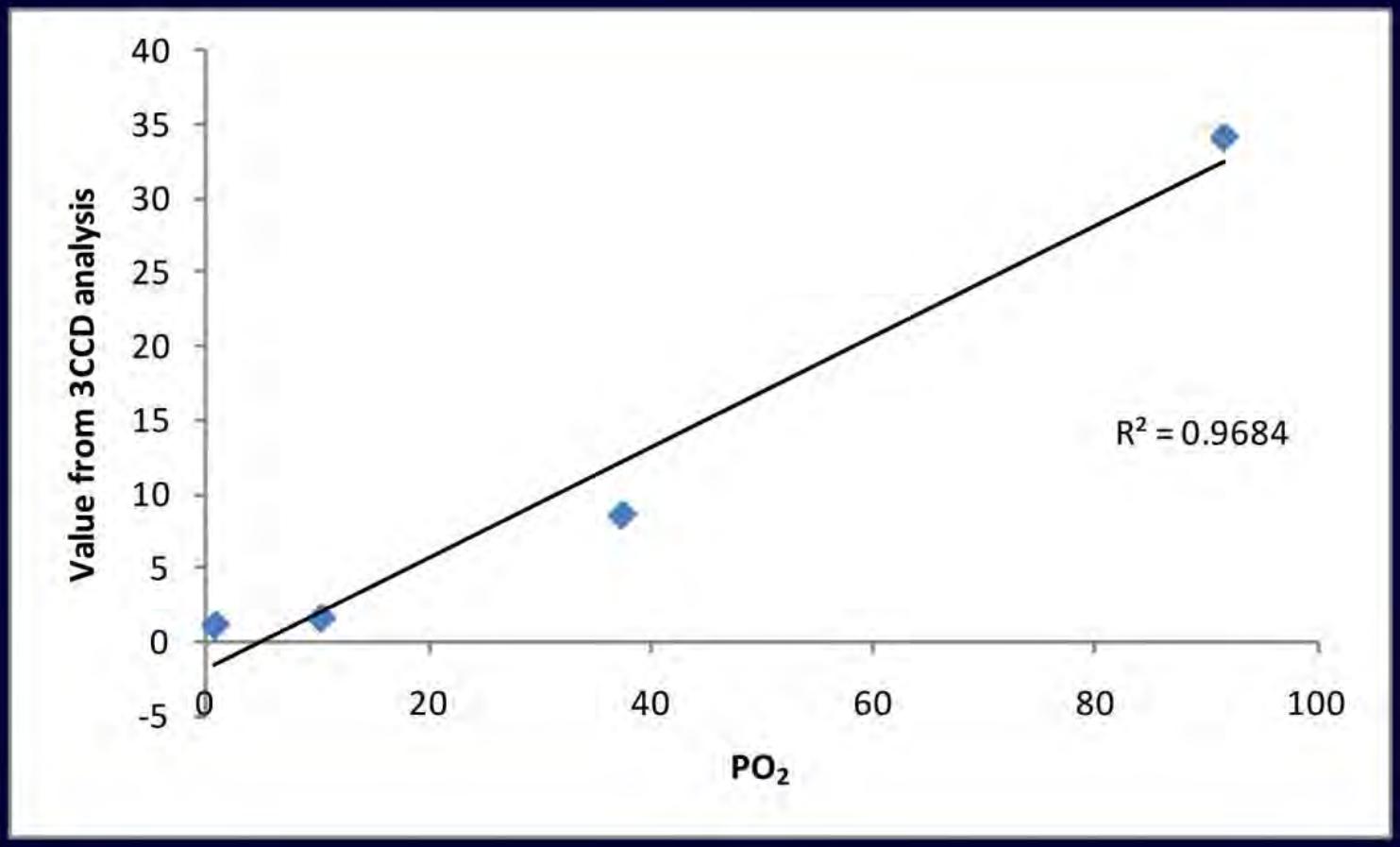

Swine Model of Limb Ischemia

Swine Limb Ischemia Protocol

- Goal: Characterize extremity injury caused by ischemia and reperfusion.

apply vessel clamps or tourniquet (120 or 210 mins)

return to cage and observe for 7 days

- To score the severity of the extremity injury the modified Tarlov scale is used.

0 – Complete paralysis
1 – Minimal movement
2 – Stands with assistance
3 – Stands alone
4 – Weak walk
5 – Normal gait

Limb Ischemia

- Study extremity ischemia and reperfusion in 2 cases.

- To simulate a vascular injury, we use direct vessel occlusion by isolating and tying the femoral artery and vein.

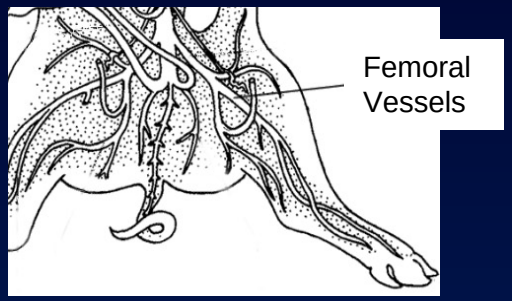

- To simulate a crush type injury, such as one sustained by an IED blast, we use a pneumatic tourniquet inflated to 250 mm Hg.

Swine Limb Ischemia Protocol - Tourniquet

- Study tourniquet induced extremity ischemia in 2 cases.
  - Case I:
    - 2 hours ischemia followed by 30 minutes of reperfusion.
    - We predicted the damage caused to be mostly “reversible”.
  - Case II:
    - 3.5 hours ischemia followed by 30 minutes of reperfusion.
    - After 3 hours of ischemia, muscle cells are much more likely to become hypoxic and die.
    - Here we predicted the damage caused to be “irreversible”.

3CCD Results

2 hr Tourniquet Ischemia and Reperfusion 3CCD Images

"Reversible Ischemia"

3.5 hr Tourniquet Ischemia and Reperfusion 3CCD Images

“Irreversible Ischemia”

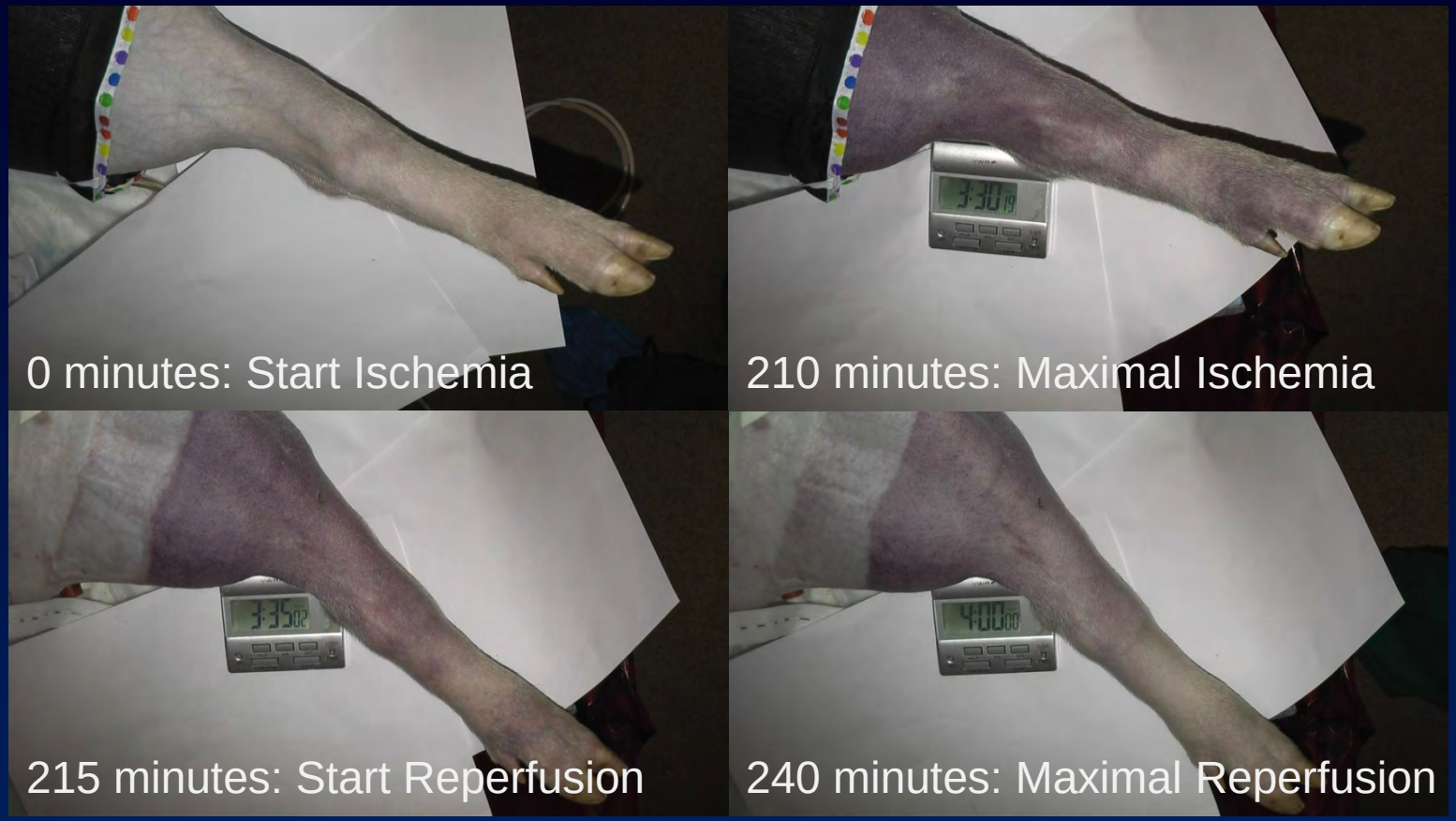

2 hr Tourniquet Ischemia and Reperfusion: Mean 3CCD R-B Values

- All R-B values were normalized to peak hypovolemic values.
- Within the 2 hour ischemia study we see 2 cases appear to be a milder ischemia than the other 5 cases.

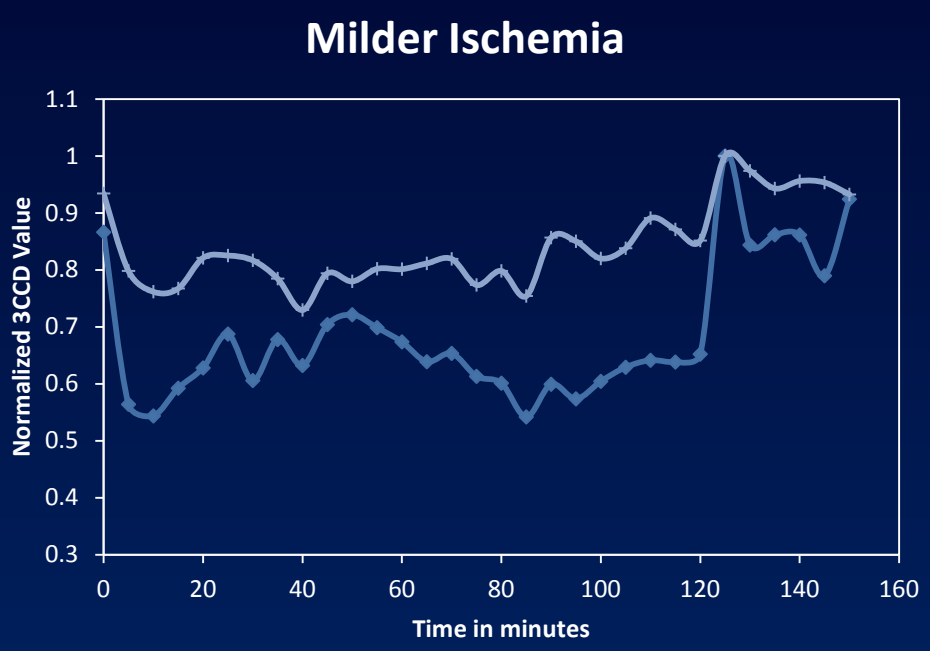

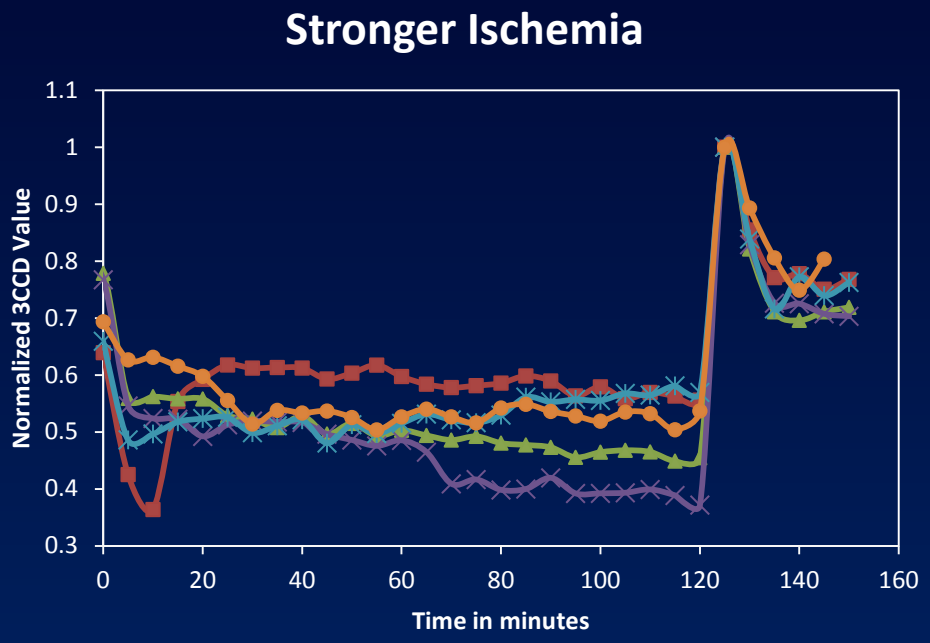

2 hr Tourniquet Reperfusion: 3CCD R-B Values

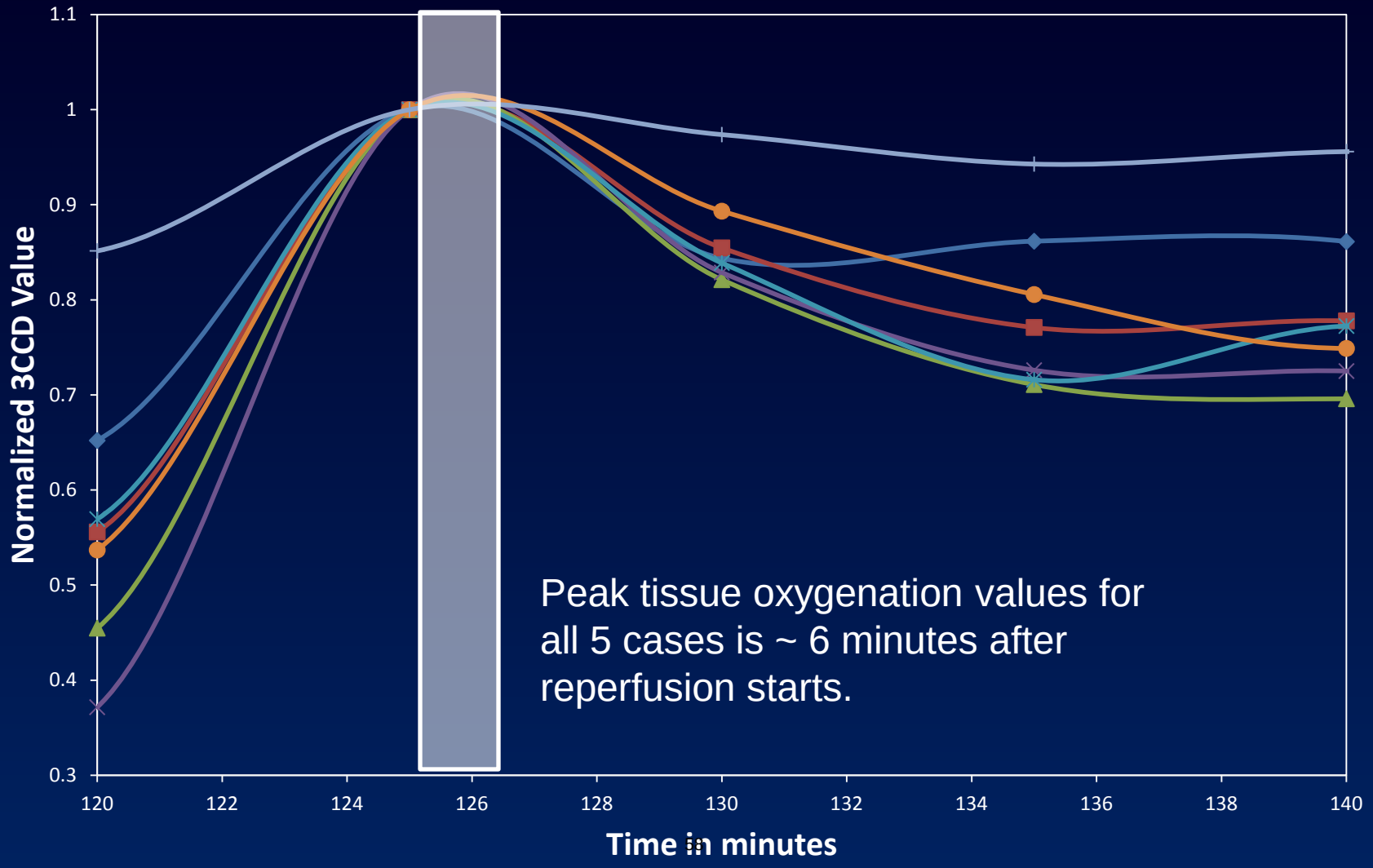

2 hr Tourniquet Reperfusion: 3CCD R-B Values

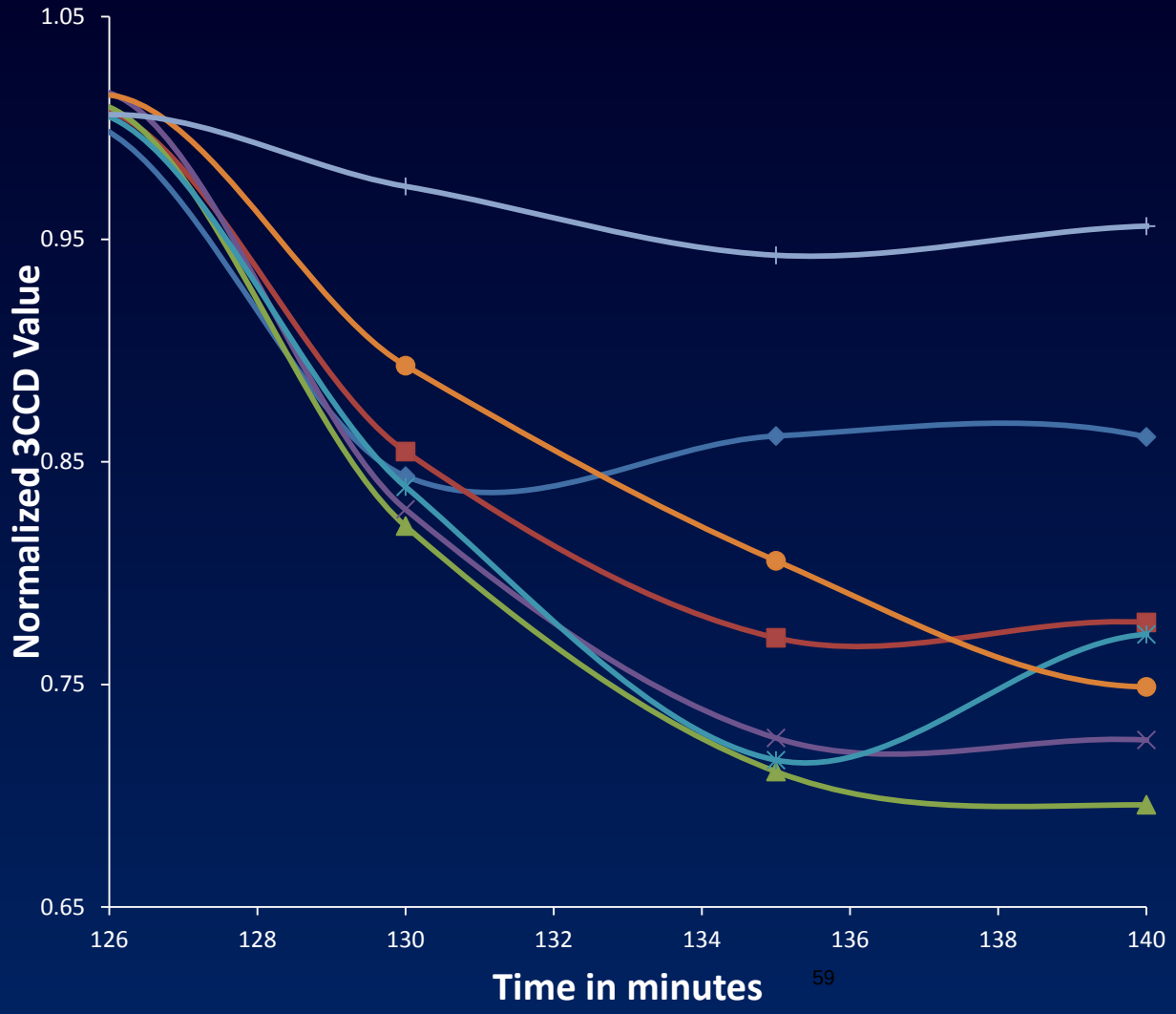

The final R-B value correlates with the severity of the extremity injury.

3.5 hr Tourniquet Ischemia and Reperfusion: Mean 3CCD R-B Values

- Again all R-B values were normalized to peak hypovolemic values.
- Here we see 2 cases appear to be a milder ischemia than the other 3 cases.

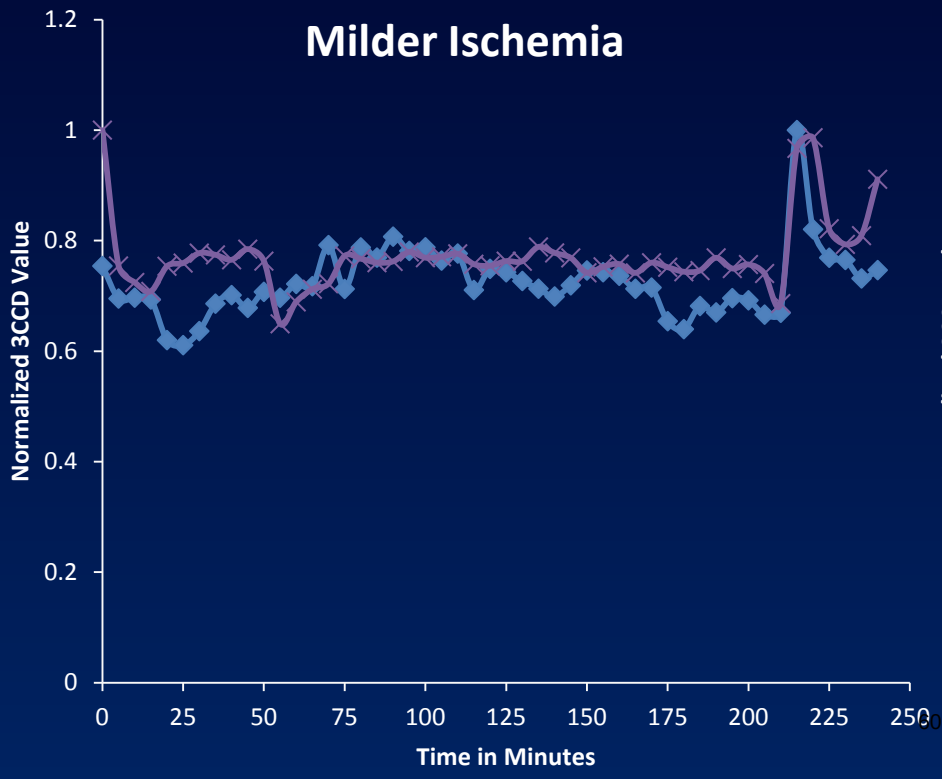

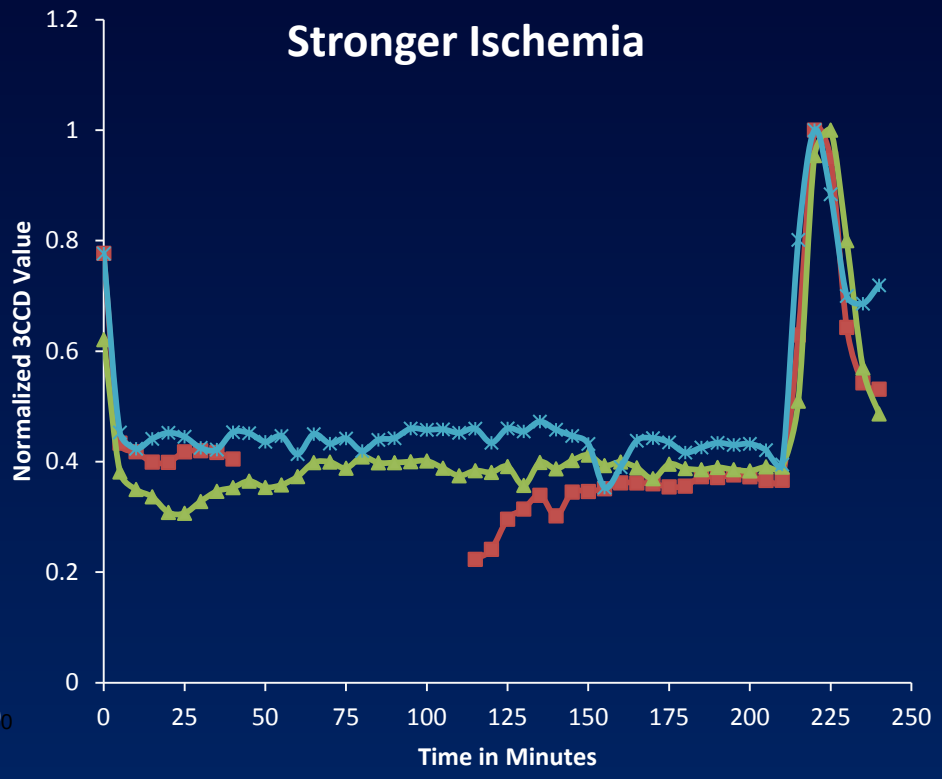

3.5 hr Tourniquet Reperfusion: 3CCD R-B Values

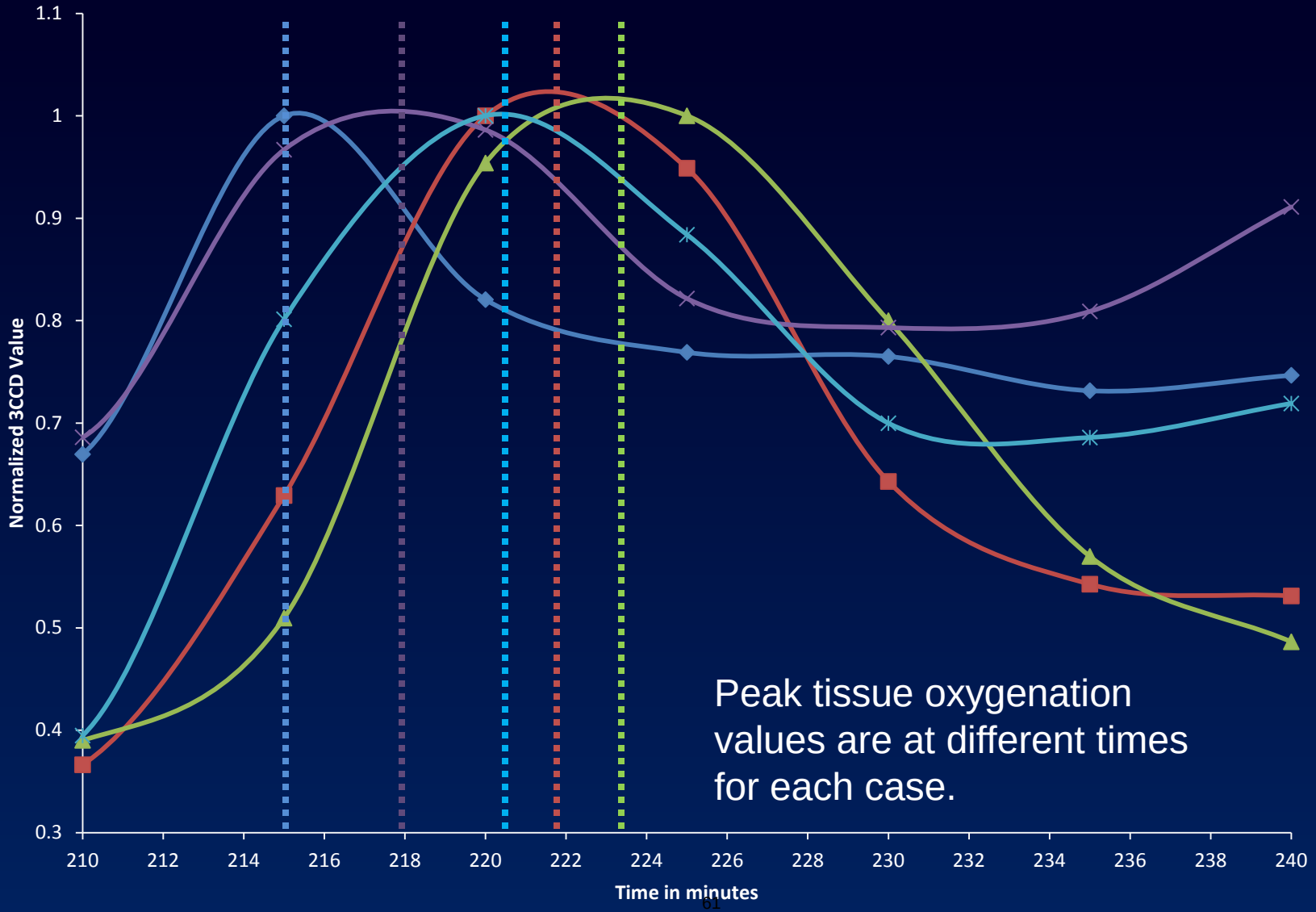

Comparison of Tarlov Scale Values and 3CCD Values

- Here we see a very good agreement between final R-B value (240 minutes) and the modified Tarlov score.
- We may be able to predict severity of tissue damage using this method.

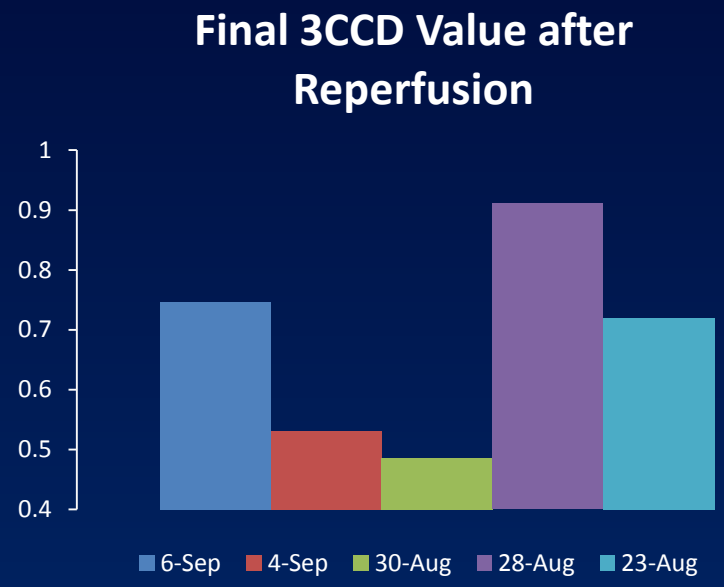

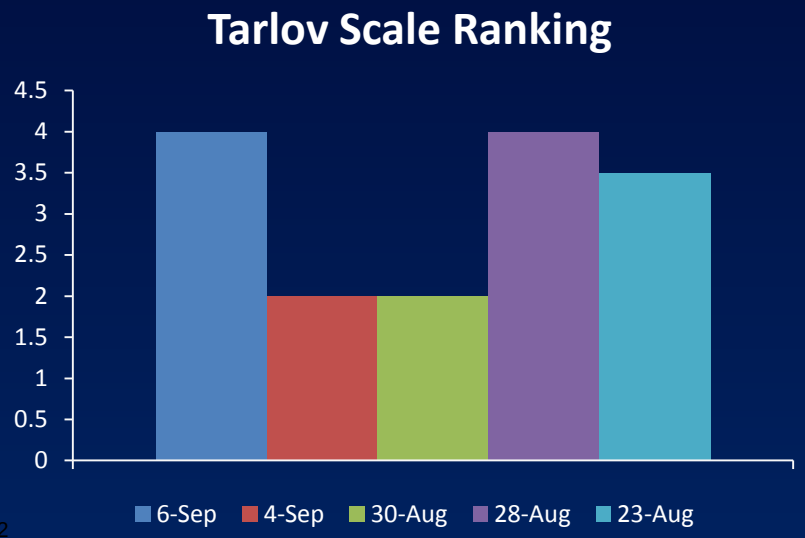

Different Peak Times due to Delayed Reperfusion?

- One explanation would be:
  - Different rates of extremity reperfusion cause different peak oxygenation values.
- To look at reperfusion we turn to IR imaging.

IR imaging Results

IR images during 2 hour Ischemia and Reperfusion

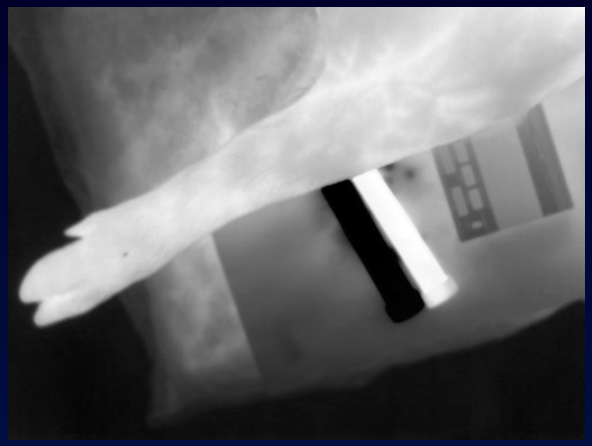

0 minutes: Start Ischemia

120 minutes: Maximal Ischemia

125 minutes: Start Reperfusion

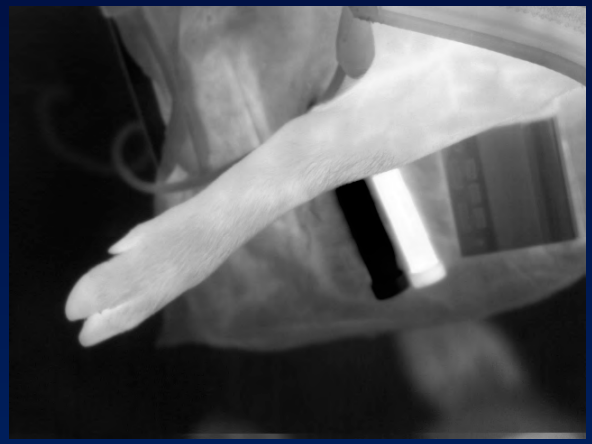

150 minutes: Maximal Reperfusion

IR images during 3.5 hour Ischemia and Reperfusion

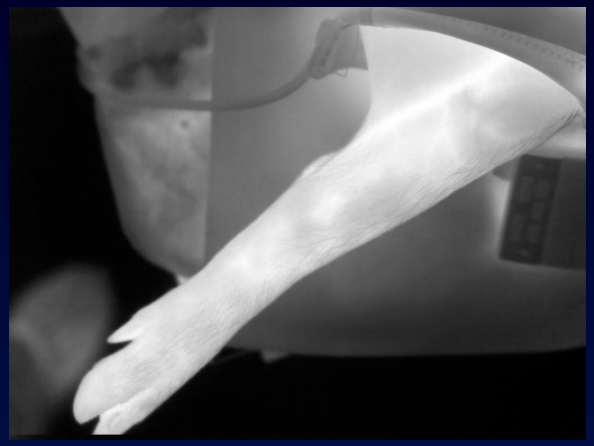

0 minutes: Start Ischemia

210 minutes: Maximal Ischemia

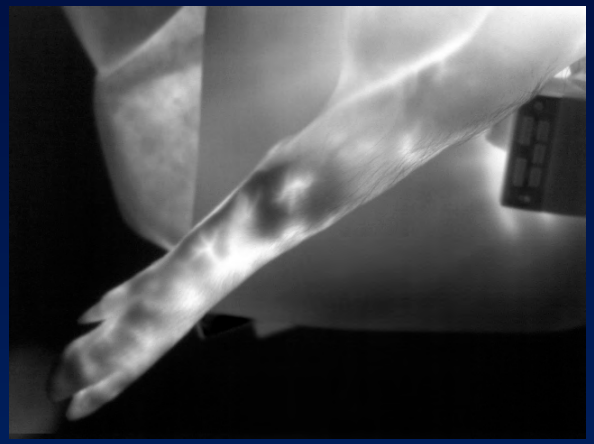

215 minutes: Start Reperfusion

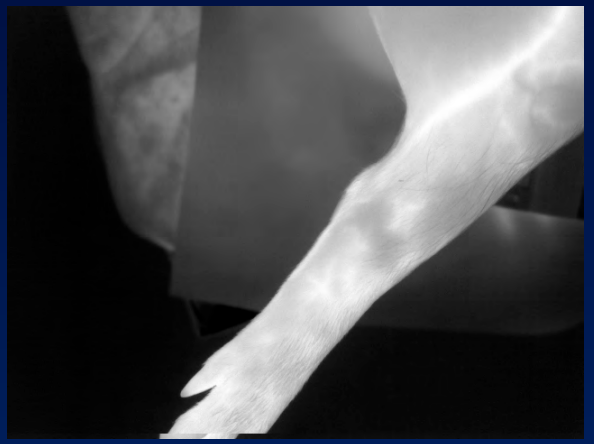

240 minutes: Maximal Reperfusion

Average extremity temperature during Ischemia and Reperfusion

- Temperature drop greater in 3.5 hr.
- No clear deviation in trends for either 2 hour or 3.5 hour cases.
- Limb temperature returns to pre-ischemic values.

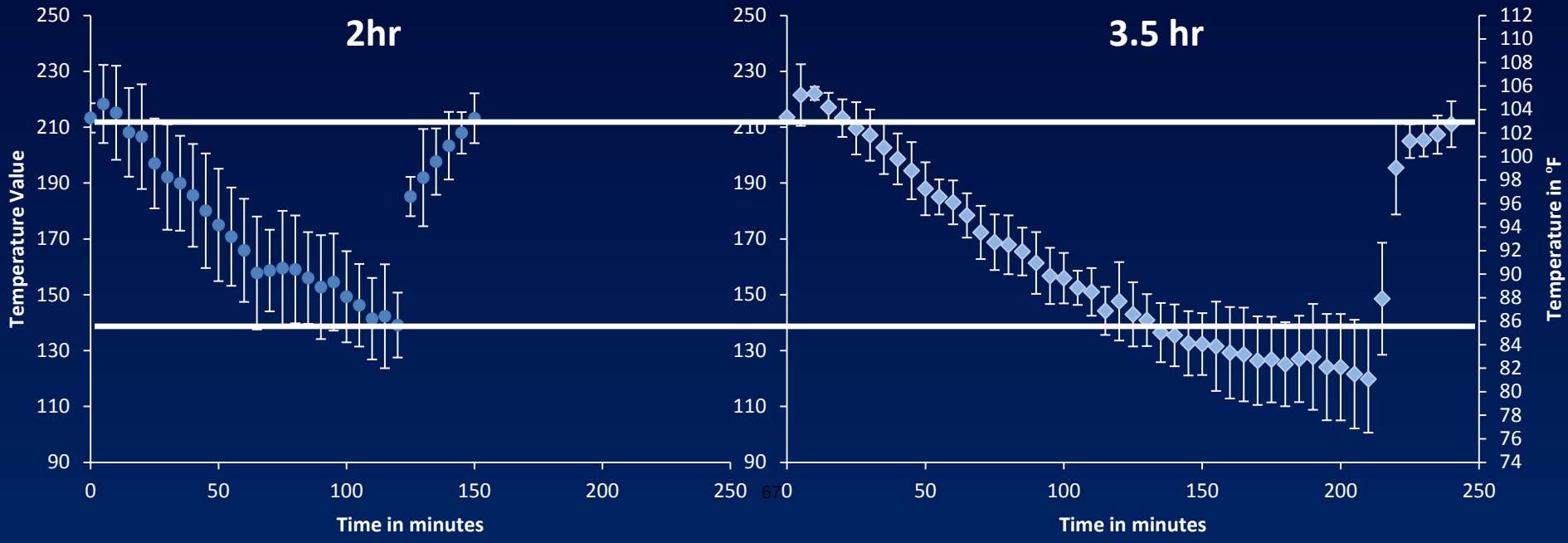

Comparing Mild and Strong Ischemic cases during Reperfusion

- Looking at 3.5 hr tourniquet cases.
- Reperfusion rates are different between the two cases.

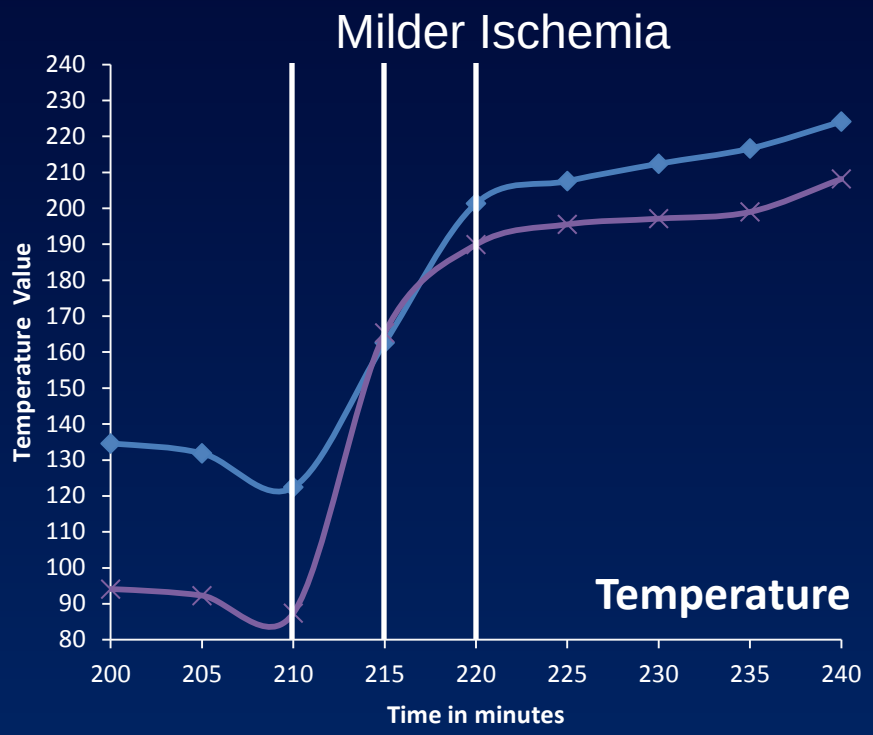

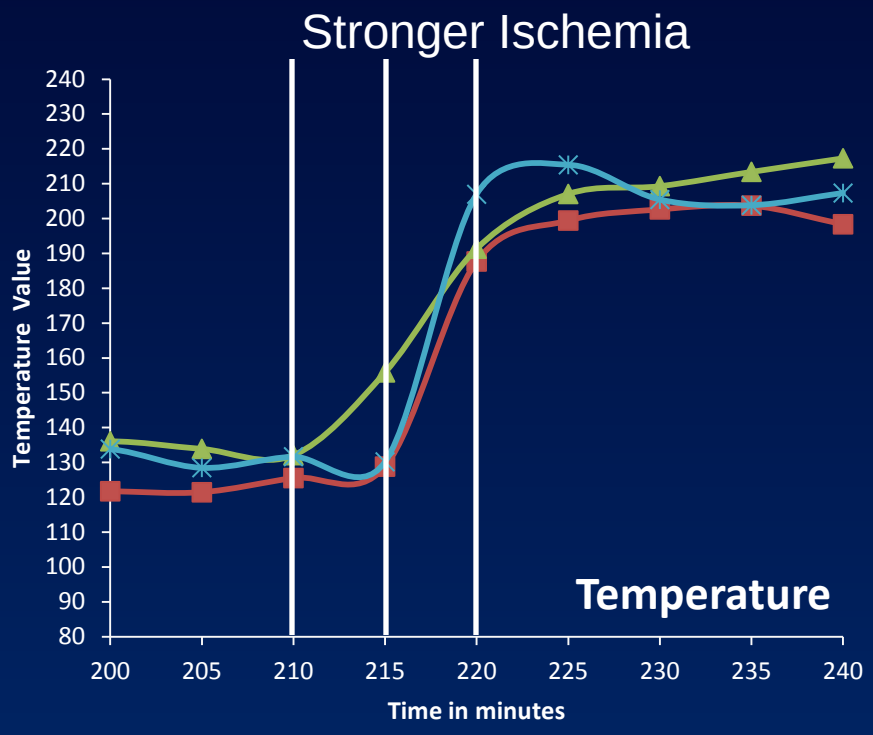

Comparing Tissue Oxygenation and Reperfusion – Milder Ischemic cases

- IR values do not directly correspond to 3CCD values.
- The delay in 3CCD value reaching its peak value is not explained well by only the reperfusion state.

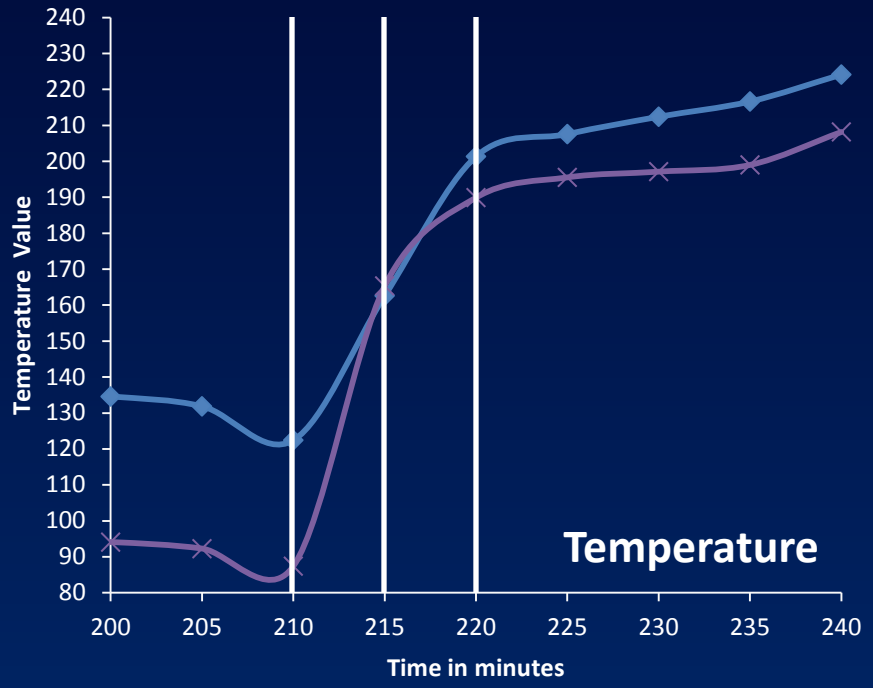

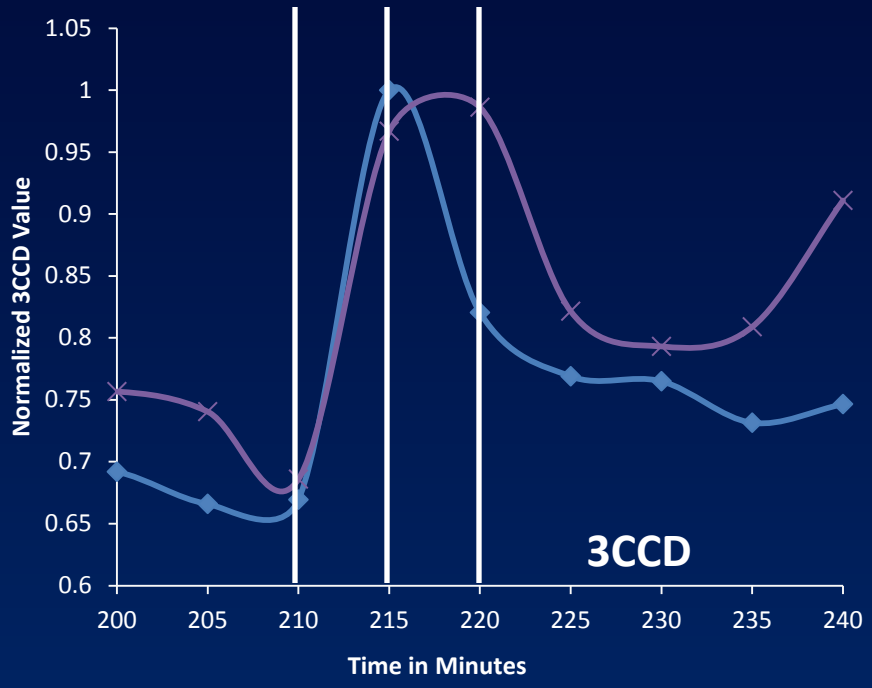

Comparing Tissue Oxygenation and Reperfusion – Stronger Ischemic cases

- Here, the fastest reperfusion case has the maximum delay to peak oxygenation.
- Possible tissue damage: reperfusion but reduced oxygentation?
- Need to monitor both reperfusion and tissue oxygenation.

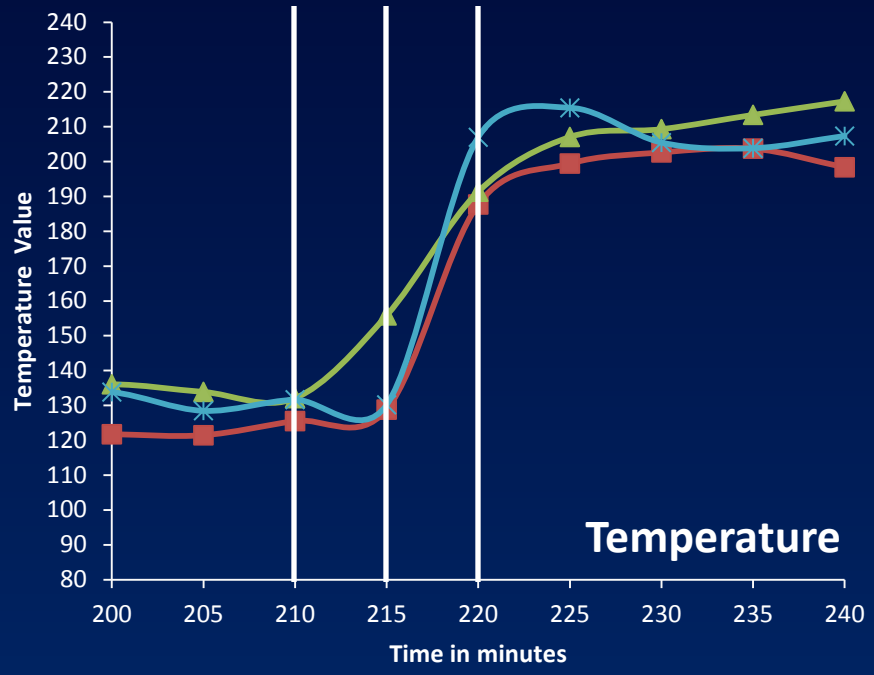

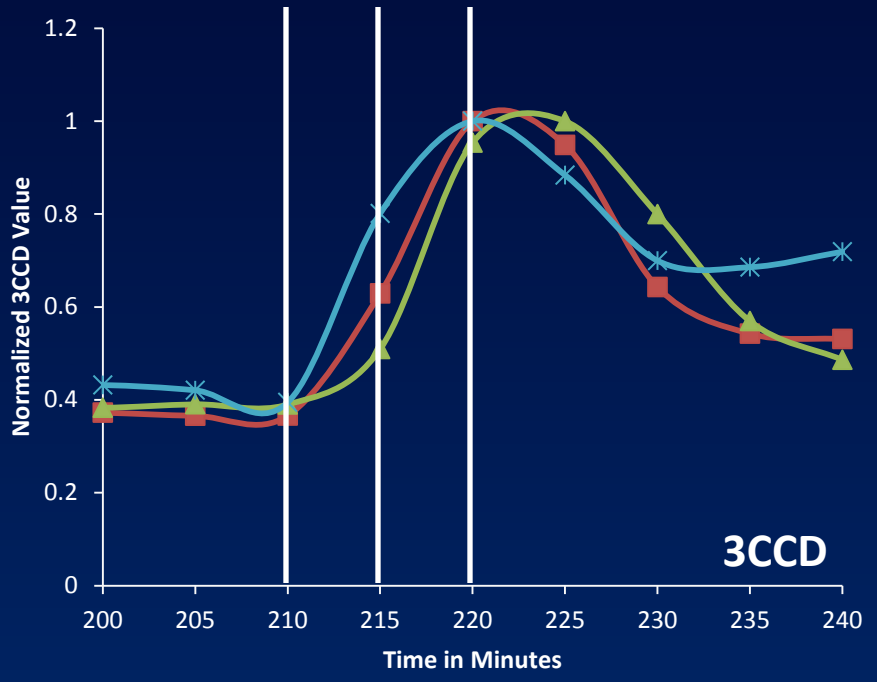

Conclusions

- We have developed a multimodal imaging system with 3CCD and infrared imaging.
- We have demonstrated that we can track changes in tissue oxygenation and perfusion in a limb ischemia model.
- A combination of R-B and IR values will likely enable prediction of limb viability.
- This technology can be easily visualized in real-time.

Visualizing Mild and Strong Ischemia

We can imagine a clinical imaging system for visualization of ischemia and reperfusion……

Mild Ischemia

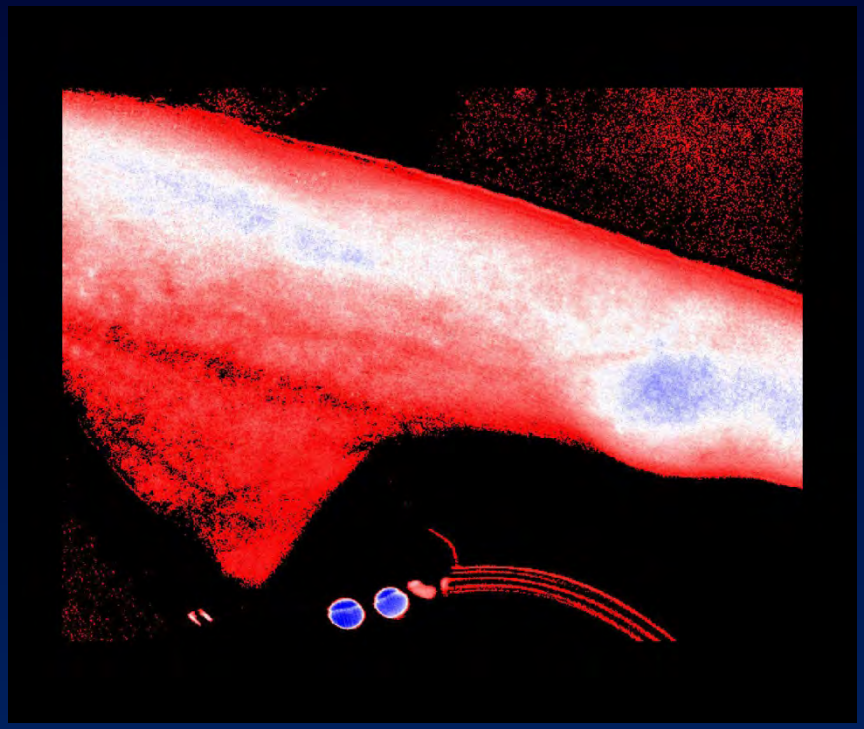

Strong Ischemia

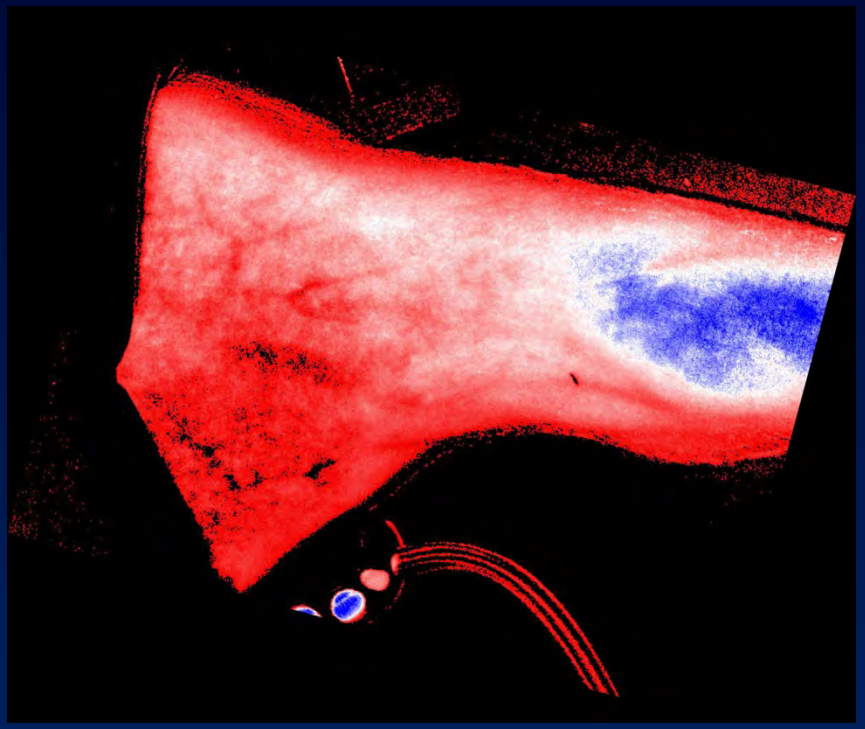

Acknowledgements

Naval Medical Research Center

Department of Regenerative Medicine

Dr. Nicole Crane
Dr. Jonathan Forsberg
Maricela Rodriguez

USUHS

Department of Surgery

Dr. Eric Elster
Tiffani Slaughter
Mitchell Harris

Laboratory Animal Medicine

WRNMMC

General Surgery

Dr. Joe Caruso
Dr. Jason Radowksy
Dr. Earl Lee
Dr. Felipe Lisboa

http://www.med.navy.mil/sites/nmrc/Pages/ccc_regenmed.htm

Disclaimer

- The multidisciplinary care of these patients would not have been possible without the dedicated efforts of everyone at WRAMC and NNMC. Both civilian and military personnel have rendered skilled and compassionate care for these casualties. All of our efforts are dedicated to those who have been placed in harm's way for the good of our nation.

- The views expressed in this manuscript are those of the authors and do not reflect the official policy of the Department of the Army, Department of the Navy, the Department of Defense or the United States Government.

- This effort was supported (in part) by the U.S. Navy Bureau of Medicine and Surgery under the Medical Development (PE 0604771N) and Office of Naval Research work unit number (602115HP.3720.001.A1015), in part by Army DMRDP grant D10-I-AR-J2-501, and in part by CDMRP PRORP award OR090136.

- We are a military service members (or employee of the U.S. Government). This work was prepared as part of our official duties. Title 17 U.S.C. 105 provides the "Copyright protection under this title is not available for any work of the United States Government." Title 17 U.S.C. 101 defines a U.S. Government work as a work prepared by a military service member or employee of the U.S. Government as part of that person's official duties.

- This study was approved by the Walter Reed National Military Medical Center Institutional Review Board in compliance with all Federal regulations governing the protection of human subjects.

Predicting Wound Outcome from Raman Spectroscopic Data: Univariate versus Multivariate Techniques

Nicole J. Crane[1,3], Rajiv Luthra[1], Jonathan A. Forsberg[1,2,3], Eric Elster[2,3]

[1]Naval Medical Research Center
[2]Walter Reed National Military Medical Center
[3]Uniformed Services University of the Health Sciences

SCIX, Kansas City, MO
October 3rd, 2012

Acute Combat Wounds

Acute Combat Wounds

- The management of modern traumatic war wounds remains a significant challenge for clinicians.
  - Extensive osseous and soft-tissue damage caused by blasts and high-energy projectiles.
- The ensuing inflammatory response ultimately dictates the pace of wound healing and tissue regeneration.
- The timing of wound closure or definitive coverage is subjectively based.
- Despite the use and application of novel wound-specific treatment modalities, some wounds fail to close, or dehisce.

Acute Combat Wounds – Current Treatment

Surgical debridements are performed every 2-3 days.

- remove devitalized tissue
- decrease bacterial load

Negative pressure wound therapy (NPWT) is applied between debridements. NPWT promotes wound closure.

Wound assessment involves:

- patient's general condition
- injury location
- adequacy of perfusion
- gross appearance of the wound

Acute Combat Wounds – The Challenge

Monitor wound healing *in vivo*, i.e. monitor wound healing during surgical debridements.

- Is it the best time to close the wound?
- Is the wound developing HO?
- Is the wound infected? With what?

Develop an objective and predictive model for wound healing.

The Toolbox

Our Toolbox

Real-time PCR

Multiplex Protein Assay

Raman Spectroscopy

FTIR Imaging

Thermography

Visible Reflectance Imaging

Bayesian Belief Network modeling

Sample Collection

Wound is surgically cleaned

Collect 1 cm³ tissue biopsy from center of wound bed

RT-PCR
Raman spectroscopy
Micro culture

NPWT is applied

Serum is collected

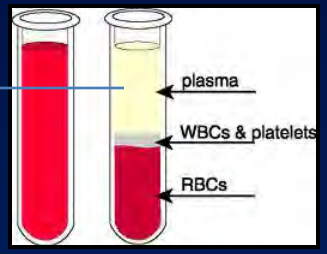

Protein assay

Effluent is collected

Protein assay

Raman spectroscopy
Micro culture

Preliminary Study – Raman Mapping Results

- Previous study demonstrated the potential of Raman spectroscopic analysis of wound biopsies for classification of wounds as normal or impaired healing.

Wound Rep Regen. 18(4): 409-416, 2010.

Ann Surg. 250(6):1002-7, 2009.

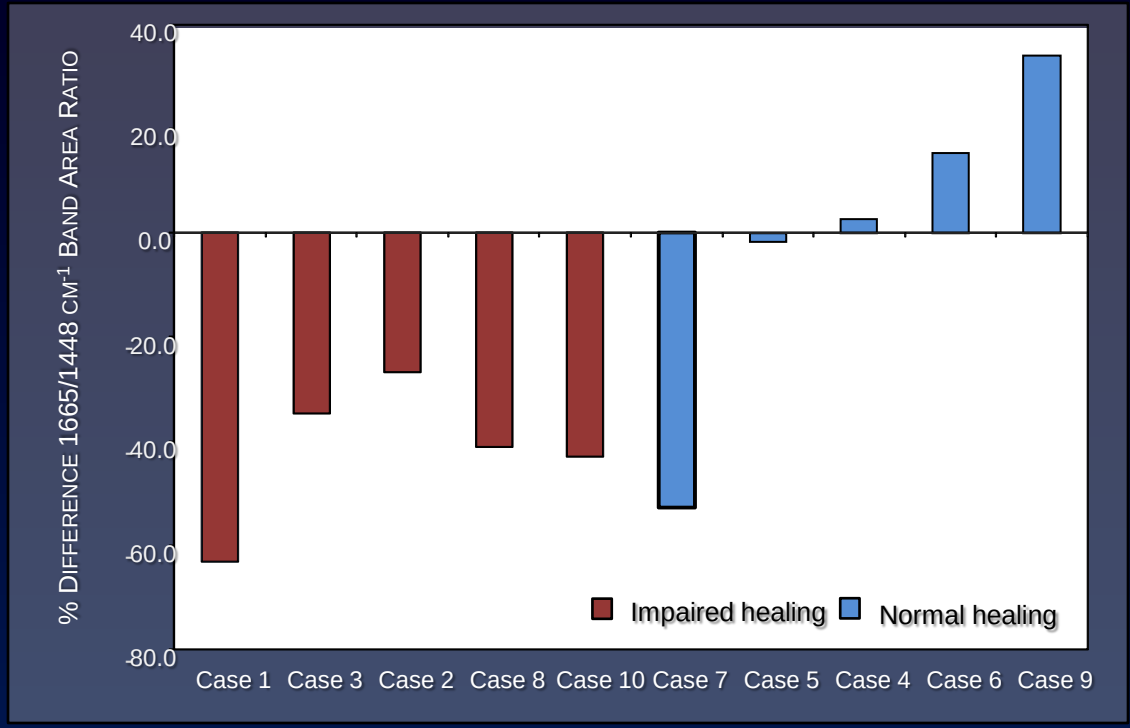

- Impaired healing wounds demonstrate a significant decrease in the 1665/1445 cm^{-1} band area ratio compared to normal healing wounds - these results were corroborated with collagen gene expression in the same samples.

Could this type of analysis be extended to intact wound biopsies and ultimately obviate the need for excisional wound biopsies?

Chronicling Wound Healing with Raman Spectroscopy

Raman Fiber Probe Data Collection

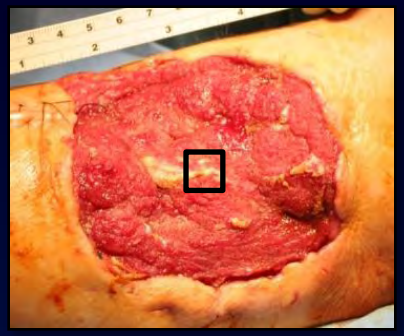

Approximately 1 cm^2 tissue biopsy is excised from the center of the wound bed.

Tissue is fixed in 10% neutral buffered formalin for storage.

Prior to spectral acquisition, samples are rinsed in 0.9% NaCl saline solution.

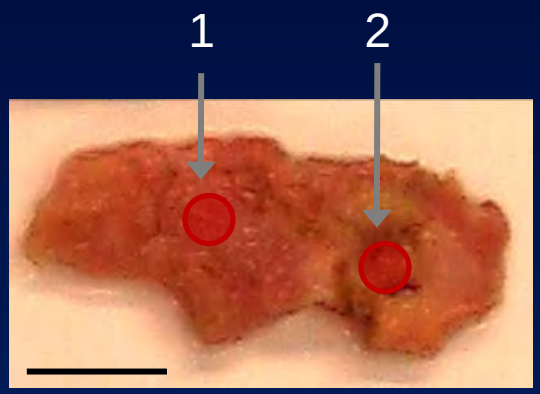

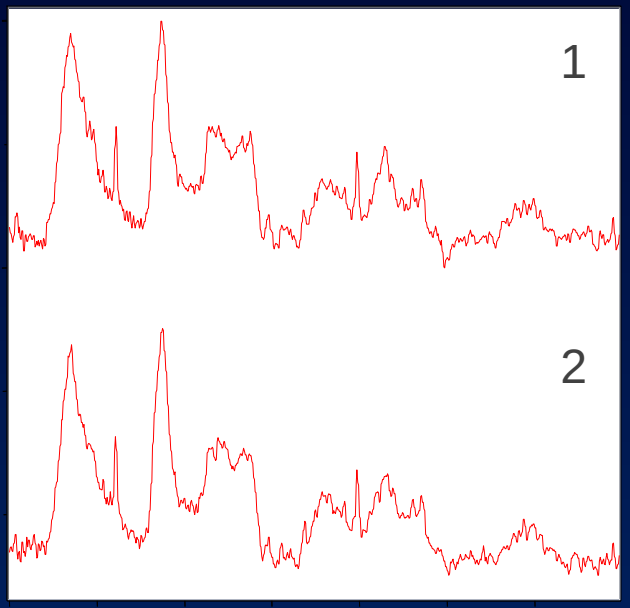

Examine multiple spots across the tissue.

14 accumulations, 5s spectrum
7 accumulations, 10s spectrum

Monitoring a Wound Over Time

First Debridement

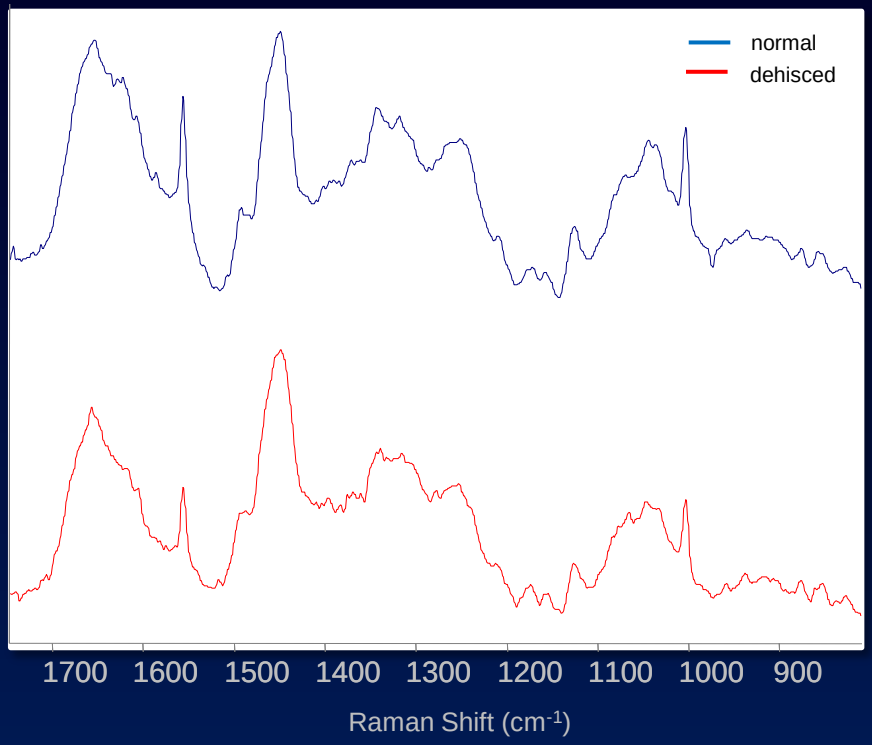

Final Debridement

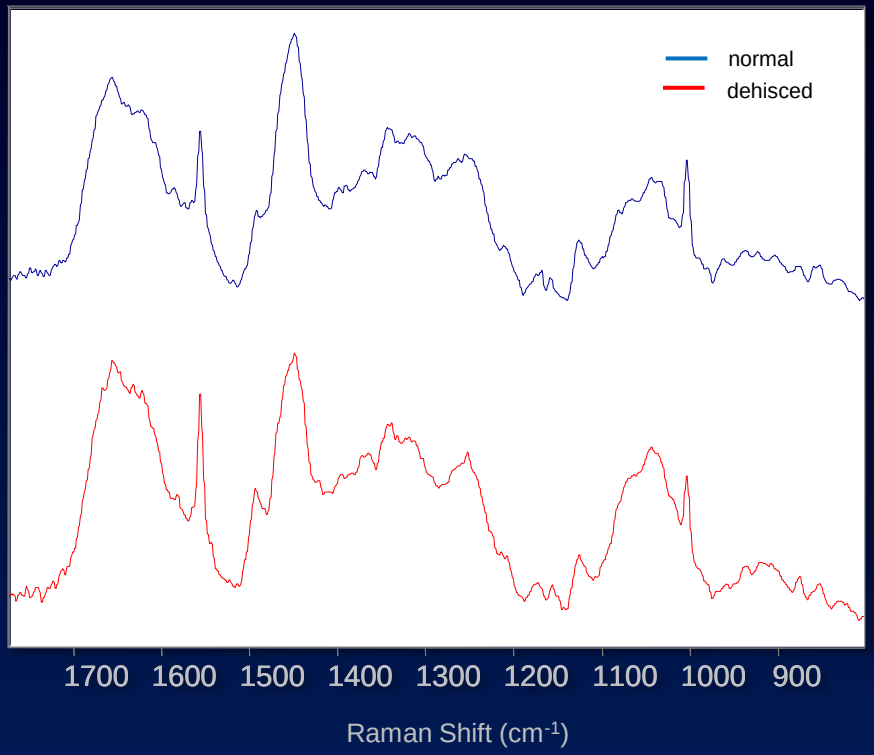

- Spectral differences between biopsies collected from normal healing wounds (n=12) and dehisced wounds (n=13) are not readily apparent.

Peakfitting for Spectral Deconvolution

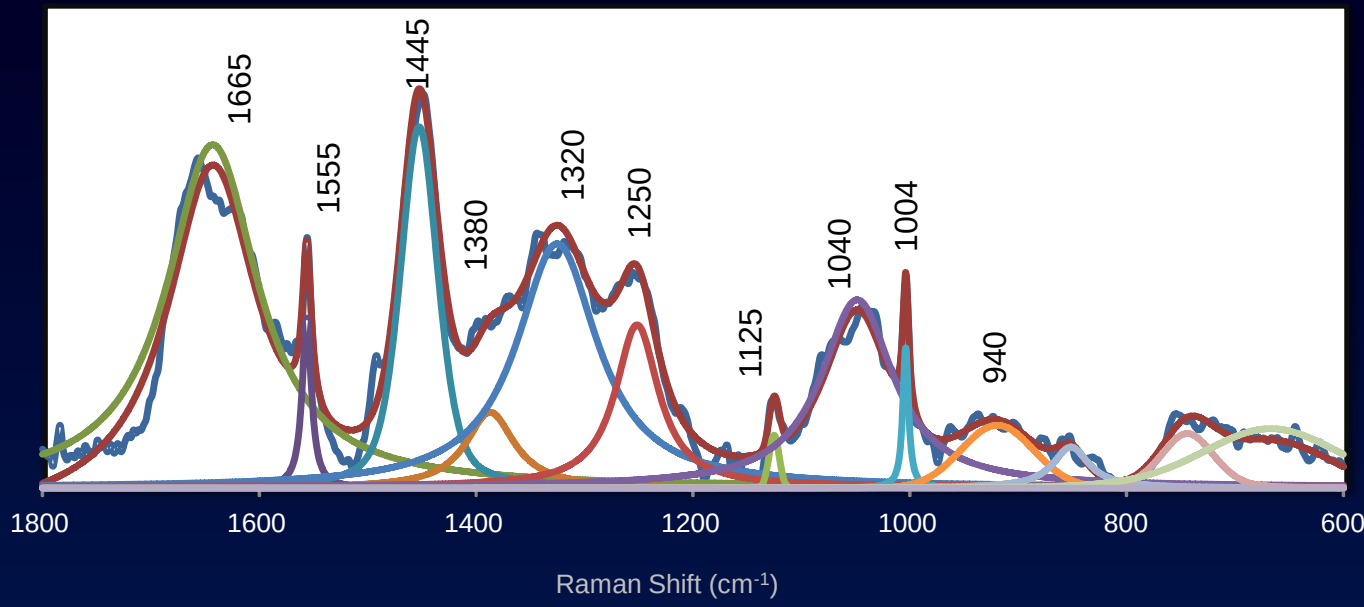

Raman Shift (cm^{-1})	Vibrational Band Assignment	Component
860	ν(C-C)	nucleic acids
920,940	ν(C-N), ν(C-C)	nucleic acids, keratin
1004	ν(C-C) ring	phenylalanine
1040	ν(C-C) skeletal	nucleic acids, protein
1125	ν(C-C), ν(C-N)	nucleic acids, protein
1250	ν (C-N) and δ(N-H); Amide III	protein
1320	$\delta(CH_2)$ twisting	nucleic acids, protein
1445	$\delta(CH_3)$ and $\delta(CH_2)$ scissoring	protein
1555		aromatic amino acids, heme
1665	ν(C=O); Amide I	protein

Univariate Analysis of Band Areas

First Debridement

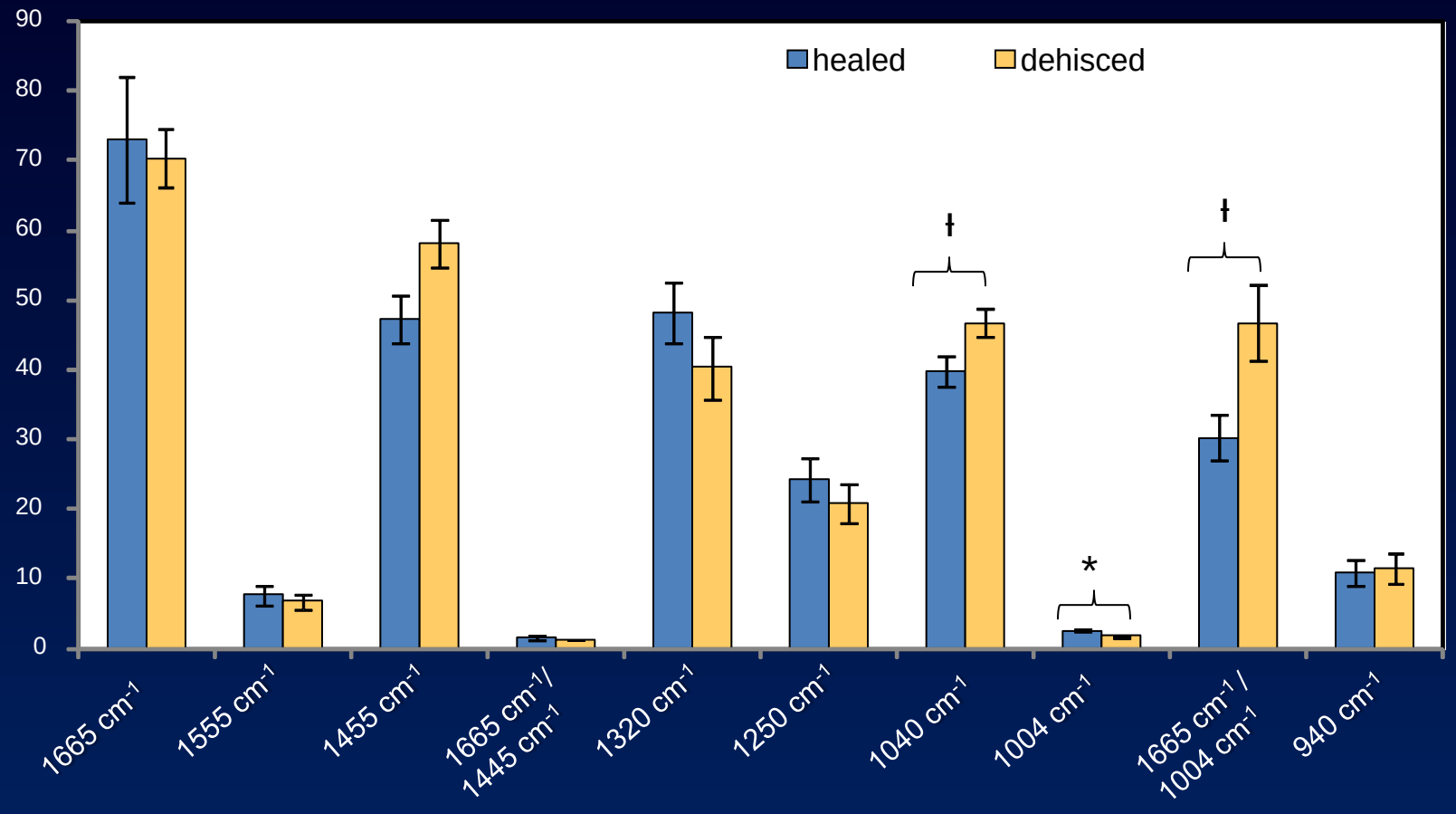

Univariate Analysis of Band Areas

Second Debridement

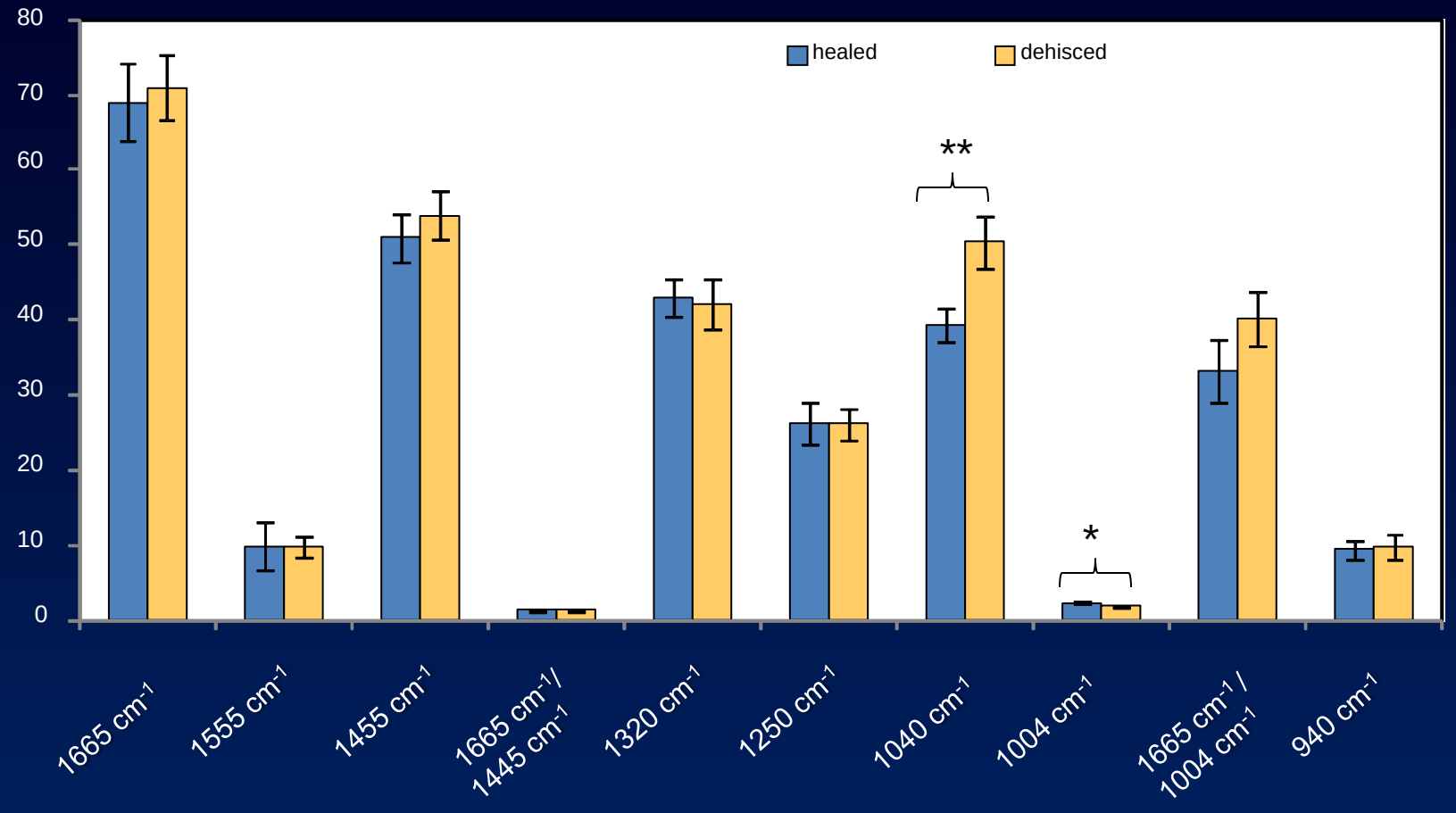

Univariate Analysis of Band Areas

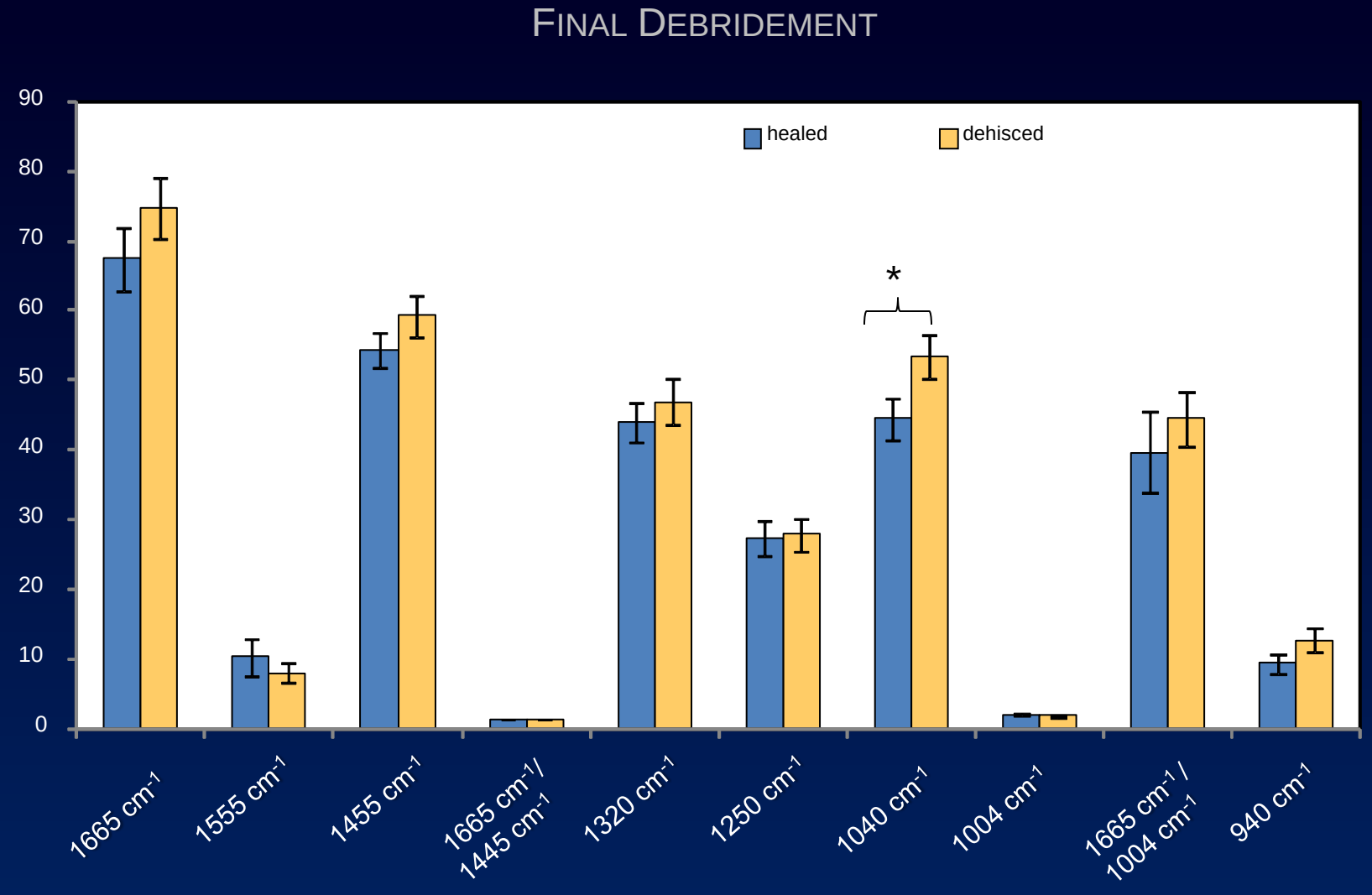

Univariate Analysis of Band Areas

- Based on a univariate analysis, there are only three band areas that differ based on outcome (healed or dehisced) - 1004 cm^{-1}, 1040 cm^{-1}, and the band area ratio 1665/1004 cm^{-1}.

- We can also look for changes in the band area profiles of healed and dehisced wounds over time, i.e. first debridement versus final debridement.

  For wounds that heal, there are no statistically significant difference between calculated band areas chronologically.

  For wounds that dehisce, the band area at 1250 cm^{-1} demonstrates a statistically significant difference between the first and final debridement ($p < 0.03$).

Is this reflective of wound "stability"?

Univariate Analysis of Band Areas: Thresholds

Predicting outcome based on univariate analysis of band areas would misclassify 31% of dehisced wounds and 33% of healed wounds.

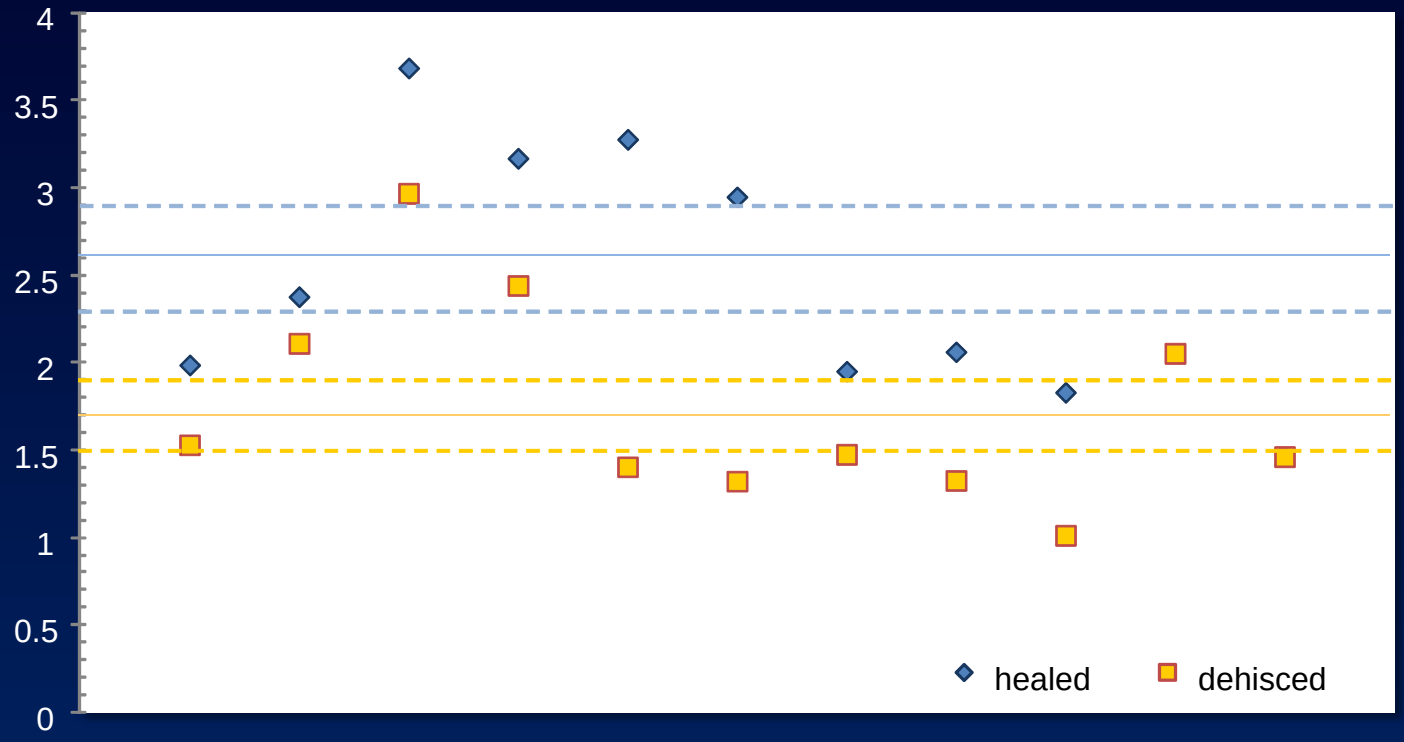

Multivariate Analysis: BBNs

- Bayesian Belief Networks fall under the umbrella of machine learning.

  Input = empirical data ⟶ output = patterns or predictions that are believed to be responsible for generating the data

- Applies the Bayes probabilistic theory for analyzing data sets.

- Bayesian Belief Networks (BBNs) demonstrate probabilistic relationships – relationships in which knowledge of the value of a variable affects the belief about the likelihood of other variables taking certain values.

  - Data mining
  - Prediction

BBN Analysis of Band Areas: Data Mining

Bayesian Belief Network (BBN) machine learning can elucidate some of the relationships between band area changes.

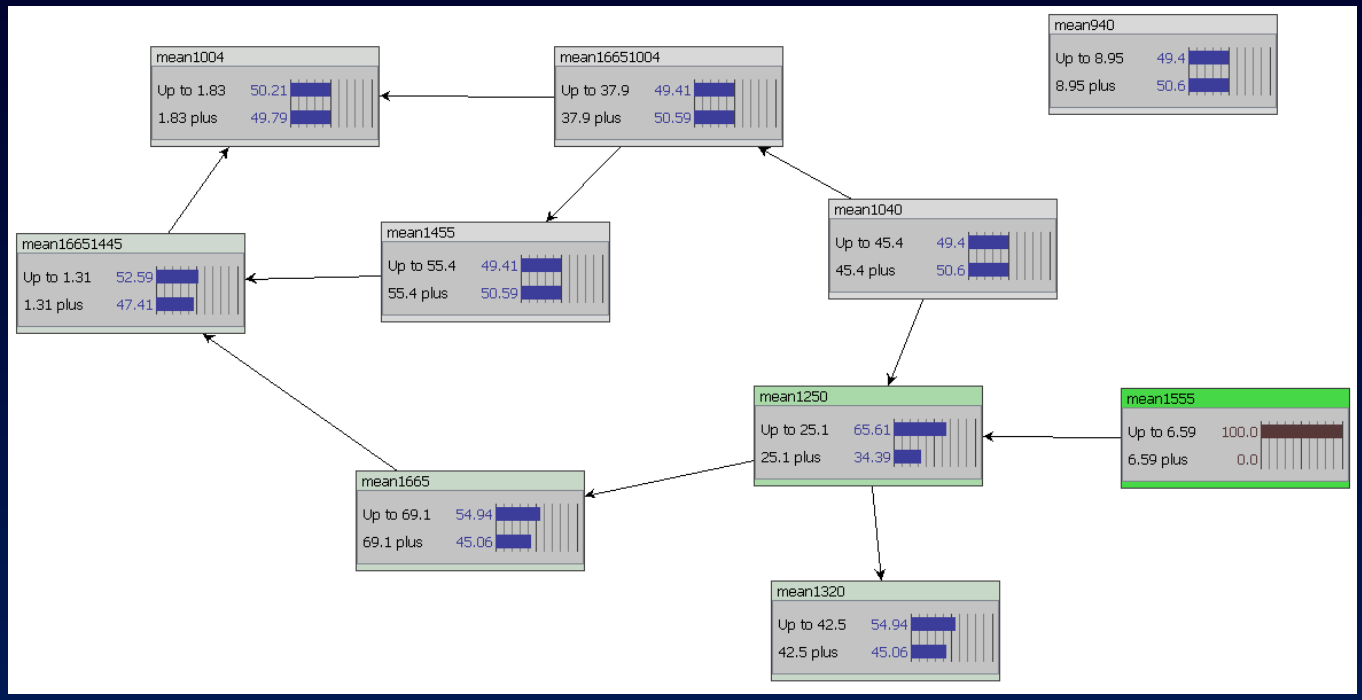

- 1555 cm^{-1} → 1250 cm^{-1} → 1320 cm^{-1} & 1665 cm^{-1} → 1665/1445 cm^{-1} → 1004 cm^{-1}
- 1040 cm^{-1} → 1250 cm^{-1} → 1665/1004 cm^{-1} → 1004 and 1455 cm^{-1} → 1665/1004 cm^{-1}

BBN Analysis of Band Areas: Prediction

A naïve Bayes model for outcome as the target reveals that outcome is largely dependent on mean 1040 cm^{-1} and mean 1455 cm^{-1} band area ratios.

Note, this data set incorporates different collection parameters, operators and regions of the biopsy.

Healed wounds

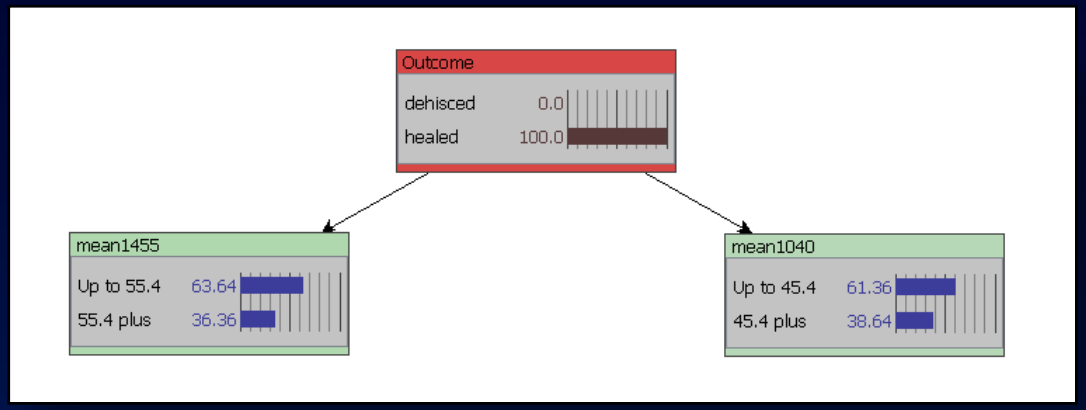

Dehsiced wounds

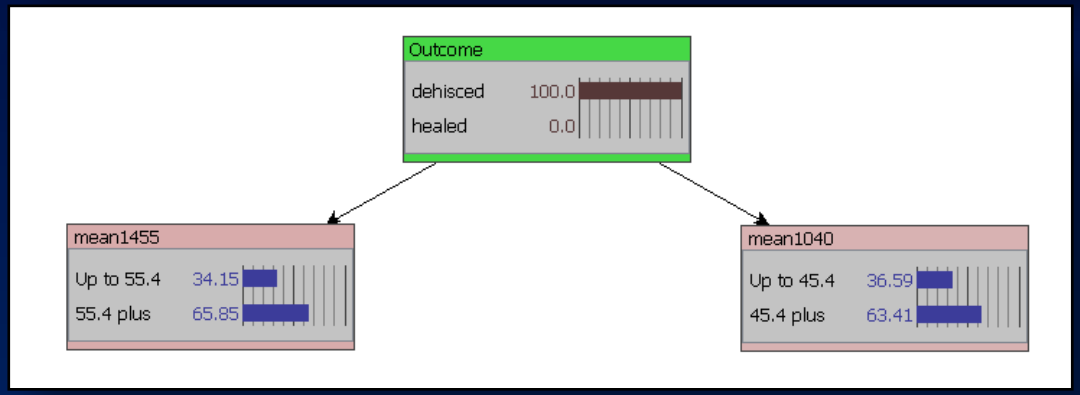

BBN Analysis of Band Areas: Prediction

Here, we generated a naïve Bayes model based on a training data set of all debridements except final debridements and used it to predict the wound healing outcome for final debridements.

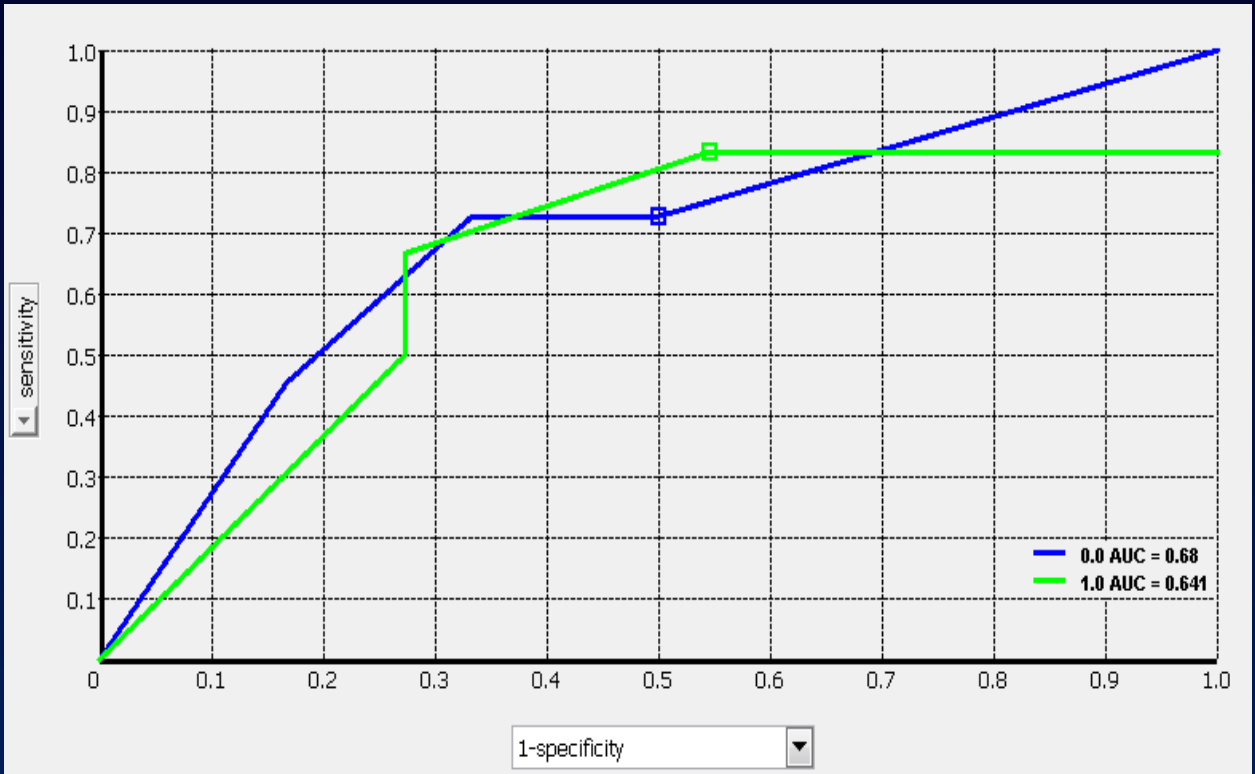

Unfortunately, the accuracy of the prediction model is only *68%* for *normal healing* wounds and *64%* for *dehisced wounds*.

Multivariate Analysis: Support Vector Machine

Supervised classification method based on a non-probabailistic binary linear classifier.

- *assumes that groups are separated by a wide boundaries*
- *places samples in the two classes as far apart as possible*
- *able to handle non-linear data*
- *can be susceptible to overfitting*
- *may perform better on data sets with more examples of training and fewer labels*

Mulitvariate Analysis: Support Vector Machine

Support Vector Machine

Developed a subset of spectra for a training data set (N=61), randomly selected from the whole data set.

Used the entire spectrum with no pre-processing (derivatization, smoothing, normalization).

Actual	Predicted	
	Healed	Dehisced
Healed	36	0
Dehisced	0	25

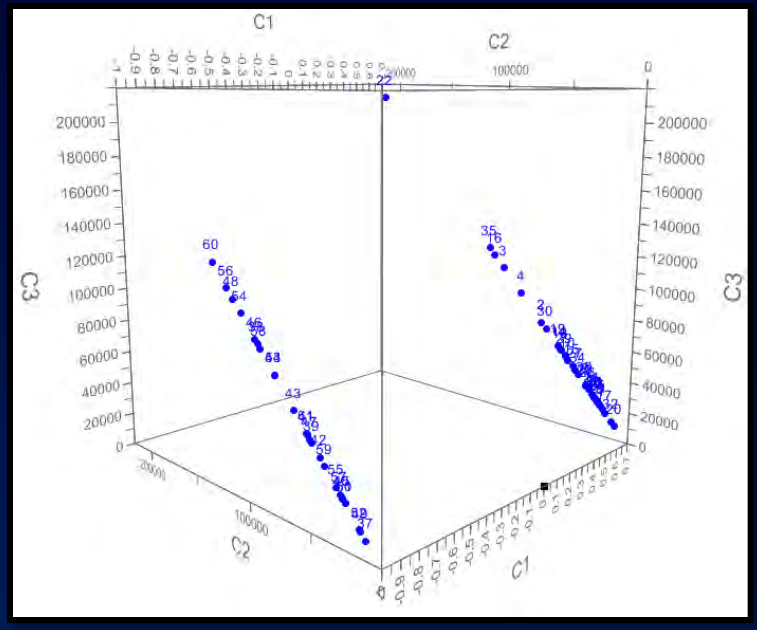

For a test data set (N=20), 80% of the wound spectra were classified correctly as dehisced.

Mulitvariate Analysis: Linear Discriminant Analysis

Supervised classification method based on Bayes' formula.

- *assumes a normal distribution*
- *assumes that the variability between each group has the same structure*
- *uses PCA to reduce dimensionality*
- *places samples in the same class close to one another but samples not in the same class far apart*
- *may perform better than SVM in cases of many labels and little training data*

Mulitvariate Analysis: Linear Discriminant Analysis

Linear Discriminant Analysis

Developed a subset of spectra for a training data set (N=61), randomly selected from the whole data set.

Used the entire spectrum with no pre-processing (derivatization, smoothing, normalization).

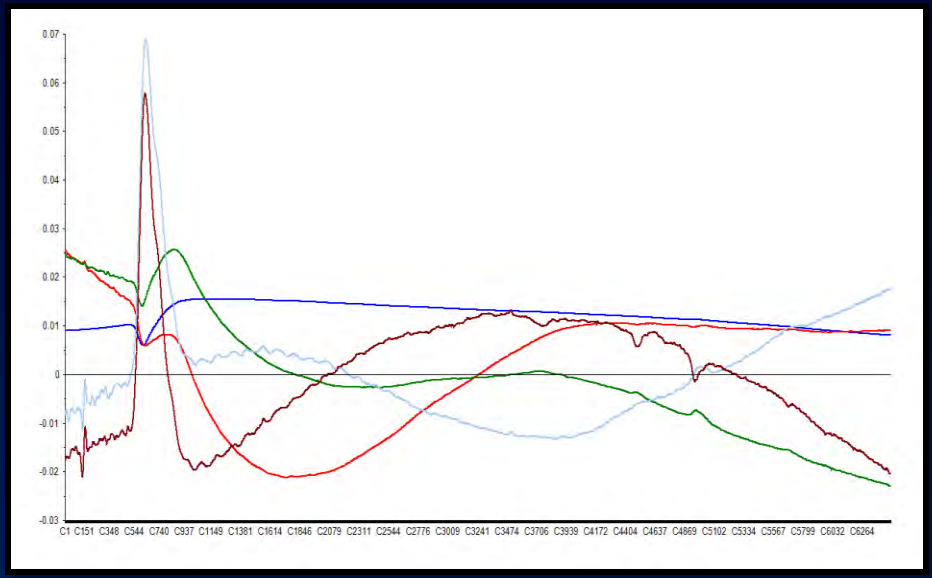

Actual	Predicted	
	Healed	Dehisced
Healed	33	2
Dehisced	3	23

For a test data set (N=20), 90% of the spectra were classified correctly as dehisced.

Which Model to Choose?

- The models shown require significant optimization.
- We need to ensure complete data sets for training (include different acquisition parameters, multiple acquisitions, different instrument operators – i.e. build robustness into our model).
- The final evaluation of the prediction model will require both the highest sensitivity and specificity.
- Preliminary results demonstrate promise for the use of Raman spectroscopy to predict wound outcome.

Ongoing Projects

- Currently, we are continuing to build our biopsy database for Bayesian Belief Network modeling and other multivariate analysis techniques.
- We have over 250 tissue biopsies from over 50 patients, most of which we have collected spectra in triplicate (over 4 years).
- Peak fitting needs to be performed over the entire spectrum to determine which vibrational bands provide optimal sensitivity and specificity. Some regions of the spectrum require a more in depth peak fitting (Amide I and III bands).
- Other aspects of the spectra, such as the fluorescence background, may also provide indications of the status of the tissue overall.

Project Goals

- Determine threshold values (band area ratios, fluorescence background, etc.) that are capable of differentiating normal healing wounds and wounds that are susceptible to dehiscence.

- Validate spectroscopic wound healing prediction models in a military and civilian population.

Acknowledgements

Naval Medical Research Center

Department of Regenerative Medicine

Dr. Jonathan Forsberg
Dr. Trevor Brown
Dr. Doug Tadaki
Tala Ghadimi
Dr. Felipe Lisboa
Stacia Moreno
Frederick Gage
Rajiv Luthra
Maricela Rodriguez

USUHS

Department of Surgery

Dr. Eric Elster

WRNMMC

General Surgery, Orthopaedics and Rehabilitation

http://www.med.navy.mil/sites/nmrc/Pages/ccc_regenmed.htm

Disclaimer

- The multidisciplinary care of these patients would not have been possible without the dedicated efforts of everyone at WRAMC and NNMC. Both civilian and military personnel have rendered skilled and compassionate care for these casualties. All of our efforts are dedicated to those who have been placed in harm's way for the good of our nation.

- The views expressed in this manuscript are those of the authors and do not reflect the official policy of the Department of the Army, Department of the Navy, the Department of Defense or the United States Government.

- This effort was supported (in part) by the U.S. Navy Bureau of Medicine and Surgery under the Medical Development (PE 0604771N) and Office of Naval Research work unit number (602115HP.3720.001.A1015), in part by Army DMRDP grant D10-I-AR-J2-501, and in part by CDMRP PRORP award OR090136.

- This study was approved by the Walter Reed National Military Medical Center Institutional Review Board in compliance with all Federal regulations governing the protection of human subjects.

Profiling wound healing with wound effluent: Raman spectroscopic indicators of infection

Nicole J. Crane*[a], Eric A. Elster[a,b,c]

[a]Department of Regenerative Medicine, Operational and Undersea Medicine Directorate, Naval Medical Research Center, Silver Spring, Maryland
[b]Department of Surgery, Uniformed Services University of Health Sciences, Bethesda, Maryland
[c]Department of Surgery, Walter Reed National Military Medical Center, Bethesda, Maryland

ABSTRACT

The care of modern traumatic war wounds remains a significant challenge for clinicians. Many of the extremity wounds inflicted during Operation Enduring Freedom and Operation Iraqi Freedom are colonized or infected with multi-drug resistant organisms, particularly *Acinetobacter baumannii*. Biofilm formation and resistance to current treatments can significantly confound the wound healing process. Accurate strain identification and targeted drug administration for the treatment of wound bioburden has become a priority for combat casualty care. In this study, we use vibrational spectroscopy to examine wound exudates for bacterial load. Inherent chemical differences in different bacterial species and strains make possible the high specificity of vibrational spectroscopy.

Keywords: combat wounds; wound effluent; Raman spectroscopy; bacteria; Acinetobacter baumannii

1. INTRODUCTION

Infections are common complications of combat wounds and affect not only quality of life but also wound outcome (healing or non-healing). At the beginning of the twentieth century, improvements in military hygiene and disease control significantly reduced the number of war-time deaths due to pestilence.[1] While deaths from "war-time" pestilence are not common in recent conflicts such as Operation Iraqi Freedom (OIF) and Operation Enduring Freedom (OEF), infection control of multi-drug resistant organisms such as *Acinetobacter*, *Klebsiella*, and *Pseudomonas* has presented a challenge.[2] *Acinetobacter* isolates were the most predominant microorganisms found in a recent study of combat wounds, accounting for over 60% of all bacterial isolates.[3] Multi-drug resistant *Acinetobacter* infections can be problematic due to the small number of effective drugs for treatment – carbapenems and tigecycline.[4] Thus, accurate identification of the species and strain of the infecting organism becomes important. Currently, we are evaluating wound effluent from combat-wounded soldiers for bacterial and correlating wound colonization to wound outcome.

Wound effluent is the fluid that is exudated from the wound during the wound healing process. The composition of wound effluent changes over the course of wound healing and is a complex milieu of blood, plasma, cells, immunoglobulins, other various proteins such as enzymes, cytokines and chemokines, and bacteria, in the case of infection. In a previous study, Brown and coworkers have shown that inflammatory cytokine and chemokine profiles extracted from wound effluent are associated with the extent of wound colonization.[5] In this study, we explore the use of Raman spectroscopy to probe wound effluent for bacterial infection.

Raman spectroscopy is a molecularly specific technique that is capable of probing samples noninvasively and nondestructively. It has been used to assess tissues at the molecular level with diverse clinical and diagnostic applications to include the analysis of cellular structure and the determination of tumor grade and type.[6-22] This makes Raman spectroscopy an ideal technology for evaluating wound effluent, particularly for detecting bioburden. There have been numerous Raman spectroscopic studies of microorganisms, many focusing on rapid identification

of the microorganisms.[23-31] By creating a Raman spectral database of microorganisms, it is possible to identify bacteria at the strain level. We hypothesized that Raman spectroscopy could evaluate bioburden in wound effluent and differentiate strains of the same species of bacteria, namely *Acinetobacte baumannii*.

2. MATERIALS AND METHODS

2.1 Clinical Studies and Sample Collection

The clinical studies were approved by the institutional review boards of the National Naval Medical Center (NNMC) and the Walter Reed Army Medical Center (WRAMC). All study participants were recruited from wounded Operation Iraqi Freedom and Operation Enduring Freedom U.S. service members evacuated to the National Capital Area. Informed consent was obtained from all participating patients.

For the treatment of combat wounds, surgical debridement and pulse lavage were performed in the operating room every 48-72 hours until definitive wound closure or coverage. Negative pressure wound therapy (NPWT) was applied to the wounds between surgical debridements, as per current standard practice at NNMC and WRAMC.[32] All wounds were examined once daily following wound closure or coverage until the sutures were removed. All patients were followed clinically for 30 days. Wound effluent was collected from the NPWT canister (without gel pack; Kinetic Concepts, Inc., San Antonio, TX) two hours following the first surgical debridement and over a 12 hour period prior to each subsequent wound debridement. Samples were stored at 4ºC prior to spectral acquisition.

2.2 Culturing *Acinetobacter baumannii*

Thirty Acinetobacter baumannii isolates were streaked onto lysogeny broth agar (LBA) plates and placed in a 37ºC incubator. After approximately three days of growth, at least 10 μL of each isolate was available for analysis by Raman spectroscopy. Additionally, microorganisms were cultured from the wound effluent itself by plating 50-100 μL of effluent onto a blood agar plate. Bacteria counts are reported as CFU/mL by plate.

2.3 Raman Spectroscopy

Raman spectra of reference standards (plasma, whole blood, cells, bacteria and immunoglobulin G) were transferred to an aluminum foil covered weighing dish for spectral acquisition. Uncentrifuged, unfiltered wound effluent samples were placed in a 1 cm^3 quartz cuvette for spectral acquisition. Bacterial isolates were transferred to an aluminum foil covered weighing dish with a 10 μL inoculating loop for spectral acquisition. A 785 nm Raman PhAT system (Kaiser Optical Systems, Inc., Ann Arbor, MI) was used to collect spectra of the effluent and bacteria. Final spectra were the accumulation of twenty 5 second spectra (for bacteria) and thirty 5 second spectra (for effluent), acquired using the 3 mm spot size. For some bacteria isolates, fluorescence signal overwhelmed the Raman scatter. To reduce the fluorescence, the bacteria isolates were transferred to a 0.5 mL centrifuge vial and rinsed with deionized water. The vial was then centrifuged at 10,000 rpm for 5 minutes. The bacteria isolates were transferred back to the weighing dish for spectral acquisition. The rinsing process was repeated until fluorescence reduction was appreciable.

2.5 Data Analysis

For the effluent samples, all spectral preprocessing was performed in GRAMS/AI software (Thermo Fisher Scientific, Madison, WI). Raman spectra were truncated to 1800-400 cm^{-1} and baseline corrected with a sixth degree polynomial. For effluent samples, spectral subtraction of blood was performed if spectral interference of blood was noted.

Hierarchical clustering of *Acinetobacter baumannii* isolates was performed in Unscrambler X 10.1 software (CAMO Software, Woodbridge Township, NJ). Prior to classification, spectra were transformed with a first derivative function (5^{th} order, 13 points) and truncated to 930-1080 cm^{-1}.

3. RESULTS

3.1 Wound Effluent

The spectral profiles of wound effluent components are displayed in Figure 1 – plasma, whole blood, human mesenchymal stem cells, bacteria and immunoglobulin G, respectively.

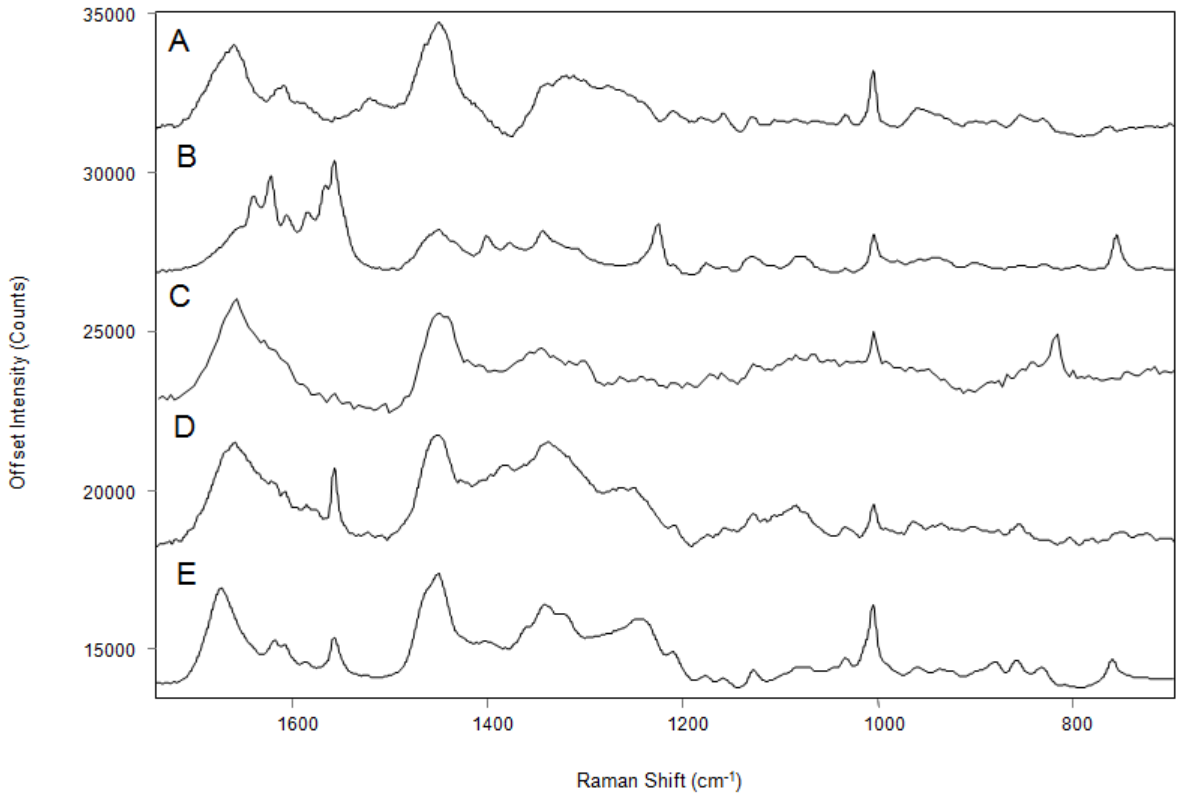

Figure 1. Spectral comparison of Raman spectra of wound effluent components – A) plasma, B) whole blood, C) cells, D) bacteria, and E) immunoglobulin G.

Major bands exhibited in the spectra 1665 cm^{-1} (amide I), 1620 cm^{-1} ($_{\nu}C=C$), 1557 cm^{-1} ($_{\nu}C$-C ring stretching), 1450 cm^{-1} (CH_2 scissoring), 1340 cm^{-1} ($_{\delta}CH_2$), 1270 cm^{-1} (amide III), 1245 cm^{-1} (amide III), 1070-1080 cm^{-1} (C-O stretch), and 1004 cm^{-1} ($_{\nu}$C-C aromatic ring). [25, 33-40] In plasma and whole blood, bands at 1620 $cm^{-1}$and 1557 cm^{-1}, are particularly prominent. In plasma and whole blood, these bands can be attributed to hemoglobin. Only the cell and bacteria spectra in Figures 1C and 1D exhibit a significant, broad band at 1070 cm^{-1}; this band confirms the presence of nucleic acids. While there is a significant amount of overlap in some of the spectra, each demonstrates uniqueness when examined as a whole.

Some of these spectral features are clearly present in the spectrum of fresh wound effluent (Figure 2A), namely whole blood. After the Raman spectrum of whole blood is subtracted from the Raman spectrum of effluent, the resulting spectrum (Figure 2B) shares spectral features with both *Acinetobacter baumannii* (Figure 2C) and cells Figure 2D), but most closely resembles the Raman spectrum of the bacteria. Additionally, the Raman spectrum of effluent can be used to monitor the amount of cellular matter (human or bacteria) throughout the course of treatment for the wounded warriors. Figure 3 shows the Raman spectra of wound effluent collected from the same patient at the fifth, sixth, seventh, and eighth surgical debridements. Evidence of cellular matter is apparent in debridements five through seven (Figures 3A-C), as denoted by the presence of the 1450 cm^{-1}, 1240 cm^{-1}, and 1004 cm^{-1} bands,

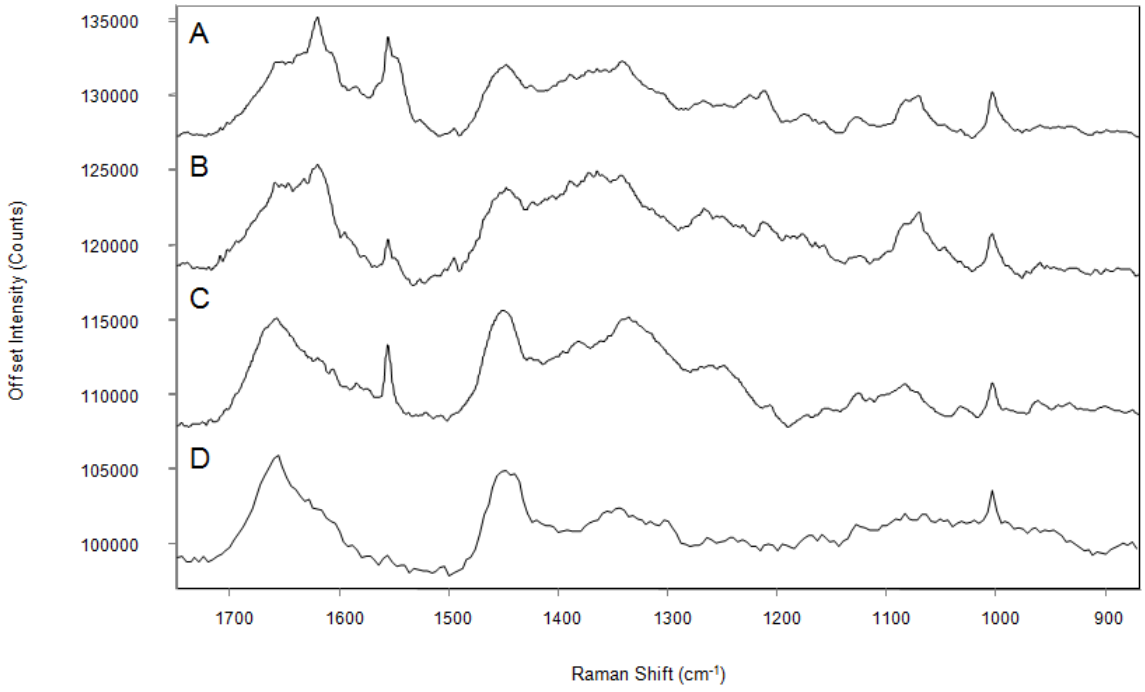

Figure 2. Raman spectrum of wound effluent before (A) and after subtracting whole blood from the spectrum (B). The resulting spectrum is compared to *Acinetobacter baumannii* (C) and cells (D).

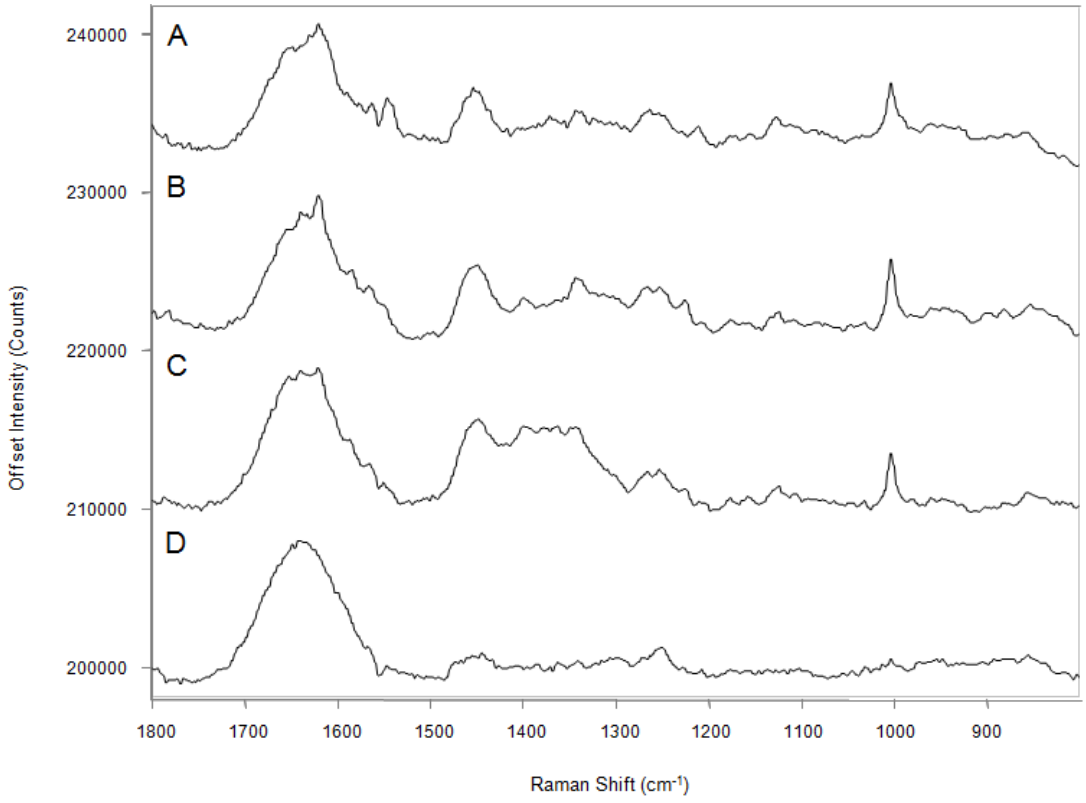

Figure 3. Raman spectra of wound effluent collected from the same wound after the fifth (A), sixth (B), seventh (C), and eighth (D) debridement.

but becomes drastically reduced by the eighth debridement (Figure 3D). Bacteria counts for these samples also decrease with time (3.5×10^5 CFU/mL, 2.1×10^3 CFU/mL, and 2.0×10^3 CFU/mL for the fifth, sixth, and eighth debridements respectively).

3.2 *Acinetobacter baumannii* Isolates

We also used Raman spectroscopy to profile thirty isolates of *Acinetobacter baumannii*. Hierarchical clustering was used to delineate the spectral relationships between the different strains of *Acinetobacter baumannii* (Figure 4), specifically Spearman's rank hierarchical clustering with complete linkage over the wavelength range of 930-1080 cm^{-1}. Apa1 digestion (restriction enzyme digestion of DNA) and optical mapping (high-resolution restriction maps from single, stained molecules of DNA) were also performed on the isolates (data not shown) and subjected to hierarchical clustering.

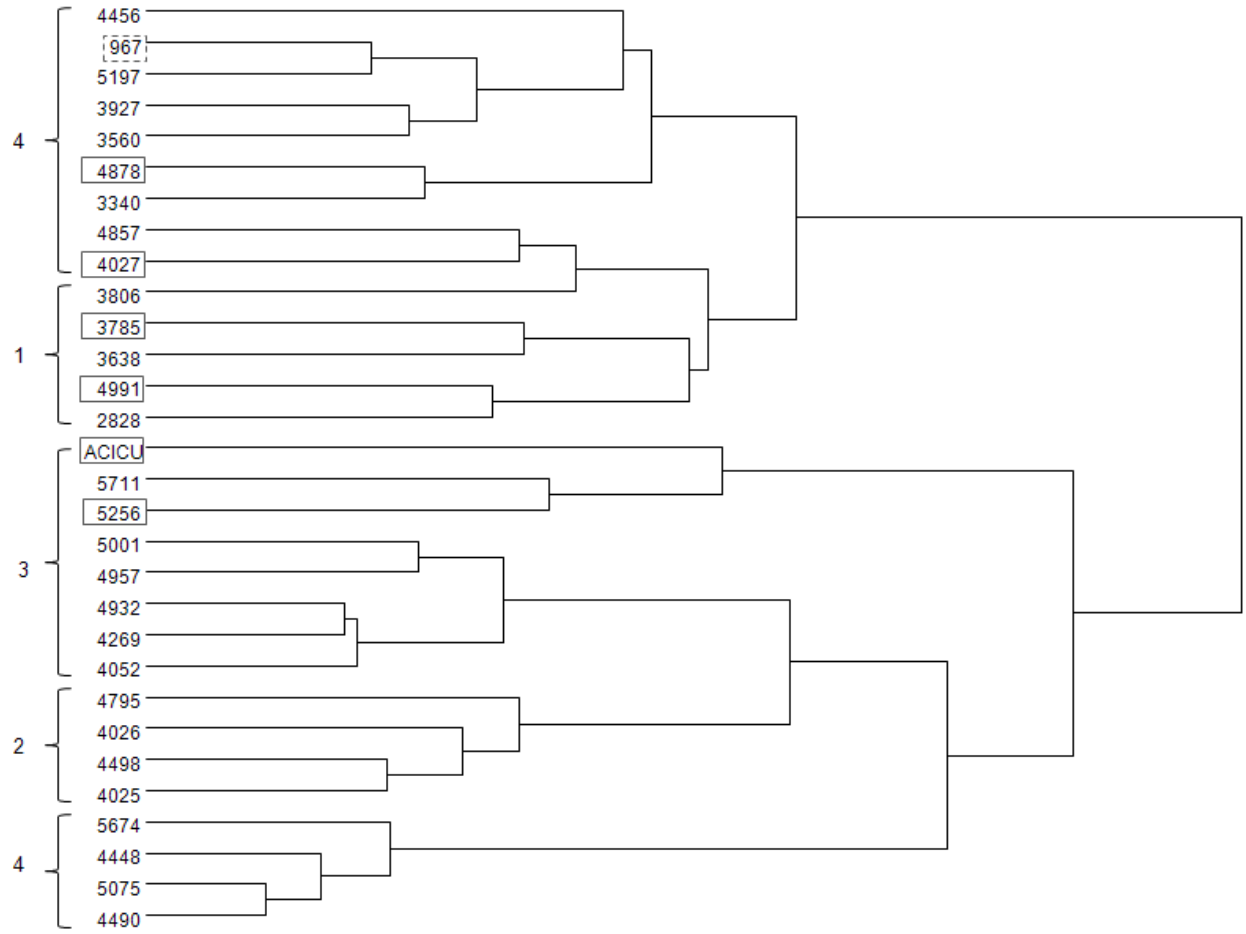

Figure 4. Hierarchical clustering of 30 *Acinetobacter baumannii* isolates into subgroups of strains. Boxes highlight strains that were misclassified according to optical mapping and/or Apa1 digest data.

Clustering by optical mapping and Apa1 digestion were compared to the results of the Raman spectral clustering. Genetically determined subgroup assignments are indicated by the numbers to the left of the brackets, while gray boxes indicate the strains that did not classify correctly according to Apa1 digestion and optical mapping. Hierarchical clustering of the Raman spectra correctly classified 77% of the thirty isolates examined. Performance of the classification technique could potentially be improved with alternate spectral preprocessing and additional spectral region optimization.

4. DISCUSSION

Current microbiological methods use culture from tissue homogenate or from wound fluid directly to determine the species of bacteria present as well as to quantify the bacteria present. At the time of wounding, or the inoculation event, 100% of wounds are contaminated. Not long after inoculation wounds become colonized, though not all microorganisms are harmful to the host. The signs of infection can be obvious is a healthy patient, but may be less conspicuous in a sick patient. Some combat wounded soldiers suffer from an exaggerated inflammatory response, similar to that observed in acutely ill states like sepsis.[32] This exposes some noncosomial bacteria like *Acinetobacter baumannii* with the perfect opportunity for infection. Previously, critical wound colonization has been correlated with the inflammatory cytokine and chemokine profiles of combat-wounded soldiers.[5] There has been some controversy over the culture methodology used for bacterial quantification, though some schools of thought believe that timing of the timing of sampling is more critical than the sampling itself. Current methodologies require 24-48 hours for results from microbial tests. Raman spectroscopy, a noninvasive and nondestructive technique, holds promise for the development of faster microbial testing.

In this preliminary study, Raman spectroscopic profiling of wound effluent during wound surgical debridements demonstrates a decrease in bands associated with cellular material, notably 1450 cm^{-1}, 1240 cm^{-1}, and 1004 cm^{-1}; these changes in the spectral profile of the wound effluent are possibly indicative of reduced bacterial load over the course of wound healing. In addition, Raman spectroscopy was able to correctly classify 77% of thirty *Acinetobacter baumannii* isolates into their respective strain subgroups. These results corroborate genetic mapping data performed on the same *Acinetobacter baumannii* isolates. Thus, it is conceivable that the Raman spectrum collected from the wound effluent itself could be compared to Raman spectra of bacterial isolates for identification. This kind of rapid assessment may eventually help to direct antibiotic therapy and prevent over- or under-treatment of bacterial infection.

We have demonstrated that Raman spectroscopy can be utilized to examine wound effluent, in addition to bacterial isolates. One advantage of Raman spectroscopy is that it can be employed in a non-invasive manner, such as a fiber probe-coupled system. It is possible to incorporate such a Raman spectroscopic system into the operating room. For microbial studies, however, a microscope coupled Raman system will allow for probing of smaller sample sizes, such as single colonies of bacteria.

5. CONCLUSIONS

This study demonstrates the potential of vibrational spectroscopy as a technique capable of affording an objective measurement regarding wound effluent colonization. Such a capability could allow for real-time point of care analysis of wounds, allowing subjective decisions to be supplanted by objective data. This is a critical need as constraints on medical education reduce clinical exposure and decision-making is moved from the subjective arena to personalized, data driven decisions. The use of such methodologies as presented herein, may allow for evaluation of wound bioburden in a shorter time frame than is currently possible. We need to expand the scope of our study to a larger patient population and a more diverse microbial to better delineate Raman spectroscopic trends to develop a classification model for wound infection.

6. ACKNOWLEDGEMENTS

The authors would like to thank Tala Ghadimi and Felipe Lisboa for the collection of effluent samples examined in these studies. The authors would also like to thank Dr. Daniel Zurawski for providing the reference bacterial strains and subsequent microbial analysis presented in this study. This work was prepared as part of the authors' official duties. Title 17 U.S.C. §105 provides that 'Copyright protection under this title is not available for any work of the United States Government.' Title 17 U.S.C. §101 defines a U.S. Government work as a work prepared by a military service member or employee of the U.S. Government as part of that person's official duties. The views expressed in this article are those of the author and do not necessarily reflect the official policy or position of the Department of the Navy, Department of Defense, nor the U.S. Government. This work was supported by funded by work unit number 602115HP.3720.001.A1015. This study was approved by the National Naval Medical Center Institutional

Review Board (protocol NNMC.2005.069) in compliance with all Federal regulations governing the protection of human subjects. I/We certify that all individuals who qualify as authors have been listed; each has participated in the conception and design of this work, the analysis of data (when applicable), the writing of the document, and the approval of the submission of this version; that the document represents valid work; that if we used information derived from another source, we obtained all necessary approvals to use it and made appropriate acknowledgements in the document; and that each takes public responsibility for it.

7. REFERENCES

[1] C. K. Murray, M. K. Hinkle, and H. C. Yun, "History of infections associated with combat-related injuries," J Trauma, 64(3 Suppl), S221-31 (2008).

[2] D. R. Hospenthal, and H. K. Crouch, "Infection control challenges in deployed US military treatment facilities," J Trauma, 66(4 Suppl), S120-8 (2009).

[3] F. R. Sheppard, P. Keiser, D. W. Craft *et al.*, "The majority of US combat casualty soft-tissue wounds are not infected or colonized upon arrival or during treatment at a continental US military medical facility," Am J Surg, 200(4), 489-95 (2010).

[4] X. Bertrand, and M. J. Dowzicky, "Antimicrobial Susceptibility Among Gram-Negative Isolates Collected From Intensive Care Units in North America, Europe, the Asia-Pacific Rim, Latin America, the Middle East, and Africa Between 2004 and 2009 as Part of the Tigecycline Evaluation and Surveillance Trial," Clin Ther, in press (2011).

[5] T. S. Brown, H. J. S., F. R. Sheppard *et al.*, "Inflammatory response is associated with critical colonization in combat wounds," Surg Infect, 12(5), 351-357 (2011).

[6] H. Wills, R. Kast, C. Stewart *et al.*, "Raman spectroscopy detects and distinguishes neuroblastoma and related tissues in fresh and (banked) frozen specimens," J Pediatr Surg, 44(2), 386-91 (2009).

[7] T. J. Harvey, E. C. Faria, A. Henderson *et al.*, "Spectral discrimination of live prostate and bladder cancer cell lines using Raman optical tweezers," J Biomed Opt, 13(6), 064004 (2008).

[8] P. O. Andrade, R. A. Bitar, K. Yassoyama *et al.*, "Study of normal colorectal tissue by FT-Raman spectroscopy," Anal Bioanal Chem, 387(5), 1643-8 (2007).

[9] H. P. Buschman, G. Deinum, J. T. Motz *et al.*, "Raman microspectroscopy of human coronary atherosclerosis: biochemical assessment of cellular and extracellular morphologic structures in situ," Cardiovascul Pathol, 10, 69-82 (2001).

[10] A. Carden, R. M. Rajachar, M. D. Morris *et al.*, "Ultrastructural changes accompanying the mechanical deformation of bone tissue: a Raman imaging study," Calcified Tissue International, 72, 166-175 (2003).

[11] K. L. Chan, G. Zhang, M. Tomic-Canic *et al.*, "A Coordinated Approach to Cutaneous Wound Healing: Vibrational Microscopy and Molecular Biology," J Cell Mol Med, 12(5B), 2145-2154 (2008).

[12] M. V. Chowdary, K. K. Kumar, K. Thakur *et al.*, "Discrimination of normal and malignant mucosal tissues of the colon by Raman spectroscopy," Photomed Laser Surg, 25(4), 269-74 (2007).

[13] N. J. Crane, V. Popescu, M. D. Morris *et al.*, "Raman spectroscopic evidence for octacalcium phosphate and other transient mineral species deposited during intramembraneous mineralization," Bone, 39, 434-442 (2006).

[14] A. S. Haka, Z. Volynskaya, J. A. Gardecki *et al.*, "In vivo margin assessment during partial mastectomy breast surgery using raman spectroscopy," Cancer Res, 66(6), 3317-22 (2006).

[15] P. R. Jess, D. D. Smith, M. Mazilu *et al.*, "Early detection of cervical neoplasia by Raman spectroscopy," Int J Cancer, 121(12), 2723-8 (2007).

[16] S. Koljenovic, T. C. Schut, R. Wolthuis *et al.*, "Raman spectroscopic characterization of porcine brain tissue using a single fiber-optic probe," Anal Chem, 79(2), 557-64 (2007).

[17] G. Leroy, G. Penel, N. Leroy *et al.*, "Human tooth ename: a Raman polarized approach," Appl Spectrosc, 56(8), 1030-1034 (2002).

[18] N. McGill, P. A. Dieppe, M. Bowden *et al.*, "Identification of pathological mineral deposits by Raman microscopy," The Lancet, 337, 77-78 (1991).

[19] A. Robichaux-Viehoever, E. Kanter, H. Shappell *et al.*, "Characterization of Raman spectra measured in vivo for the detection of cervical dysplasia," Appl Spectrosc, 61(9), 986-93 (2007).

[20] G. Shetty, C. Kendall, N. Shepherd *et al.*, "Raman spectroscopy: elucidation of biochemical changes in carcinogenesis of oesophagus," Br J Cancer, 94(10), 1460-4 (2006).

[21] M. G. Shim, B. C. Wilson, E. Marple *et al.*, "Study of fiber-optic orobes for *in vivo* medical Raman spectroscopy," Applied Spectroscopy, 53(6), 619-627 (1999).
[22] T. D. Wang, and J. Van Dam, "Optical biopsy: a new frontier in endoscopic detection and diagnosis," Clin Gastroenterol Hepatol, 2(9), 744-53 (2004).
[23] P. C. Buijtels, H. F. Willemse-Erix, P. L. Petit *et al.*, "Rapid identification of mycobacteria by Raman spectroscopy," J Clin Microbiol, 46(3), 961-5 (2008).
[24] M. F. Escoriza, J. M. VanBriesen, S. Stewart *et al.*, "Raman spectroscopy and chemical imaging for quantification of filtered waterborne bacteria," J Microbiol Methods, 66(1), 63-72 (2006).
[25] K. Maquelin, C. Kirschner, L. P. Choo-Smith *et al.*, "Identification of medically relevant microorganisms by vibrational spectroscopy," J Microbiol Methods, 51(3), 255-71 (2002).
[26] Q. Wu, W. H. Nelson, S. Elliot *et al.*, "Intensities of E. coli nucleic acid Raman spectra excited selectively from whole cells with 251-nm light," Anal Chem, 72(13), 2981-6 (2000).
[27] L. Zeiri, B. V. Bronk, Y. Shabtai *et al.*, "Surface-enhanced Raman spectroscopy as a tool for probing specific biochemical components in bacteria," Appl Spectrosc, 58(1), 33-40 (2004).
[28] K. Maquelin, L. Dijkshoorn, T. J. van der Reijden *et al.*, "Rapid epidemiological analysis of Acinetobacter strains by Raman spectroscopy," J Microbiol Methods, 64(1), 126-31 (2006).
[29] K. Maquelin, L. P. Choo-Smith, T. van Vreeswijk *et al.*, "Raman spectroscopic method for identification of clinically relevant microorganisms growing on solid culture medium," Anal Chem, 72(1), 12-9 (2000).
[30] K. S. Kalasinsky, T. Hadfield, A. A. Shea *et al.*, "Raman chemical imaging spectroscopy reagentless detection and identification of pathogens: signature development and evaluation," Anal Chem, 79(7), 2658-73 (2007).
[31] L. Zeiri, B. V. Bronk, Y. Shabtai *et al.*, "Silver metal induced surface enhanced Raman of bacteria," Colloids and Surfaces A: Physicochemical and Engineering Aspects, 208, 357-362 (2002).
[32] J. S. Hawksworth, A. Stojadinovic, F. A. Gage *et al.*, "Inflammatory biomarkers in combat wound healing," Ann Surg, 250(6), 1002-7 (2009).
[33] B. R. Wood, and D. McNaughton, "Raman excitation wavelength investigation of single red blood cells in vivo," J Raman Spectrosc, 33(7), 517-523 (2002).
[34] S. U. Sane, S. M. Cramer, and T. M. Przybycien, "A holistic approach to protein secondary structure characterization using amide I band Raman spectroscopy," Anal Biochem, 269(2), 255-72 (1999).
[35] J. L. Lippert, D. Tyminski, and P. J. Desmeules, "Determination of the secondary structure of proteins by laser Raman spectroscopy," J Am Chem Soc, 98(22), 7075-80 (1976).
[36] N. C. Maiti, M. M. Apetri, M. G. Zagorski *et al.*, "Raman spectroscopic characterization of secondary structure in natively unfolded proteins: alpha-synuclein," J Am Chem Soc, 126(8), 2399-408 (2004).
[37] M. Pezolet, M. Pigeon, D. Menard *et al.*, "Raman spectroscopy of cytoplasmic muscle fiber proteins. Orientational order," Biophys J, 53(3), 319-25 (1988).
[38] J. Wohlrab, A. Vollmann, S. Wartewig *et al.*, "Noninvasive characterization of human stratum corneum of undiseased skin of patients with atopic dermatitis and psoriasis as studied by Fourier transform Raman spectroscopy," Biopolymers, 62(3), 141-6 (2001).
[39] B. G. Frushour, and J. L. Koenig, "Raman scattering of collagen, gelatin, and elastin," Biopolymers, 14, 379-391 (1975).
[40] L. Chrit, C. Hadjur, S. Morel *et al.*, "In vivo chemical investigation of human skin using a confocal Raman fiber optic microprobe," J Biomed Opt, 10(4), 44007 (2005).

Journal of Biomedical Optics

SPIEDigitalLibrary.org/jbo

Vibrational spectroscopy: a tool being developed for the noninvasive monitoring of wound healing

Nicole J. Crane
Eric A. Elster

Vibrational spectroscopy: a tool being developed for the noninvasive monitoring of wound healing

Nicole J. Crane[a] and Eric A. Elster[a,b,c]
[a]Naval Medical Research Center, Department of Regenerative Medicine, Silver Spring, Maryland 20910
[b]Walter Reed National Military Medical Center, Department of Surgery, Bethesda, Maryland 20892
[c]Uniformed Services University of the Health Sciences, Department of Surgery, Bethesda, Maryland 20892

Abstract. Wound care and management accounted for over 1.8 million hospital discharges in 2009. The complex nature of wound physiology involves hundreds of overlapping processes that we have only begun to understand over the past three decades. The management of wounds remains a significant challenge for inexperienced clinicians. The ensuing inflammatory response ultimately dictates the pace of wound healing and tissue regeneration. Consequently, the eventual timing of wound closure or definitive coverage is often subjective. Some wounds fail to close, or dehisce, despite the use and application of novel wound-specific treatment modalities. An understanding of the molecular environment of acute and chronic wounds throughout the wound-healing process can provide valuable insight into the mechanisms associated with the patient's outcome. Pathologic alterations of wounds are accompanied by fundamental changes in the molecular environment that can be analyzed by vibrational spectroscopy. Vibrational spectroscopy, specifically Raman and Fourier transform infrared spectroscopy, offers the capability to accurately detect and identify the various molecules that compose the extracellular matrix during wound healing in their native state. The identified changes might provide the objective markers of wound healing, which can then be integrated with clinical characteristics to guide the management of wounds. [DOI: 10.1117/1.JBO.17.1.010902]

Keywords: wound healing; acute wounds; chronic wounds; combat wounds; Raman spectroscopy; Fourier transform infrared spectroscopy.

Paper 11485V received Sep. 6, 2011; revised manuscript received Nov. 29, 2011; accepted for publication Nov. 30, 2011; published online Jan. 25, 2012.

1 Introduction

There is no healthcare specialty that is free from the morbidity and costs of wound development in a patient. In 2009, U.S. hospitals discharged over 1,300,000 patients with chronic wounds and more than 547,000 with traumatic wounds (classified as >10% body surface area burn or open wound).[1] U.S. healthcare costs related to wound treatment are well over $20 billion yearly, and the impact of wound healing on these expenditures is extensive.[2] In addition, if every surgical procedure is considered a case of an acute wound, the significance of wound healing is simply tremendous.

Although the wound-healing process of acute wounds such as surgical incisions is fairly well understood, the modified wound-healing process encountered in patients with chronic wounds and some traumatic acute wounds still requires elucidation. Normal healing of an acute wound is directed by a cascade of growth factors and cell signaling that allows the wounds to repair quickly. Chronic wounds and some traumatic acute wounds are much slower to heal and behave differently for several underlying reasons. There may be a pathologic process such as infection that prevents the wound from healing normally. Additionally, wound healing may be complicated by a prolonged inflammatory phase that inhibits normal levels of chemical mediators and cell recruitment. Finally, the patient's general condition contributes to the rate of wound healing; malnutrition and comorbidities such as diabetes are associated with impaired wound healing.[3]

Improved objective assessment of wounds would be conducive to better treatment of them, which might result in faster healing times, decreased infection rates, and decreased local and systemic complications of injury. For instance, if visits to the operating room were reduced by one instance per patient for 140 patients at one hospital, the cost savings would be over $2 million. The eventual timing of wound closure is often subjective, and there exists a need for an objective evaluation of the molecular environment of wounds throughout the wound-healing process. The use of vibrational spectroscopy and imaging for increased diagnostic accuracy and better wound treatment can produce improved clinical outcomes and decreased patient morbidity, resulting in an earlier return to an improved quality of life.

2 Wound Pathophysiology and the Process of Wound Healing

Several parameters are used to classify wounds: the layers of tissue involved, the origin and duration of the wound, and the type of wound closure used (i.e., surgical closure with sutures or formation of scar tissue). Origin and duration dictate whether a wound is classified as chronic or acute. Wounds resulting from trauma or surgery are acute wounds and generally proceed normally through the wound-healing process. An incision site in the abdomen, a third-degree burn, or a crushed limb

Address all correspondence to: Nicole J. Crane, Naval Medical Research Center, Department of Regenerative Medicine, Silver Spring, Maryland 20910. Tel: 301 319 7304; E-mail: Nicole.Crane@med.navy.mil

0091-3286/2012/$25.00 © 2012 SPIE

is termed an "acute wound." Wounds arising from chronic inflammation, repetitive insult, or vascular compromise that fail to heal normally or in a timely manner are called "chronic wounds." Pressure ulcers and diabetic foot ulcers are examples of chronic wounds. Acute wounds generally begin with a single, abrupt insult and progress through the healing process in an orderly manner. Conversely, chronic wounds are usually caused by a pathologic process such as infection or poor circulation.

In general, the wound-healing process proceeds through regeneration and/or repair. "Wound regeneration" is the renewal of the damaged tissue with healthy tissue that is the same, whereas "wound repair" is the replacement of the damaged tissue by scar tissue. Wounds that are confined to the superficial layers of skin heal by regeneration, but wounds that penetrate deep into the subcutaneous layers are not able to regenerate and heal by scar formation. The overall sequence of events that precedes injury is thought to be similar for chronic and acute wounds whereby chronic wounds simply stall at one or more stages during the wound-healing process.[4]

The first step in wound healing is hemostasis, the vascular response that triggers platelet activation and aggregation, clot formation, and vasoconstriction. The second step in wound healing is inflammation—capillaries vasodilate, and neutrophils and macrophages migrate to the wound bed to debride the wound and secrete growth factors to promote angiogenesis and connective tissue synthesis (tissue inhibitors of matrix metalloproteases, matrix metalloproteases, transforming growth factor-α and transforming growth factor-β, interleukin-1, interleukin-6, interleukin-8, epidermal growth factor, and keratinocyte growth factor). The third step in wound healing is proliferation, a multistep process involving epithelialization (early formation of the new wound bed from fibroblasts), neoangiogenesis (induction of new vasculature), and matrix and/or collagen deposition. The final step in wound healing is wound contraction and maturation and/or remodeling—the wound edges close, and a stronger, more orderly matrix forms scar tissue.[4]

Numerous factors that can affect the wound-healing process make an already complicated process even more difficult to accurately assess. These factors include age, stress, nutrition, tissue perfusion and oxygenation, infection, and other comorbidities, such as obesity, diabetes mellitus, immunosuppression, pulmonary disease, renal disease, and vascular disease. Unfortunately, in some cases, wound healing is complicated by dehiscence, in which "closed" wounds fall apart and reopen. The events leading up to wound dehiscence are not well understood but are suspected to result from an intensely exaggerated inflammatory response.[4] Currently, wounds are evaluated on the basis of parameters such as location of injury, adequacy of perfusion, gross appearance of the wound, wound tensile strength, and the patient's general condition. Although parameters such as the location of injury, the gross appearance of the wound, and the patient's general condition are fairly obvious and can be reasonably assessed, parameters such as the adequacy of perfusion and tensile strength are not readily quantifiable during surgery. It has previously been demonstrated that there is a greater incidence of associated vascular injury in slowly healing wounds than in normally healing wounds.[5] It is also well established that the tensile strength of the wound is dependent on collagen deposition.[6] There exists a need for technologies that can be used to noninvasively and objectively assess these challenging parameters.

3 Raman and Fourier Transform Infrared Spectroscopy

Raman and Fourier transform infrared (FTIR) spectroscopy are types of vibrational spectroscopy that measure the vibrational frequencies of molecules as the molecules are excited by incident photons. Every molecule has a unique fingerprint of vibrational frequencies, which makes Raman and FTIR spectroscopy highly specific techniques for molecular identification. Both techniques can be employed noninvasively, making them ideal for biomedical applications. Raman spectroscopy and FTIR spectroscopy are sometimes referred to as "sister" techniques and provide complementary information about molecules, but they differ in several fundamental ways.

Raman spectroscopy arises from the inelastic scattering of ultraviolet, visible, or near-infrared light when a photon interacts with a molecule. Raman scattering is an inherently weak process, and, as such, samples are typically illuminated by laser light. Light scattered by the sample is diffracted into individual wavelengths by a spectrograph and collected by a detector such as a CCD or CMOS sensor.[7] Raman systems can be coupled to a microscope and motorized stage for high-resolution imaging[8–14] or to a fiberoptic probe for bulk *in vivo* sampling.[15–20] Raman spectroscopy's independence from a specific sample thickness and lack of spectral interference from water make it an ideal technique for biomedical applications. One disadvantage of Raman spectroscopy in the biomedical arena, however, is its inherently weak signal, which can be overwhelmed by sample fluorescence. Often this is overcome by excitation in the near-infrared region of the spectrum where biological molecules tend not to fluoresce. There are other advanced configurations and applications of Raman spectroscopy, but they lie outside the scope of this review.[21–25].

FTIR spectroscopy consists of the absorbance of frequencies of light by a molecule that contains the same vibrational frequencies within its molecular bonds. A beam of infrared light is passed through or reflected by a sample. Some light is absorbed by the sample's vibrational frequencies, and the remaining light is transmitted to an interferometer and then collected by a detector, such as a mercury cadmium telluride photoconductive detector or an indium gallium arsenide photodiode detector.[26] As with Raman spectroscopic systems, FTIR systems can be coupled to a microscope[27–39] or a fiberoptic probe.[40] FTIR spectroscopy is sensitive to the presence of water, however, and *in vivo* sampling can be challenging. One disadvantage of FTIR spectroscopy is that it requires that light be able to pass through the sample and thus is confined to use with thin samples, such as tissue sections on optically transparent windows.

Both Raman spectroscopy and FTIR spectroscopy offer the capability to accurately detect and identify the various molecules that compose the extracellular matrix in their native state during wound healing. They are both imaging techniques in which the precise biochemical composition of biologic samples can be obtained by noninvasive and nondestructive means.[41–44] Both have been proven to be effective in studying tissues at the molecular level using diverse clinical and diagnostic applications, including the analysis of cellular structure and the determination of tumor grade and type.[9,42,45–48] Pathologic alterations of wounds are accompanied by fundamental changes in the molecular environment that can be analyzed by

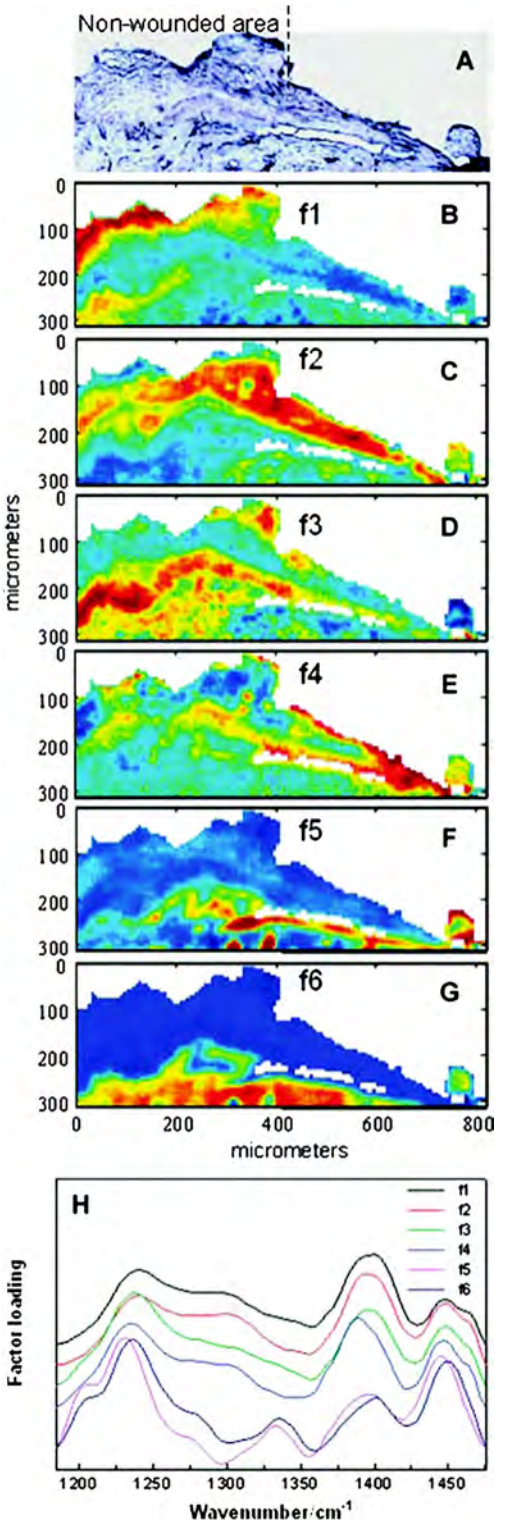

Fig. 1 Infrared characterization (factor analysis conducted over the 1185 to 1475/cm region) of wounded and nonwounded areas six days after wounding is shown. (a) Optical image of an unstained section with the edge of the wounded area marked by a vertical dashed line. (b—g) The score images are shown for various components of the tissue. (b) f1 is the stratum corneum and part of the viable epidermis. (c) f2 is the suprabasal epidermis. (d) f3 is the basal epidermal layer. (e) f4 is the outer leading edge of the migrating epithelial tongue. (f and g) f5 and f6 are the collagen-rich areas, respectively. (h) The factor loadings of f1 to f4 are characteristic of keratin-rich areas. The factor loadings of f5 and f6 are characteristic of collagen-rich areas. Reprinted with permission from John Wiley and Sons [J. Cell. Mol. Med. 12(5B), 2145–2154 (2008)].

vibrational spectroscopy.[49,50] The identified changes might provide the objective markers of acute wound healing, which could then be integrated with clinical characteristics to guide the management of traumatic wounds. For instance, changes in collagen vibrational bands could be correlated with alterations in collagen deposition and reepithelialization of the wound bed.

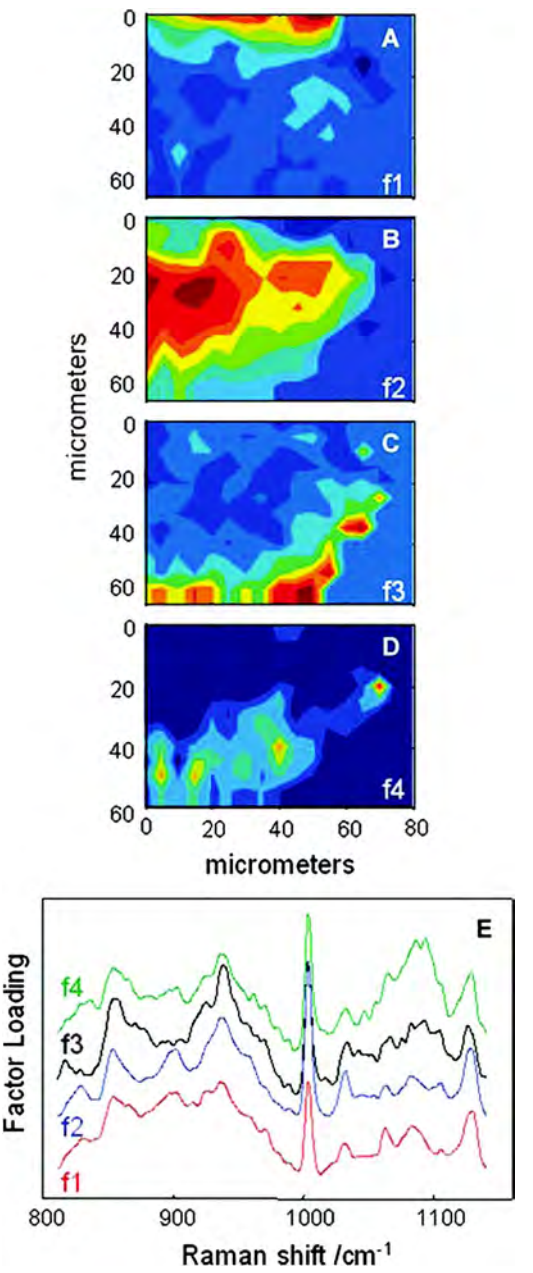

Fig. 2 Factor analysis of a confocal Raman dataset delineates skin regions near a wound edge 0.5 days after wounding. Data analysis was conducted over the 800 to 1140/cm region, yielding four factor loading images that map to anatomically distinct regions in the skin. (a) The spatial distribution of scores for f1 highlights the stratum corneum region of the skin, which is rich in keratin-filled corneocytes and lipids. (b) f2 shows high scores in the underlying epidermal region. (c) High scores for f3 reside near the dermal-epidermal boundary region. (d) The size, location, and spatial distribution of several smaller regions with high scores for f4 are identified as cell nuclei. (e) Factor loadings reveal several spectral features specific to the microanatomy of the epidermis in human skin. Reprinted with permission from John Wiley and Sons [J. Cell. Mol. Med. 12(5B), 2145–2154 (2008)].

4 Vibrational Spectroscopic Studies of Wound Healing

4.1 *Wounds*

The application of vibrational spectroscopy, such as Raman spectroscopy and FTIR spectroscopy, to study wound healing is a developing field of interest. Both *ex vivo* and *in vivo* models of wound healing have been explored in animals and humans, but all studies published to date have focused on acute wounds versus chronic wounds.

In all surgical cases, an acute wound is inflicted once a surgical incision is made. Thus, all surgical wounds are classified as acute wounds and are typically examples of the normal healing process. In early *ex vivo* studies by Wijelath and co-workers, FTIR attenuated total reflection (ATR) spectroscopy illustrated modified healing patterns in arterial grafts implanted into dogs. Standard histological analysis of the graft implants showed little or no activity in the first 10 days after implantation, but FTIR-ATR spectroscopy demonstrated changes within the fibrin layer of the graft that could be correlated to endothelialization of the wound.[51,52] Gough et al. utilized synchrotron FTIR spectroscopic mapping to monitor peridural scarring in rats following laminectomy.[53] Their results derived from untreated rats were compared to data from rats treated with L-2-oxothiazolidine-4-carboxylate (OTC). FTIR spectroscopic maps of laminectomized tissue sections indicated a decrease in lipid and phosphate bands, which are indicators of inflammatory cells. Immunohistochemistry confirmed these results and showed a diminished number of activated macrophages in OTC-treated rats. More recently, investigators successfully employed Raman spectroscopy to differentiate normal from injured tissue in rodent models of brain injury[54] and spinal cord injury.[55] In two rodent models of incisional wound healing, Raman spectra collected *in vivo* demonstrated increased protein configuration surrounding the wounds and increased cellularity[56] as well as conformational changes within the proteins themselves.[57]

To date, published applications of vibrational spectroscopy to study wound healing in humans have been performed on *ex vivo* biopsies of wounds. In 2008, Mendelsohn et al. utilized both FTIR and Raman spectroscopy to correlate spectroscopic changes with the reepithelialization of the wound bed of cutaneous incisional wounds.[49] Spectroscopic results were compared directly with immunohistochemical images of serial tissue sections and gene array analysis data. FTIR images collected four days after wounding precisely depicted the keratin-rich migrating epithelial tongue from the collagen-rich wound bed with focal data analysis of the 1185/cm to 1475/cm spectral region (Fig. 1). Similar spectral features are exhibited by factors 1 to 4 (f1 to f4), but the factors are spatially distinct within the sample itself. These represent keratin-rich areas confirmed by immunohistochemistry. Factors 5 and 6 are spectrally distinct from factors 1 to 4 and represent collagen-rich areas of the sample. Confocal Raman microspectroscopic images of tissue sections demonstrate the time dependence of elastin distribution in the wound up to six days after wounding (Fig. 2).[49] By day 2, the elastin distribution (f1) and the distribution of a collagen factor (f3) were significantly decreased, whereas the distribution of a second collagen factor (f2) decreased. Their study clearly demonstrates the utility of vibrational spectroscopy and imaging to monitor component-specific changes in skin in an acute wound-healing model.

Our group has used Raman spectroscopic mapping to monitor changes within the wound bed. Tissue biopsies were collected from Operation Iraqi Freedom and Operation Enduring Freedom combat-wounded soldiers at each surgical debridement during the wound-healing process.[58] Spectral maps revealed differences in the amide I/CH_2 scissoring band area ratios that correlated with wound outcome (Fig. 3), i.e., normal healing or impaired healing. Raman spectroscopic results were

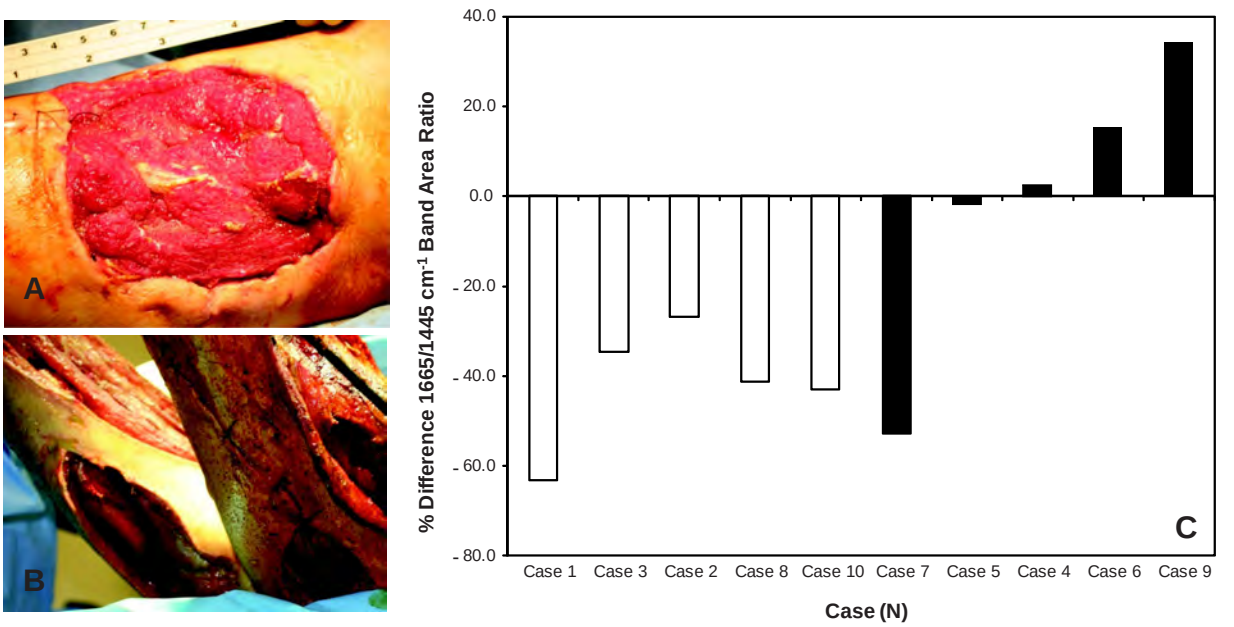

Fig. 3 Photographs are shown for a patient with a normal healing wound (a) and one whose wound healing was impaired (b). (c) This graph shows the percentage difference of the 1665-to-1445/cm band area ratios calculated from the first and last debridement 1665-to-1445/cm band area ratios for wounds classified as healing normally (black bars) and those wounds in which healing was classified as impaired (white bars).

corroborated with collagen gene expression profiles. In impaired healing wounds, a decrease in collagen-like bands was confirmed by decreased expression of the *COL1A1* and *COL3A1* genes (for type I and type III collagens, respectively).[58] In addition to monitoring the wound bed itself, FTIR and Raman spectroscopy were utilized to monitor complications of wound healing, such as infection, the formation of biofilm from subsequent infection, and heterotopic ossification (HO), to which acute and chronic wounds are susceptible.

4.2 *Infection*

For acute wounds such as surgical incisions, infection is the most prevalent postsurgical complication.[59] Chronic wounds provide a bed of growth for pathogens—they are warm, deep, and sometimes full of necrotic tissue. Chronic wounds are more often infected than acute wounds, but acute combat wounds present a subset of acute wounds with a high infection rate.[60] Identifying the pathogens responsible for wound bioburden is especially important because the prevalence of multidrug-resistant bacteria is increasing, necessitating treatment with appropriate antimicrobial agents. Because of the specificity of Raman and FTIR spectroscopy, they can also be used to evaluate the bioburden of wounds. There have been numerous FTIR and Raman spectroscopic studies of microorganisms, many of which have been focused on rapid identification of the microorganisms.[61–72] Differences in the Raman spectral profile of three bacterial species as well as three bacterial strains are evident in Fig. 4 (unpublished data). Both *Klebsiella pneumoniae* and *Acinetobacter baumannii* are Gram-positive bacteria, whereas methicillin-resistant *Staphylococcus aureus* is a Gram-negative bacterium. Differences in the Raman spectral profile, however, are due not strictly to peptidoglycan content but to other structural differences in the proteins as well. Inherent chemical differences in different bacterial species and strains, as demonstrated in Fig. 4, make possible the high specificity of Raman spectroscopy. When the Raman spectra of wound effluent collected from two patients colonized with different bacteria are compared (Fig. 4), the spectral profiles show differences in amino acid content and alterations in glycosidic linkages.

4.3 *Heterotopic Ossification*

Another complication of wound healing, "heterotopic ossification," is defined as the pathological formation of bone in soft tissue. HO formation has been observed following orthopedic surgery (total hip arthroplasty as well as acetabular and elbow fracture surgery), burn injury, traumatic brain injury, and spinal cord injury.[73] HO formation is not commonly observed in civilian traumatic wounds without the presence of head injury or spinal injury and develops in only 20% and 11% of these patients, respectively.[74] During the current military conflicts in Iraq and Afghanistan, HO has been a frequent and common clinical problem in soldiers with traumatic combat wounds. Currently, operative excision is the only treatment for mature, symptomatic HO. Identifying tissue that will develop into HO is not trivial, however, and can only be confirmed once mineralized tissue is evidenced on a radiograph. Tissue mineralization could easily be monitored with Raman spectroscopy.[12,75–88] Information could be gained that would reveal the quality of the bone being formed during HO. For example, is the bone "normal" but developing in soft tissue, or is the bone "pathological," developing by an different mineralization mechanism altogether.[80,89–94]

While Raman and FTIR spectroscopy have been used extensively to study the process of biomineralization,[84–95] they have not previously been used to provide insight into the pathological process of HO. We have collected Raman spectra of uninjured muscle, injured muscle, and "pre-HO" tissue (defined as palpably firm or "woody" tissue without roentgenographic evidence of HO) found within high-energy penetrating wounds (Fig. 5).[95] When we compared uninjured to injured muscle, we found an apparent decrease in the 1340 and 1320/cm vibrational bands in the injured muscle as well as an increase in the 1266/cm vibrational band. This suggests collagen-specific alterations within the tissue as a result of traumatic injury. In one case, a patient exhibited "pre-HO" muscle during a debridement procedure.

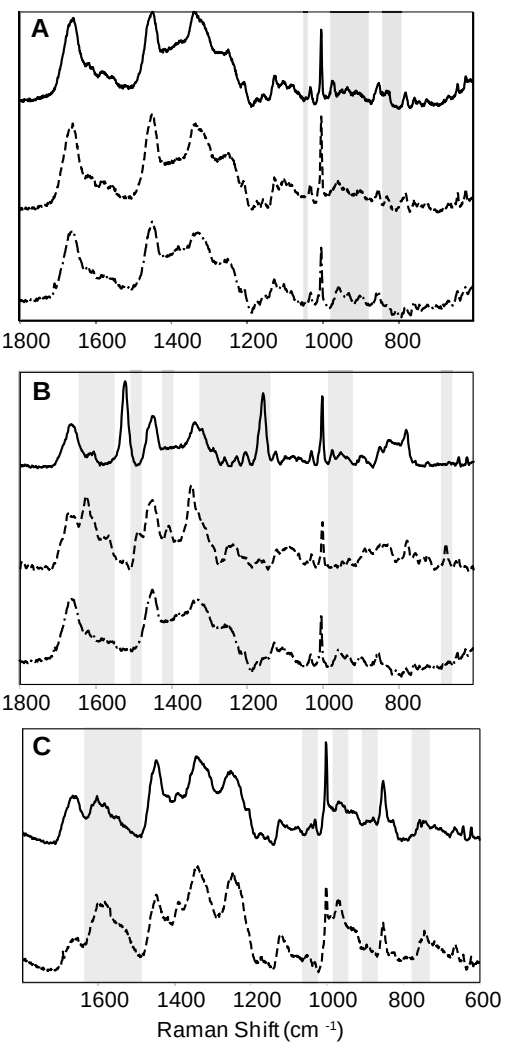

Fig. 4 Raman spectra of (a) methicillin-resistant *Staphylococcus aureus* (solid), *Klebsiella pneumoniae* (middle dashed line), and *Acinetobacter baumannii* (bottom dashed line). (b) Lines represent three different strains of *A. baumannii*. (c) Raman spectra obtained from wound effluent from a wound colonized with *Escherichia coli* (solid line) and from a wound colonized with *A. baumannii* (dashed line). Gray boxes highlight regions of the spectra where chemical differences are prevalent.

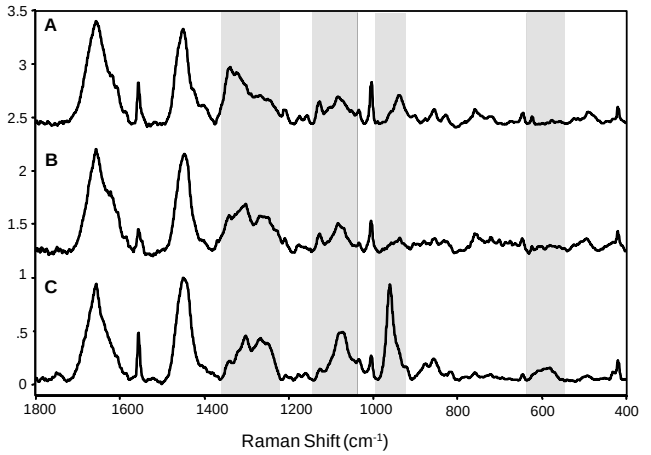

Fig. 5 Raman spectra of (a) uninjured muscle and/or control tissue, (b) combat-injured muscle, and (c) preheterotopic ossification combat-injured muscle. The gray boxes highlight spectral changes in the amide III envelope (1340 to 1240/cm) and the appearance of mineral vibrational bands at 1,070, 960, and 591/cm.

Upon Raman spectroscopic examination, it was clear that the tissue was indeed mineralized, even in "soft" tissue areas. Mineral vibrational bands at 1,070, 960, and 591/cm, typical of a carbonated apatite, were prominent in the spectrum. These vibrational bands are attributed to the phosphate and carbonate stretching modes of bone. Thus, Raman spectroscopy can potentially be utilized to identify areas of tissue affected by early HO as well as areas of tissue that may be predisposed to HO formation.

5 Conclusions

The potential of vibrational spectroscopy to provide detailed information, noninvasively, about molecular and even structural changes within the components of the wound bed itself enable a more thorough understanding of the wound-healing process. Vibrational spectroscopic modalities such as Raman and FTIR spectroscopy can provide an objective means of evaluation by monitoring key components of wound bed reepithelialization, such as keratin, elastin, and collagen; by identifying and quantifying bacterial load; and by detecting HO. These techniques have the potential to offer improved objective assessment of combat wounds, resulting in faster healing times, decreased infection rates, and decreased local and systemic complications of injury. This, in turn, will produce improved clinical outcomes, decreased patient morbidity, and reduced medical costs.

Acknowledgments

The views expressed in this paper are those of the authors and do not reflect the official policy of the Department of the Army, the Department of the Navy, the Department of Defense, or the U.S. government. We are military service members (or employees of the U.S. government). This work was prepared as part of our official duties. Title 17 U.S.C. § 105 states, "Copyright protection under this title is not available for any work of the United States Government." Title 17 U.S.C. § 101 defines a U.S. government work as a work prepared by a military service member or employee of the U.S. government as part of that person's official duties.

This effort was supported in part by the U.S. Navy Bureau of Medicine and Surgery under the Medical Development Program and Office of Naval Research work unit number 602115HP.3720.001.A1015. This study was approved by the National Naval Medical Center Institutional Review Board (NNMC IRB) in compliance with all federal regulations governing the protection of human subjects. The NNMC IRB-approved protocol number is NNMC.2005.0069/NMRC.2005.0012, and the protocol title is "The Use of Vacuum Assisted Wound Closure Device in the treatment of Extremity Wounds."

We certify that all individuals who qualify as authors have been listed; that each has participated in the conception and design of this work, the analysis of data (when applicable), the writing of the document, and the approval of the submission of this version; that the document represents valid work; that if we used information derived from another source, we obtained all necessary approvals to use it and made appropriate acknowledgments thereof in the document; and that each author takes public responsibility for it.

References

1. U.S. Department of Health & Human Services, Agency for Healthcare Research and Quality, *Healthcare Cost & Utilization Project (HCUP)*, August 22, 2011, http://www.ahrq.gov/data/hcup/, accessed December 30, 2011.
2. D. J. Samson, F. Lefevre, and N. Aronson, "*Wound-Healing Technologies: Low-Level Laser and Vacuum-Assisted Closure*", Evidence Report/Technology Assessment No. 111, prepared by the Blue Cross and Blue Shield Association Technology Evaluation Center Evidence-Based Practice Center under Contract No. 290-02-0026, AHRQ Publication No. 05-E005-2, December 2004, Rockville, MD, Agency for Healthcare Research and Quality, http://www.ahrq.gov/downloads/pub/evidence/pdf/woundtech/woundtech.pdf, accessed December 30, 2011.
3. R. A. Bryant and D. P. Nix, "Acute & Chronic Wounds: Current Management Concepts," 3rd ed., Mosby, St. Louis (2007).
4. R. A. Bryant and D. P. Nix, "Acute & Chronic Wounds: Current Management Concepts," 3rd ed., Mosby, St.Louis (2012).
5. J. S. Hawksworth et al., "Inflammatory biomarkers in combat wound healing," *Ann. Surg.* **250**6, 1002–1007 (2009).
6. F. C. Brunicardi et al., Eds., Schwartz's Manual of Surgery, 8th ed., McGraw-Hill, New York (2006).
7. I. R. Lewis and H. G. M. Edwards, Eds., "Handbook of Raman Spectroscopy: From the Research Laboratory to the Process Line", Marcel Dekker, New York (2001).
8. A. Kohler et al., "Multivariate image analysis of a set of FTIR microspectroscopy images of aged bovine muscle tissue combining image and design information," *Anal. Bioanal. Chem.* **389**4, 1143–1153 (2007).
9. T. Meyer et al., "Nonlinear microscopy, infrared, and Raman microspectroscopy for brain tumor analysis," *J. Biomed. Opt.* **16**2, 021113 (2011).
10. S. Keren et al., "Noninvasive molecular imaging of small living subjects using Raman spectroscopy," *Proc. Natl. Acad. Sci. U. S. A.* **105**15, 5844–5849 (2008).
11. M. Kazanci et al., "Bone osteonal tissues by Raman spectral mapping: orientation-composition," *J. Struct. Biol.* **156**3, 489–496 (2006).
12. M. D. Morris and W. F. Finney, "Recent developments in Raman and infrared spectroscopy and imaging of bone tissue," *Spectroscopy* **18**2, 155–159 (2004).
13. W. Gellermann et al., "Raman imaging of human macular pigments," *Opt. Lett.* **27**10, 833–835 (2002).
14. N. J. Kline and P. J. Treado, "Raman chemical imaging of breast tissue," *J. Raman Spectrosc.* **28**2–3, 119–124 (1997).
15. M. V. Schulmerich et al., "Subsurface and transcutaneous Raman spectroscopy and mapping using concentric illumination rings and collection with a circular fiber-optic array," *Appl. Spectrosc.* **61**7, 671–678 (2007).

16. Y. Hattori et al., "In vivo Raman study of the living rat esophagus and stomach using a micro-Raman probe under an endoscope," *Appl. Spectrosc.* **61**6, 579–584 (2007).
17. M. V. Schulmerich et al., "Transcutaneous Raman spectroscopy of bone tissue using a non-confocal fiber optic array probe," *Proc. SPIE* **6093**, 60930O (2006).
18. J. G. Wu et al., "Distinguishing malignant from normal oral tissues using FTIR fiber-optic techniques," *Biopolymers* **62**4, 185–192 (2001).
19. M. G. Shim et al., "Study of fiber-optic orobes for in vivo medical Raman spectroscopy," *Appl. Spectrosc.* **53**6, 619–627 (1999).
20. A. S. Haka et al., "In vivo margin assessment during partial mastectomy breast surgery using raman spectroscopy," *Cancer Res.* **66**6, 3317–3322 (2006).
21. J. Grun et al., "Identification of bacteria from two-dimensional resonant-Raman spectra," *Anal. Chem.* **79**14, 5489–5493 (2007).
22. C. A. Lieber et al., "In vivo nonmelanoma skin cancer diagnosis using Raman microspectroscopy," *Lasers Surg. Med.* **40**7, 461–467 (2008).
23. R. Manoharan et al., "Ultraviolet resonance Raman spectroscopy for detection of colon cancer," *Laser. Life Sci.* **6**4, 217–227 (1995).
24. K. R. Ward et al., "Oxygenation monitoring of tissue vasculature by resonance Raman spectroscopy," *Anal. Chem.* **79**4, 1514–1518 (2007).
25. P. S. Bernstein et al., "Resonance Raman measurement of macular carotenoids in the living human eye," *Arch. Biochem. Biophys.* **430**2, 163–169 (2004).
26. J. M. Chalmers and P. R. Griffiths, eds., Handbook of Vibrational Spectroscopy, vols. **5**, John Wiley & Sons, New York (2002).
27. C. Pezzei et al., "Characterization of normal and malignant prostate tissue by Fourier transform infrared microspectroscopy," *Mol. Biosyst.* **6**11, 2287–2295 (2010).
28. K. Wehbe et al., "FT-IR spectral imaging of blood vessels reveals protein secondary structure deviations induced by tumor growth," *Anal. Bioanal. Chem.* **392**1–2, 129–135 (2008).
29. E. Ly et al., "Combination of FTIR spectral imaging and chemometrics for tumour detection from paraffin-embedded biopsies," *Analyst* **133**2, 197–205 (2008).
30. C. Petibois et al., "Histological mapping of biochemical changes in solid tumors by FT-IR spectral imaging," *FEBS Lett.* **581**28, 5469–5474 (2007).
31. R. Bhargava, "Towards a practical Fourier transform infrared chemical imaging protocol for cancer histopathology," *Anal. Bioanal. Chem.* **389**4, 1155–1169 (2007).
32. C. H. Petter et al., "Development and application of Fourier-transform infrared chemical imaging of tumour in human tissue," *Curr. Med. Chem.* **16**3, 318–326 (2009).
33. B. Bird et al., "Infrared micro-spectral imaging: distinction of tissue types in axillary lymph node histology," *BMC Clin. Pathol.* **8**8, 8 (2008).
34. R. Zoehrer et al., "Bone quality determined by Fourier transform infrared imaging analysis in mild primary hyperparathyroidism," *J. Clin. Endocrinol. Metab.* **93**9, 3484–3489 (2008).
35. S. Gourion-Arsiquaud, P. A. West, and A. L. Boskey, "Fourier transform-infrared microspectroscopy and microscopic imaging," *Methods Mol. Biol.* **455**, 293–303 (2008).
36. X. Bi et al., "Fourier transform infrared imaging spectroscopy investigations in the pathogenesis and repair of cartilage," *Biochim. Biophys. Acta* **17587**, 934–941 (2006).
37. E. David-Vaudey et al., "Fourier Transform Infrared Imaging of focal lesions in human osteoarthritic cartilage," *Eur. Cell Mater.* **10**, 51–60 (2005).
38. I. W. Levin and R. Bhargava, "Fourier transform infrared vibrational spectroscopic imaging: integrating microscopy and molecular recognition," *Annu. Rev. Phys. Chem.* **56**, 429–474 (2005).
39. D. C. Fernandez et al., "Infrared spectroscopic imaging for histopathologic recognition," *Nat. Biotechnol.* **23**4, 469–474 (2005).
40. V. K. Katukuri et al., "Detection of colonic inflammation with Fourier transform infrared spectroscopy using a flexible silver halide fiber," *Biomed. Opt. Express.* **1**3, 1014–1025 (2010).
41. C. Kendall et al., "Exploiting the diagnostic potential of biomolecular fingerprinting with vibrational spectroscopy," *Faraday Discuss.* **149**, 279–290 (2011).
42. C. Kendall et al., "Vibrational spectroscopy: a clinical tool for cancer diagnostics," *Analyst* **134**6, 1029–1045 (2009).
43. C. Krafft et al, "Raman and FTIR microscopic imaging of colon tissue: a comparative study," *J. Biophotonics* **1**2, 154–169 (2008).
44. C. Krafft et al., "Methodology for fiber-optic Raman mapping and FTIR imaging of metastases in mouse brains," *Anal. Bioanal. Chem.* **389**4, 1133–1142 (2007).
45. C. Krafft et al., "Disease recognition by infrared and Raman spectroscopy," *J. Biophotonics* **2**1–2, 13–28 (2009).
46. C. Murali Krishna et al., "An overview on applications of optical spectroscopy in cervical cancers," *J. Cancer Res. Ther.* **4**1, 26–36 (2008).
47. C. M. Krishna et al., "FTIR and Raman microspectroscopy of normal, benign, and malignant formalin-fixed ovarian tissues," *Anal. Bioanal. Chem.* **387**5, 1649–1656 (2007).
48. S. F. Weng et al., "FTIR fiber optics and FT-Raman spectroscopic studies for the diagnosis of cancer," *Am. Clin. Lab.* **19**7, 20 (2000).
49. K. L. Chan Andrew et al., "A coordinated approach to cutaneous wound healing: vibrational microscopy and molecular biology," *J. Cell. Mol. Med.* **125**B, 2145–2154 (2008).
50. G. Chen et al., "Nonlinear spectral imaging of human hypertrophic scar based on two-photon excited fluorescence and second-harmonic generation," *Br. J. Dermatol.* **161**1, 48–55 (2009).
51. J. Murray-Wijelath, D. J. Lyman, and E. S. Wijelath, "Vascular graft healing. III. FTIR analysis of ePTFE graft samples from implanted bigrafts," *J. Biomed. Mater. Res. B Appl. Biomater.* **70**2, 223–232 (2004).
52. D. J. Lyman et al., "Vascular graft healing. II. FTIR analysis of polyester graft samples from implanted bi-grafts," *J. Biomed. Mater. Res.* **58**3, 221–237 (2001).
53. R. Wiens et al., "Synchrotron FTIR microspectroscopic analysis of the effects of anti-inflammatory therapeutics on wound healing in laminectomized rats," *Anal. Bioanal. Chem.* **387**5, 1679–1689 (2007).
54. L. L. Tay et al., "Detection of acute brain injury by Raman spectral signature," *Analyst* **136**8, 1620–1626 (2011).
55. T. Saxena et al., "Raman spectroscopic investigation of spinal cord injury in a rat model," *J. Biomed. Opt.* **16**2, 027003 (2011).
56. A. Makowski et al., "Laser preconditioning for wound healing: a Raman spectroscopy analysis," *Lasers Surg. Med.* **42**(Suppl. 22), 10–11 (2010).
57. A. Alimova et al., "In vivo molecular evaluation of guinea pig skin incisions healing after surgical suture and laser tissue welding using Raman spectroscopy," *J. Photochem. Photobiol. B* **96**3, 178–183 (2009).
58. N. J. Crane et al., "Monitoring the healing of combat wounds using Raman spectroscopic mapping," *Wound Repair Regen.* **18**4, 409–416 (2010).
59. A. J. Mangram et al., "Guideline for Prevention of Surgical Site Infection, 1999. Centers for Disease Control and Prevention (CDC) Hospital Infection Control Practices Advisory Committee," *Am. J. Infect. Control* **27**2, 96–134 (1999).
60. F. R. Sheppard et al., "The majority of US combat casualty soft-tissue wounds are not infected or colonized upon arrival or during treatment at a continental US military medical facility," *Am. J. Surg.* **200**4, 489–495 (2010).
61. P. C. Buijtels et al., "Rapid identification of mycobacteria by Raman spectroscopy," *J. Clin. Microbiol.* **46**3, 961–965 (2008).
62. M. F. Escoriza et al., "Raman spectroscopy and chemical imaging for quantification of filtered waterborne bacteria," *J. Microbiol. Methods* **66**1, 63–72 (2006).
63. K. Maquelin et al., "Identification of medically relevant microorganisms by vibrational spectroscopy," *J. Microbiol. Methods* **51**3, 255–271 (2002).
64. Q. Wu et al., "Intensities of E. coli nucleic acid Raman spectra excited selectively from whole cells with 251-nm light," *Anal. Chem.* **72**13, 2981–2986 (2000).
65. L. Zeiri et al., "Surface-enhanced Raman spectroscopy as a tool for probing specific biochemical components in bacteria," *Appl. Spectrosc.* **58**1, 33–40 (2004).
66. K. Maquelin et al., "Rapid epidemiological analysis of Acinetobacter strains by Raman spectroscopy," *J. Microbiol. Methods* **64**1, 126–131 (2006).
67. K. Maquelin et al., "Raman spectroscopic method for identification of clinically relevant microorganisms growing on solid culture medium," *Anal. Chem.* **72**1, 12–19 (2000).

68. K. S. Kalasinsky et al., "Raman chemical imaging spectroscopy reagentless detection and identification of pathogens: signature development and evaluation," *Anal. Chem.* **79**7, 2658–2673 (2007).
69. L. Zeiri et al., "Silver metal induced surface enhanced Raman of bacteria," *Colloids Surf A Physicochem. Eng. Asp* **208**, 357–362 (2002).
70. D. I. Ellis and R. Goodacre, "Metabolic fingerprinting in disease diagnosis: biomedical applications of infrared and Raman spectroscopy," *Analyst* **131**8, 875–885 (2006).
71. K. Maquelin et al., "Prospective study of the performance of vibrational spectroscopies for rapid identification of bacterial and fungal pathogens recovered from blood cultures," *J. Clin. Microbiol.* **41**1, 324–329 (2003).
72. C. L. Winder et al., "The rapid identification of Acinetobacter species using Fourier transform infrared spectroscopy," *J. Appl. Microbiol.* **96**2, 328–339 (2004).
73. F. S. Kaplan et al., "Heterotopic ossification," *Am. J. Acad. Orthop. Surg.* **12**2, 116–125 (2004).
74. D. E. Garland, "Clinical observations on fractures and heterotopic ossification in the spinal cord and traumatic brain injured populations," *Clin. Orthop. Relat. Res.* **233**, 86–101 (1988).
75. A. Carden and M. D. Morris, "Application of vibrational spectroscopy to the study of mineralized tissues," *J. Biomed. Opt.* **5**3, 259–268 (2000).
76. A. Carden et al., "Raman imaging of bone mineral and matrix: composition and function," *Proc. SPIE* **3608**, 132–138 (1999).
77. A. Carden et al., "Ultrastructural changes accompanying the mechanical deformation of bone tissue: a Raman imaging study," *Calcif. Tissue Int.* **72**2, 166–175 (2003).
78. C. J. de Grauw et al., "Investigation of bone and calcium phosphate coatings and crystallinity determination using Raman microspectroscopy," *Cells Mater* **6**1–3, 57–62 (1996).
79. M. D. Morris et al., "Bone microstructure deformation observed by Raman microscopy," *Proc. SPIE* **4254**, 81–89 (2001).
80. M. D. Morris et al., "Raman spectroscopy of early mineralization of normal and pathological calvaria," *Proc. SPIE* **4614**, 28–39 (2002).
81. M. D. Morris et al., "Raman microscopy of de novo woven bone tissue," *Proc. SPIE* **4254**, 90–96 (2001).
82. G. Penel et al., "Raman microspectrometry studies of brushite cement: in vivo evolution in a sheep model," *Bone* **25**(Suppl. 2), 81S–84S(1999).
83. G. Pezzotti and S. Sakakura, "Study of the toughening mechanisms in bone and biomimetic hydroxyapatite materials using Raman microprobe spectroscopy," *J. Biomed. Mater. Res.* **65A**2, 229–236 (2003).
84. J. A. Pezzuti et al., "Hyperspectral Raman imaging of bone growth and regrowth chemistry," *Proc. SPIE* **3261**, 270–276 (1998).
85. R. Smith and I. Rehman, "Fourier transform Raman spectroscopic studies of human bone," *J. Mater. Sci. Mater. Med.* **5**, 775–778 (1995).
86. C. P. Tarnowski, M. A. Ignelzi, Jr., and M. D. Morris, "Mineralization of developing mouse calvaria as revealed by Raman microspectroscopy," *J. Bone Miner. Res.* **17**6, 1118–1126 (2002).
87. J. Timlin et al., "Raman spectroscopic imaging markers for fatigue-related microdamage in bovine bone," *Anal. Chem.* **72**10, 2229–2236 (2000).
88. J. A. Timlin et al., "Spatial distribution of phosphate species in mature and newly generated mammalian bone by hyperspectral Raman imaging," *J. Biomed. Opt.* **4**1, 28–34 (1999).
89. N. J. Crane et al., "Raman spectroscopic evidence for octacalcium phosphate and other transient mineral species deposited during intramembraneous mineralization," *Bone* **39**3, 434–442 (2006).
90. J. J. Freeman et al., "Raman spectroscopic detection of changes in bioapatite in mouse femora as a function of age and in vitro fluoride treatment," *Calcif. Tissue Int.* **68**3, 156–162 (2001).
91. M. D. Morris et al., "Effects of applied load on bone tissue as observed by Raman spectroscopy," *Proc. SPIE* **4614**, 47–54 (2002).
92. J. D. Pasteris et al., "Lack of OH in nanocrystalline apatite as a function of degree of atomic order: implications for bone and biomaterials," *Biomaterials* **25**2, 229–238 (2004).
93. G. Penel et al., "MicroRaman spectral study of the PO_4 and CO_3 vibrational modes in synthetic and biological apatites," *Calcif. Tissue Int.* **63**6, 475–481 (1998).
94. P. Taddei et al., "Vibrational spectroscopic characterization of new calcium phosphate bioactive coatings," *Biospectroscopy* **5**73, 140–148 (2000).
95. B. K. Potter et al., "Heterotopic ossification following combat-related trauma," *J. Bone Joint Surg. Am.* **92**(Suppl. 2), 74–89(2010).

Predicting Wound Outcome from Raman Spectroscopic Data: Univariate versus Multivariate Techniques

Nicole J. Crane[1,3], Rajiv Luthra[1], Jonathan A. Forsberg[1,2,3], Eric Elster[2,3]

[1]Naval Medical Research Center, Silver Spring, MD
[2]Walter Reed National Military Medical Center, Bethesda, MD
[3]Uniformed Services University of the Health Sciences, Bethesda, MD

Email:
Nicole.Crane@med.navy.mil

IEEE AIPR
October 10th, 2012

Acute Combat Wounds

Acute Combat Wounds

- The management of modern traumatic war wounds remains a significant challenge for clinicians.
  - Extensive osseous and soft-tissue damage caused by blasts and high-energy projectiles.
- The ensuing inflammatory response ultimately dictates the pace of wound healing and tissue regeneration.
- The timing of wound closure or definitive coverage is subjectively based.
- Despite the use and application of novel wound-specific treatment modalities, some wounds fail to close, or dehisce.

Acute Combat Wounds – Current Treatment

Surgical debridements are performed every 2-3 days.

- remove devitalized tissue
- decrease bacterial load

Negative pressure wound therapy (NPWT) is applied between debridements. NPWT promotes wound closure.

Wound assessment involves:

- patient's general condition
- injury location
- adequacy of perfusion
- gross appearance of the wound

Acute Combat Wounds – The Challenge

Monitor wound healing *in vivo*, i.e. monitor wound healing during surgical debridements.

- Is it the best time to close the wound?
- Is the wound developing HO?
- Is the wound infected? With what?

Develop an objective and predictive model for wound healing.

The Toolbox

Our Toolbox

Real-time PCR

Multiplex Protein Assay

Raman Spectroscopy

FTIR Imaging

Thermography

Visible Reflectance Imaging

Bayesian Belief Network modeling

Sample Collection

Wound is surgically cleaned

Collect 1 cm³ tissue biopsy from center of wound bed

RT-PCR
Raman spectroscopy
Micro culture

NPWT is applied

Serum is collected

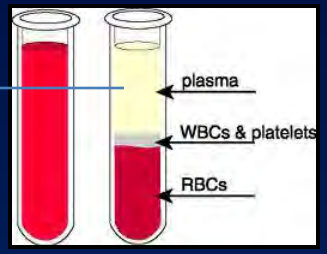

Protein assay

Effluent is collected

Protein assay

Raman spectroscopy
Micro culture

Preliminary Study – Raman Mapping Results

- Previous study demonstrated the potential of Raman spectroscopic analysis of wound biopsies for classification of wounds as normal or impaired healing.

Wound Rep Regen. 18(4): 409-416, 2010.

Ann Surg. 250(6):1002-7, 2009.

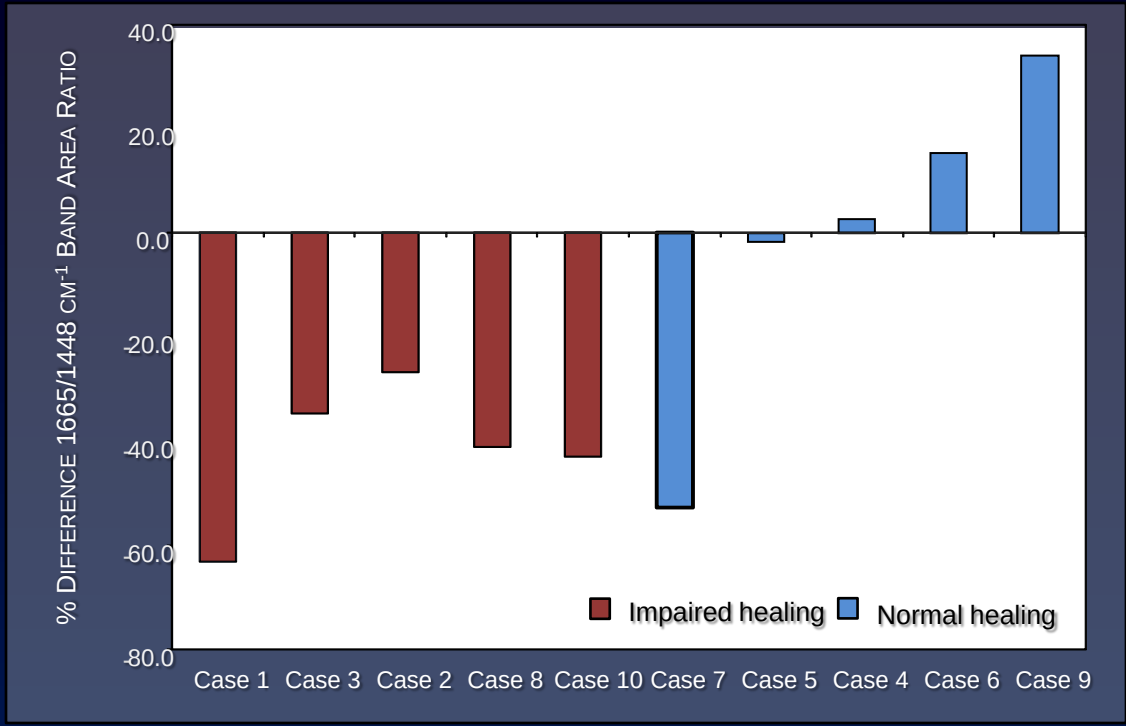

- Impaired healing wounds demonstrate a significant decrease in the 1665/1445 cm^{-1} band area ratio compared to normal healing wounds - these results were corroborated with collagen gene expression in the same samples.

Could this type of analysis be extended to intact wound biopsies and ultimately obviate the need for excisional wound biopsies?

Chronicling Wound Healing with Raman Spectroscopy

Raman Fiber Probe Data Collection

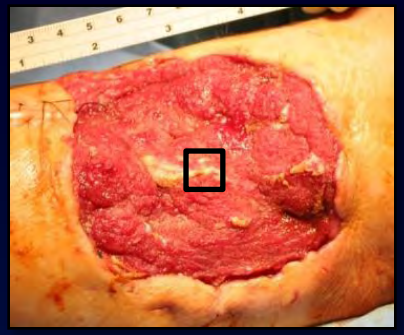

Approximately 1 cm^2 tissue biopsy is excised from the center of the wound bed.

Tissue is fixed in 10% neutral buffered formalin for storage.

Prior to spectral acquisition, samples are rinsed in 0.9% NaCl saline solution.

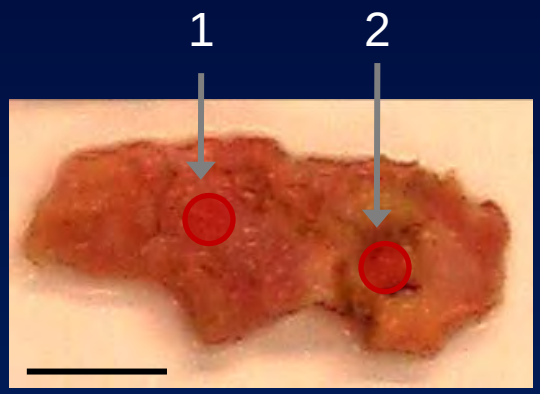

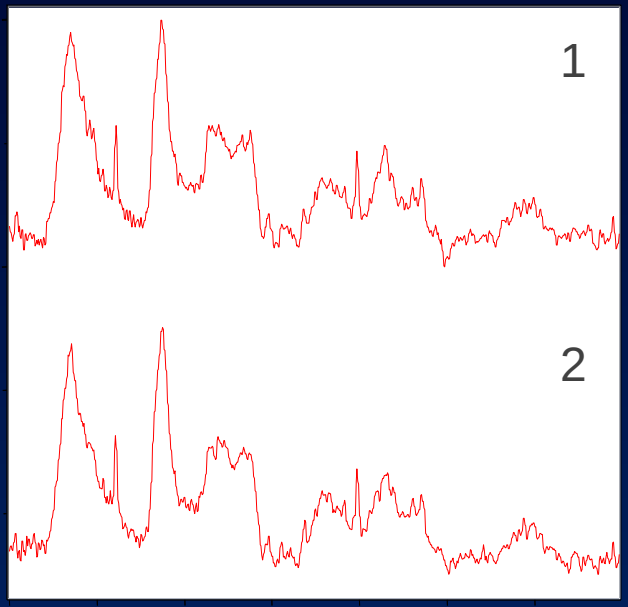

Examine multiple spots across the tissue.

14 accumulations, 5s spectrum
7 accumulations, 10s spectrum

Monitoring a Wound Over Time

First Debridement

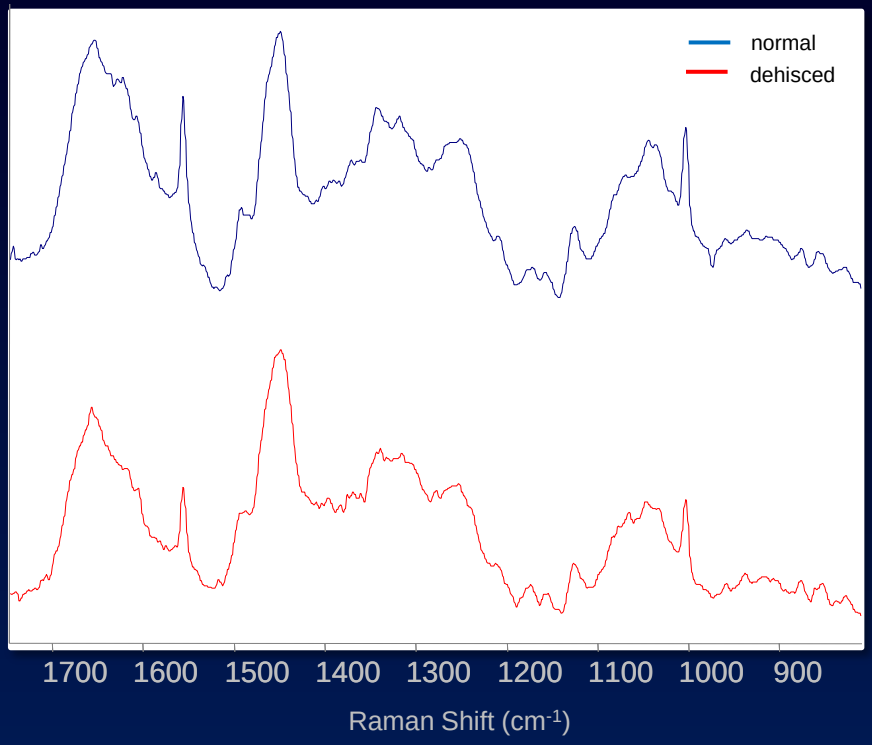

Final Debridement

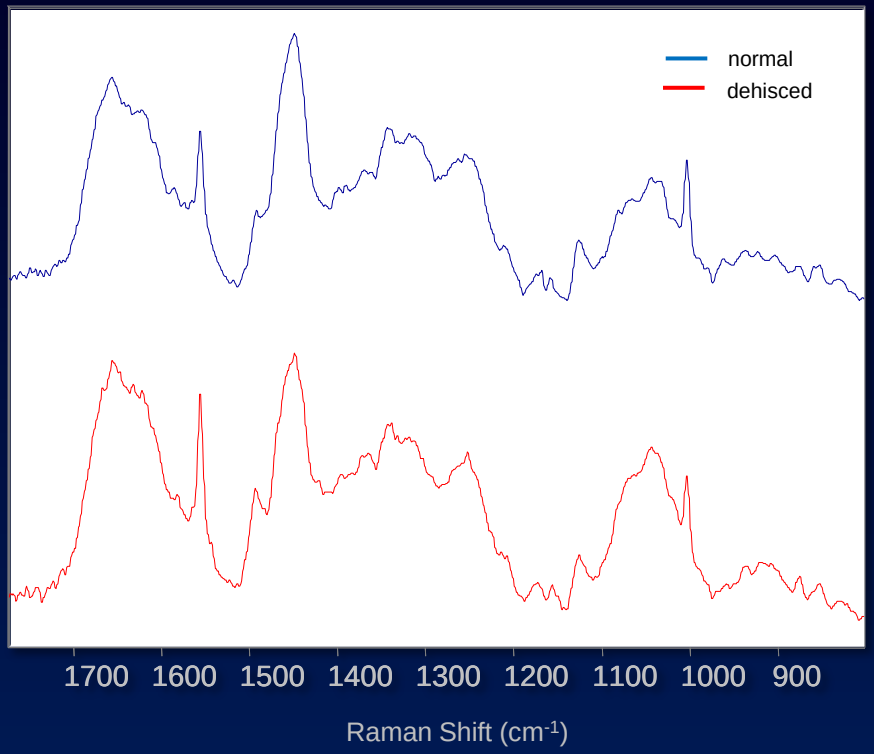

- Spectral differences between biopsies collected from normal healing wounds (n=12) and dehisced wounds (n=13) are not readily apparent.

Peakfitting for Spectral Deconvolution

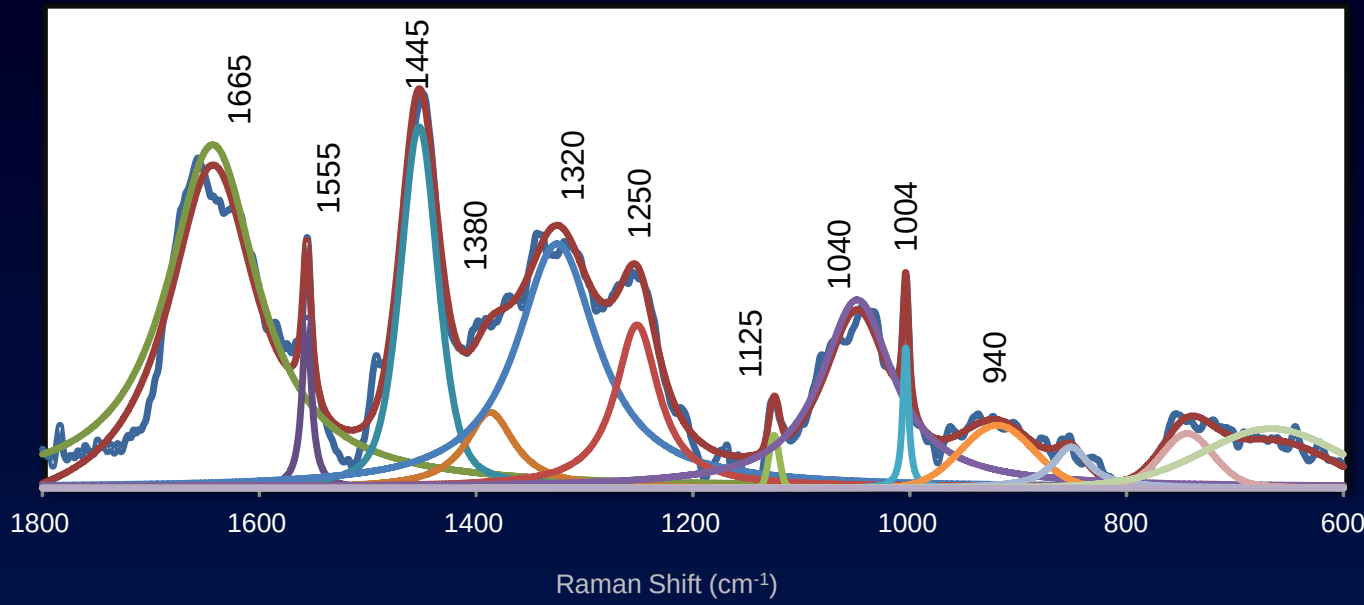

Raman Shift (cm^{-1})	Vibrational Band Assignment	Component
860	ν(C-C)	nucleic acids
920,940	ν(C-N), ν(C-C)	nucleic acids, keratin
1004	ν(C-C) ring	phenylalanine
1040	ν(C-C) skeletal	nucleic acids, protein
1125	ν(C-C), ν(C-N)	nucleic acids, protein
1250	ν (C-N) and δ(N-H); Amide III	protein
1320	$\delta(CH_2)$ twisting	nucleic acids, protein
1445	$\delta(CH_3)$ and $\delta(CH_2)$ scissoring	protein
1555		aromatic amino acids, heme
1665	ν(C=O); Amide I	protein

Univariate Data Set

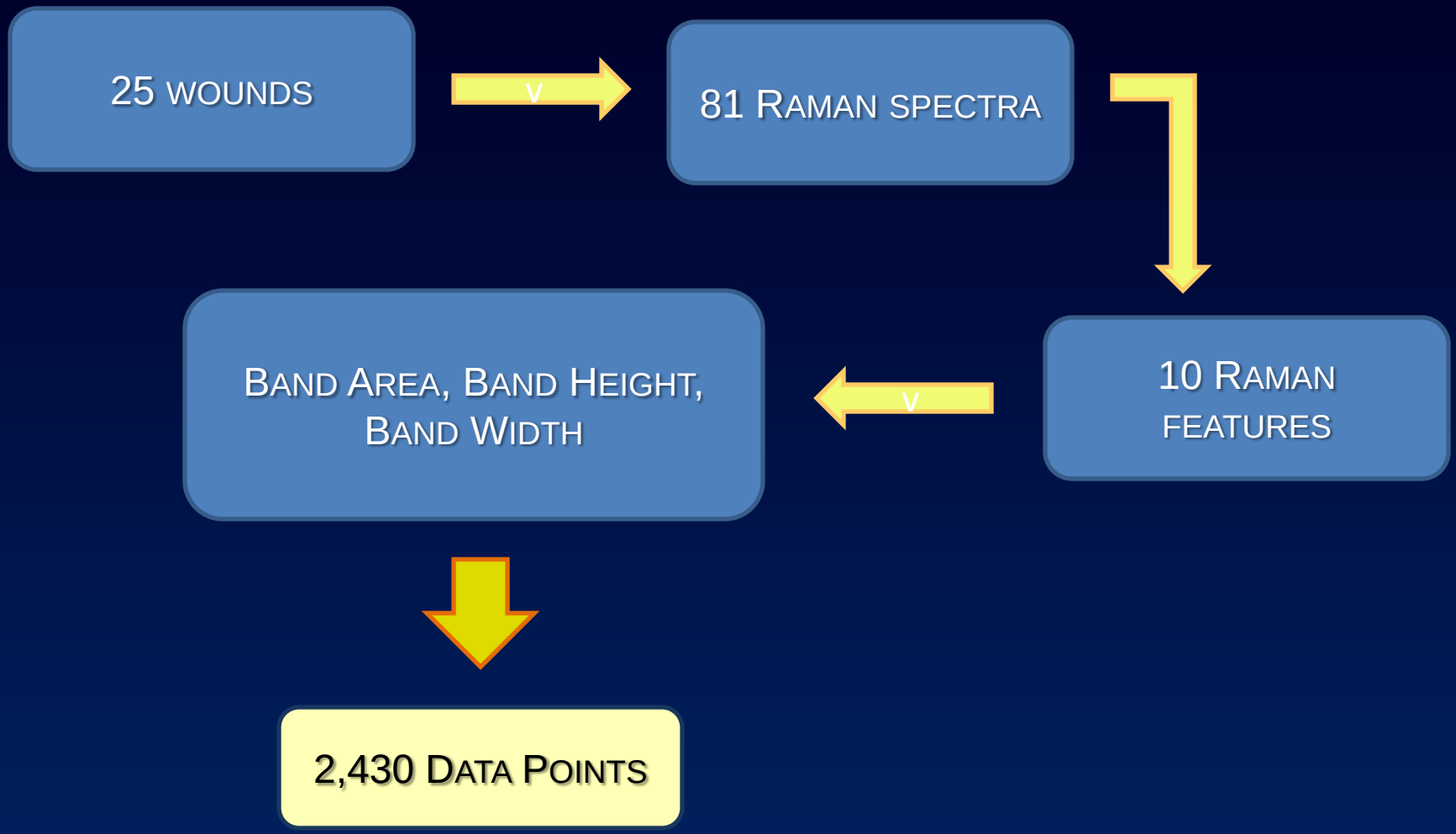

Univariate Analysis of Band Areas

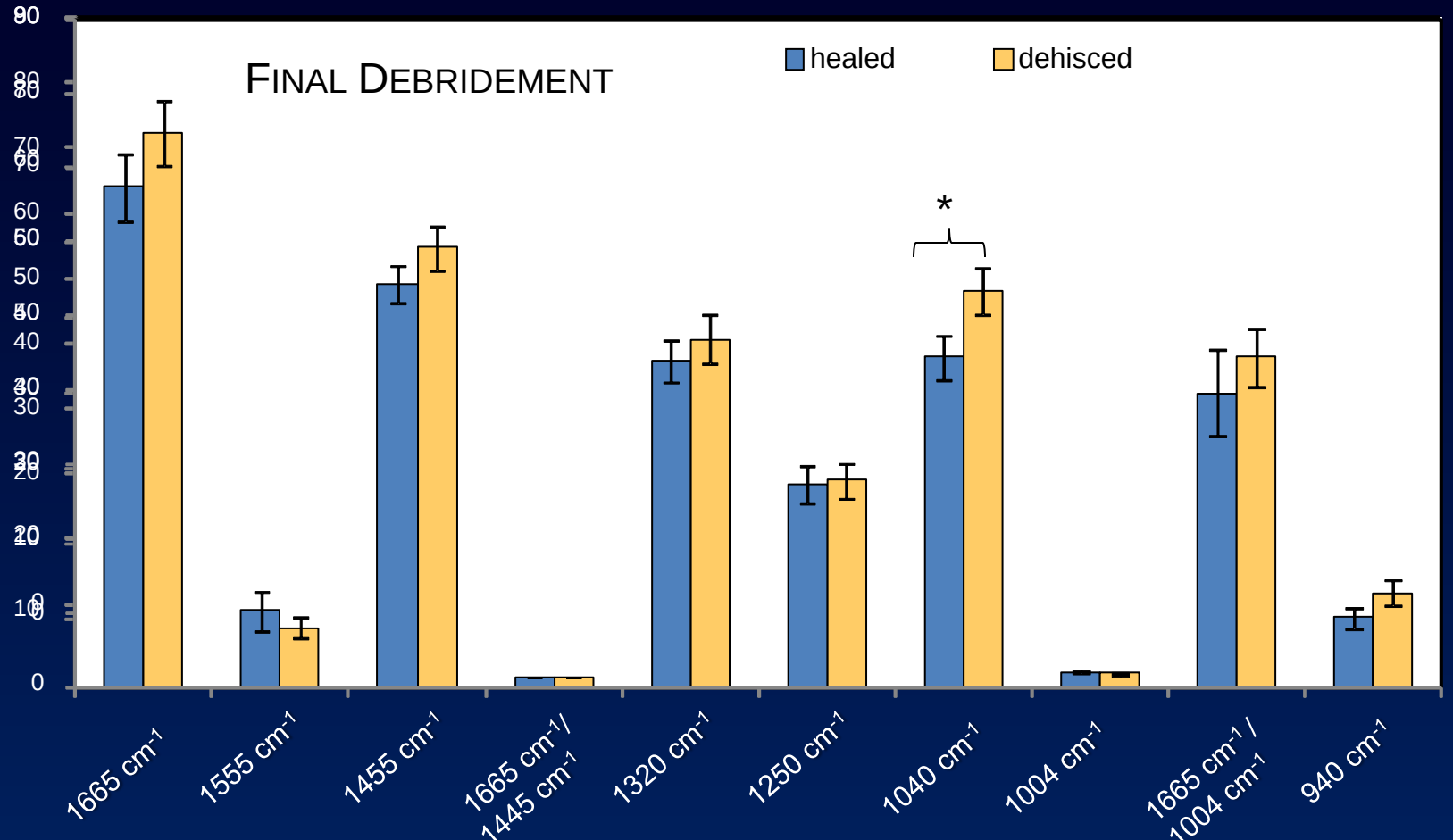

Univariate Analysis of Band Areas: Thresholds

Predicting outcome based on univariate analysis of band areas would misclassify 31% of dehisced wounds and 33% of healed wounds.

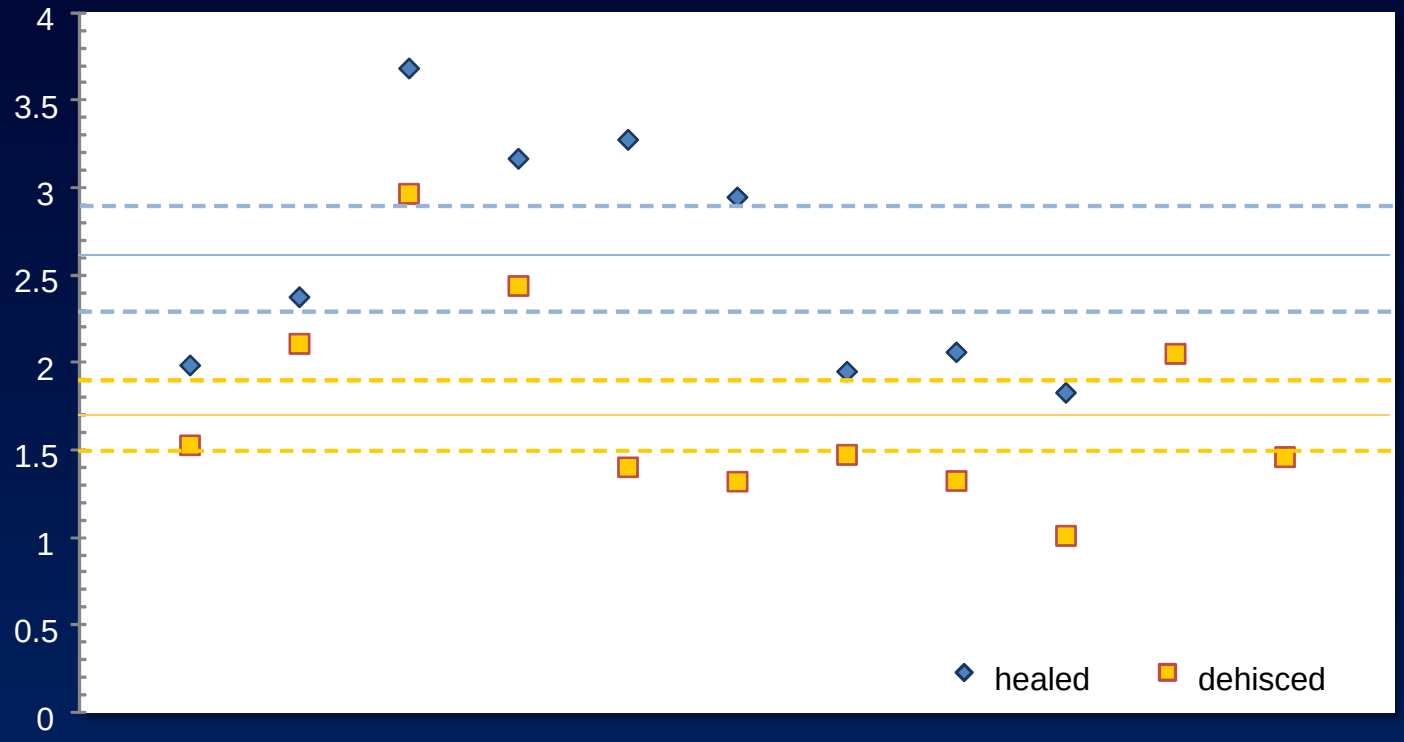

Univariate Analysis of Band Areas

- We can also look for changes in the band area profiles of healed and dehisced wounds over time, i.e. first debridement versus final debridement.

  For wounds that heal, there are no statistically significant difference between calculated band areas chronologically.

  For wounds that dehisce, the band area at 1250 cm^{-1} demonstrates a statistically significant difference between the first and final debridement ($p < 0.03$).

Multivariate Analysis: BBNs

- Bayesian Belief Networks fall under the umbrella of machine learning.

  Input = empirical data ⟶ output = patterns or predictions that are believed to be responsible for generating the data

- Applies the Bayes probabilistic theory for analyzing data sets.

- Bayesian Belief Networks (BBNs) demonstrate probabilistic relationships – relationships in which knowledge of the value of a variable affects the belief about the likelihood of other variables taking certain values.

  - Data mining
  - Prediction

Bayesian Modeling Data Set: Raman Only

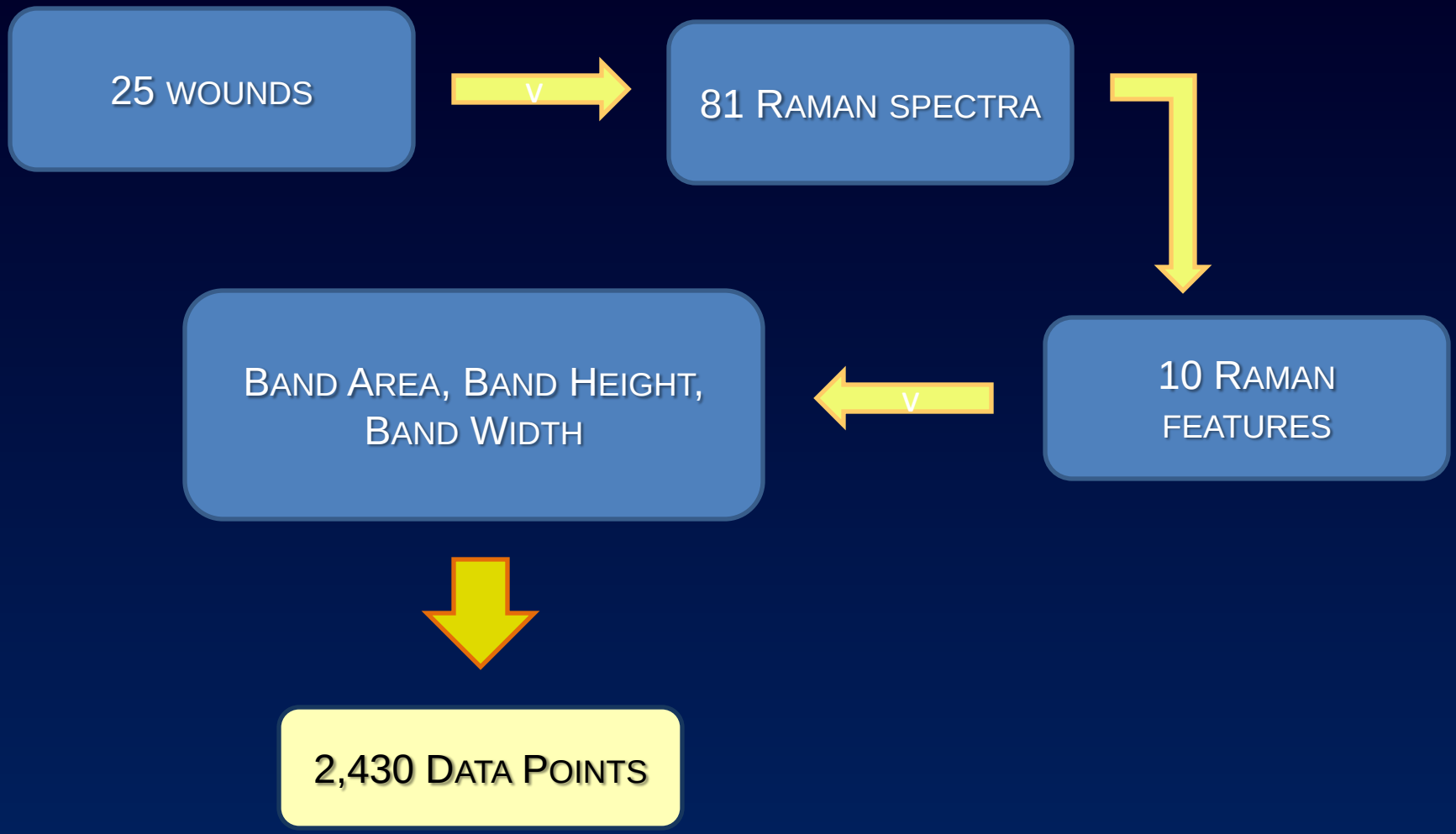

BBN Analysis of Band Areas: Data Mining

Bayesian Belief Network (BBN) machine learning can elucidate some of the relationships between band area changes.

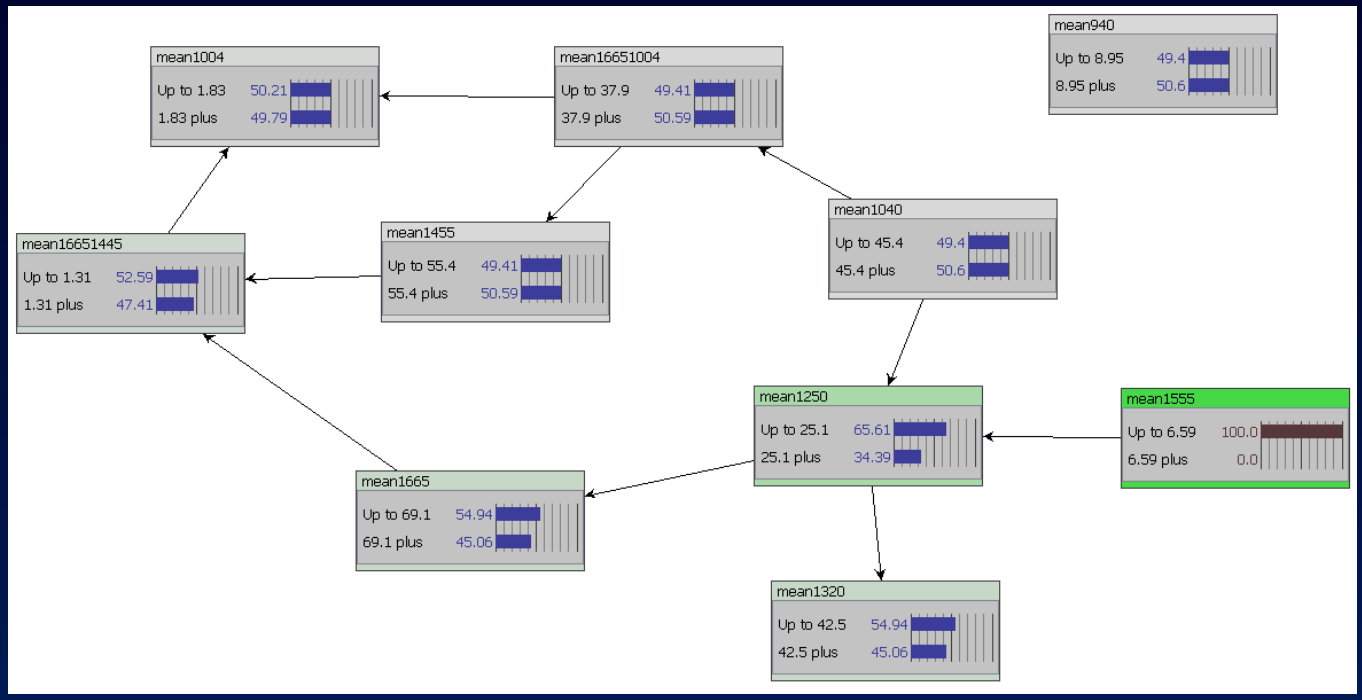

- 1555 cm^{-1} → 1250 cm^{-1} → 1320 cm^{-1} & 1665 cm^{-1} → 1665/1445 cm^{-1} → 1004 cm^{-1}
- 1040 cm^{-1} → 1250 cm^{-1} → 1665/1004 cm^{-1} → 1004 and 1455 cm^{-1} → 1665/1004 cm^{-1}

BBN Analysis of Band Areas: Prediction

A naïve Bayes model for outcome as the target reveals that outcome is largely dependent on mean 1040 cm^{-1} and mean 1455 cm^{-1} band area ratios.

Note, this data set incorporates different collection parameters, operators and regions of the biopsy.

HEALED WOUNDS

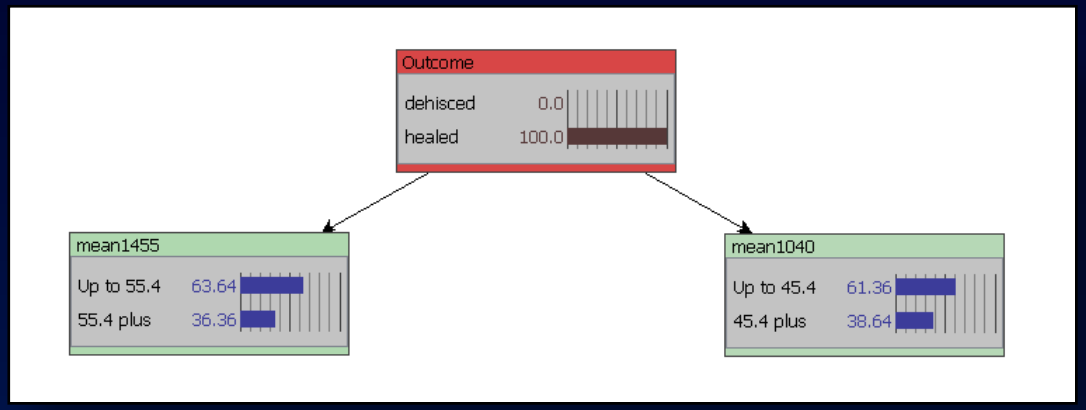

DEHSICED WOUNDS

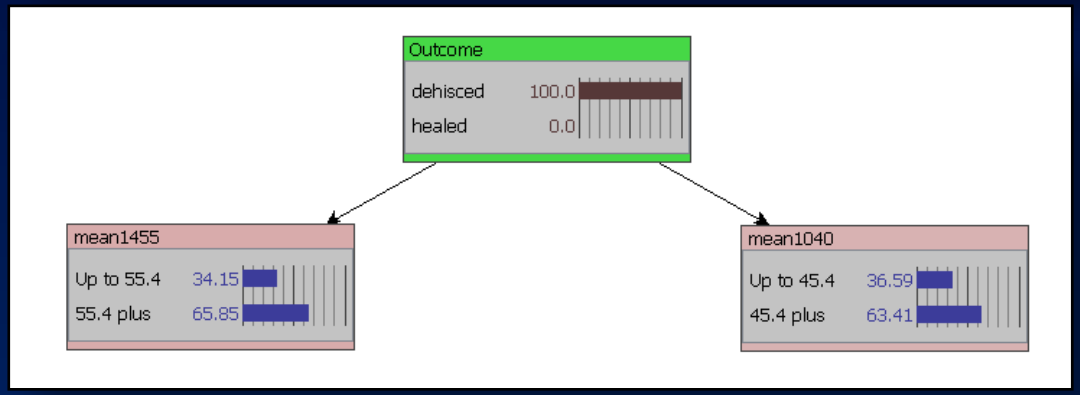

BBN Analysis of Band Areas: Prediction

Here, we generated a naïve Bayes model based on a training data set of all debridements except final debridements and used it to predict the wound healing outcome for final debridements.

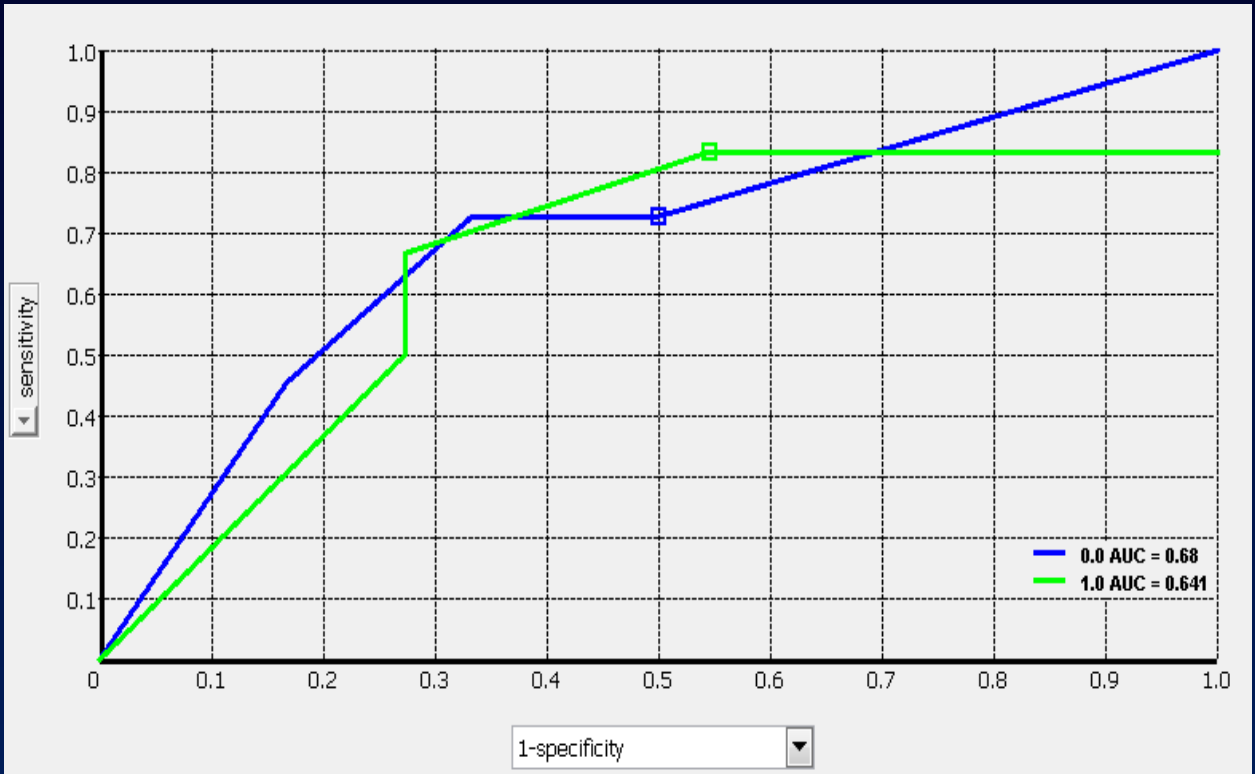

Unfortunately, the accuracy of the prediction model is only *68%* for *normal healing* wounds and *64%* for *dehisced wounds*.

Bayesian Modeling Data Set: Raman and Clinical Data

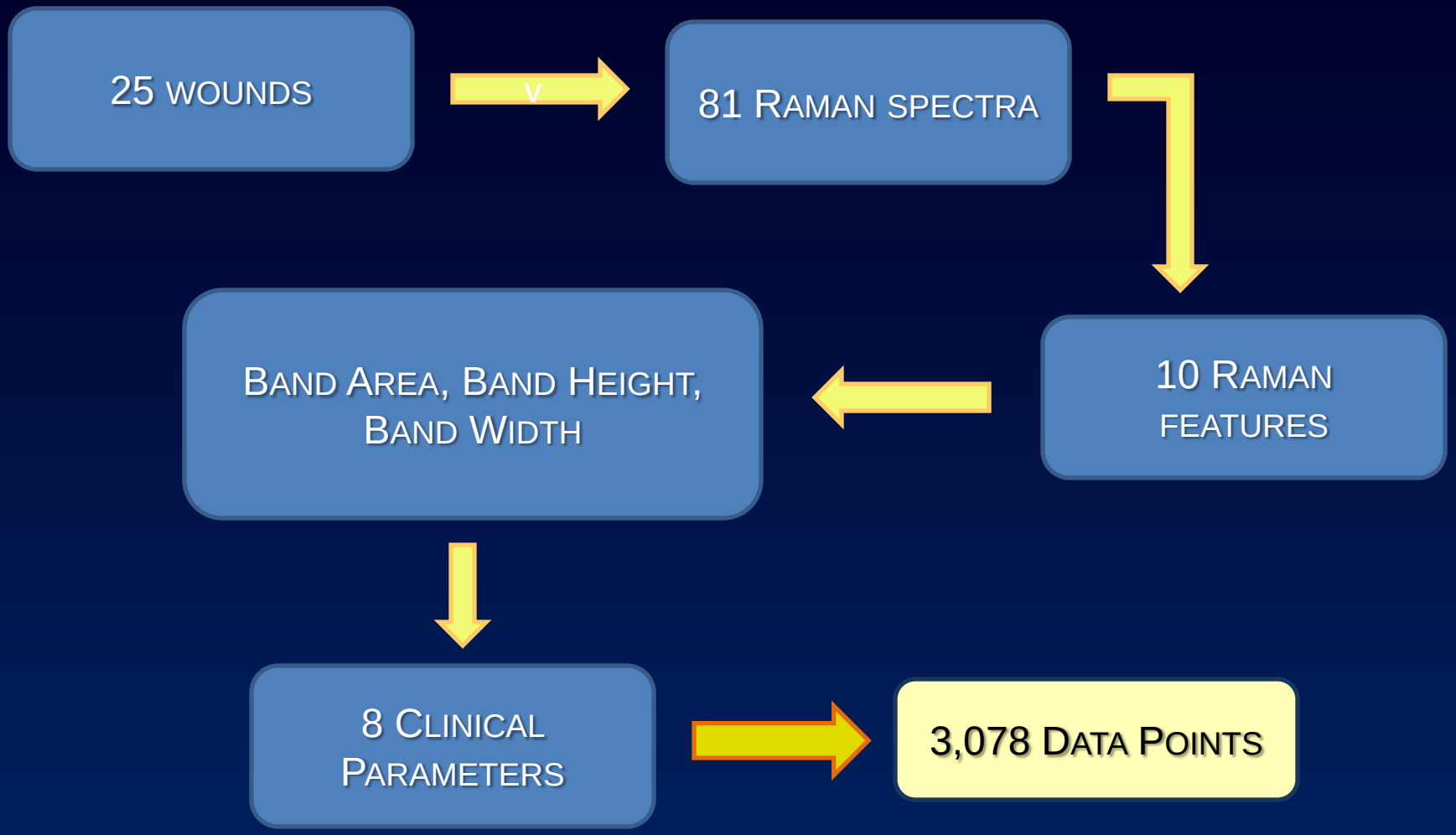

BBN Analysis of Band Areas and Clinical Data: Data Mining

What are the relationships between cljnical data and Raman spectroscopic data?

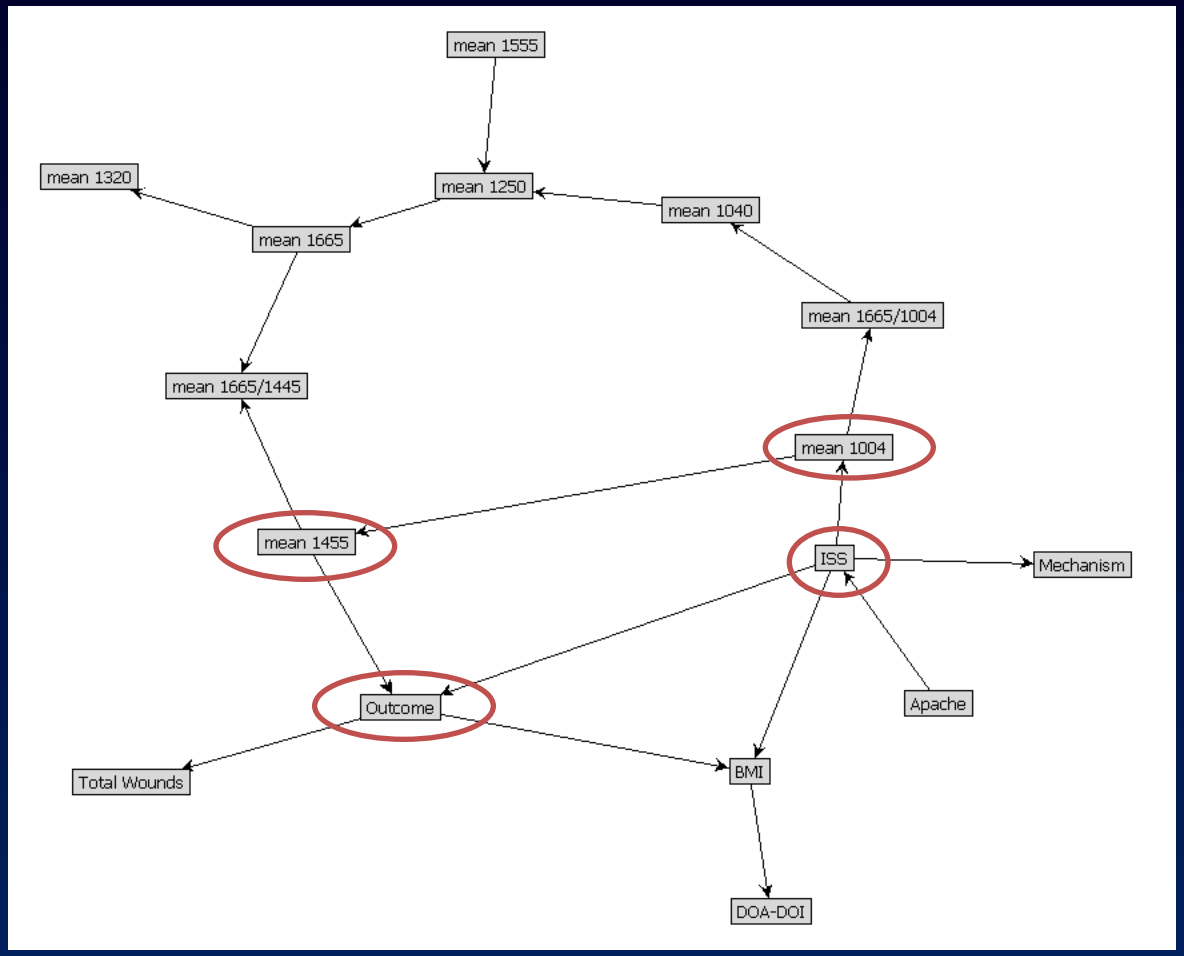

BBN Analysis of Band Areas and Clinical Data: Prediction Models

Here, we generated a naïve Bayes model based on a training data set of all debridements and used it to predict the wound healing outcome for final debridements.

HEALED WOUNDS

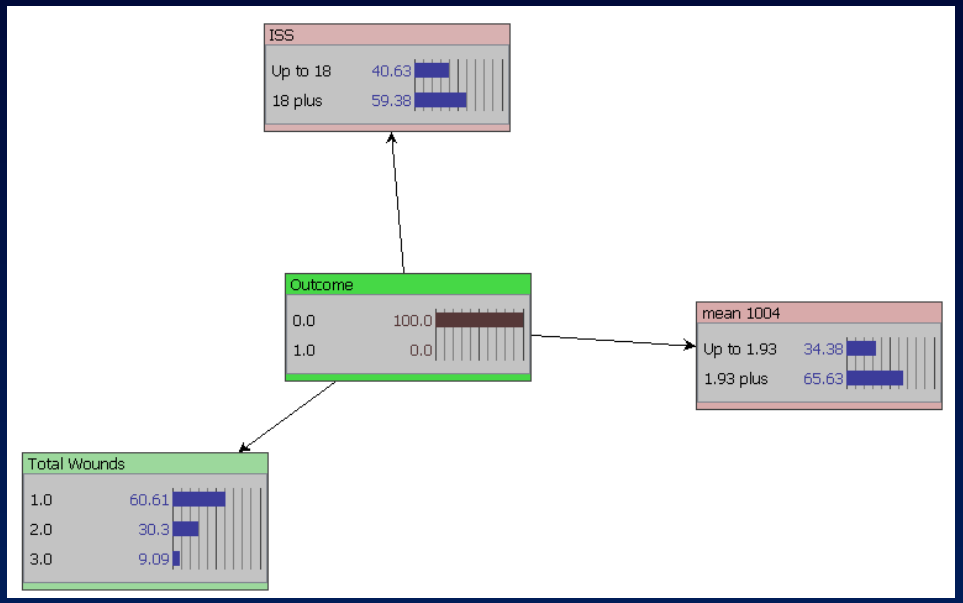

DEHSICED WOUNDS

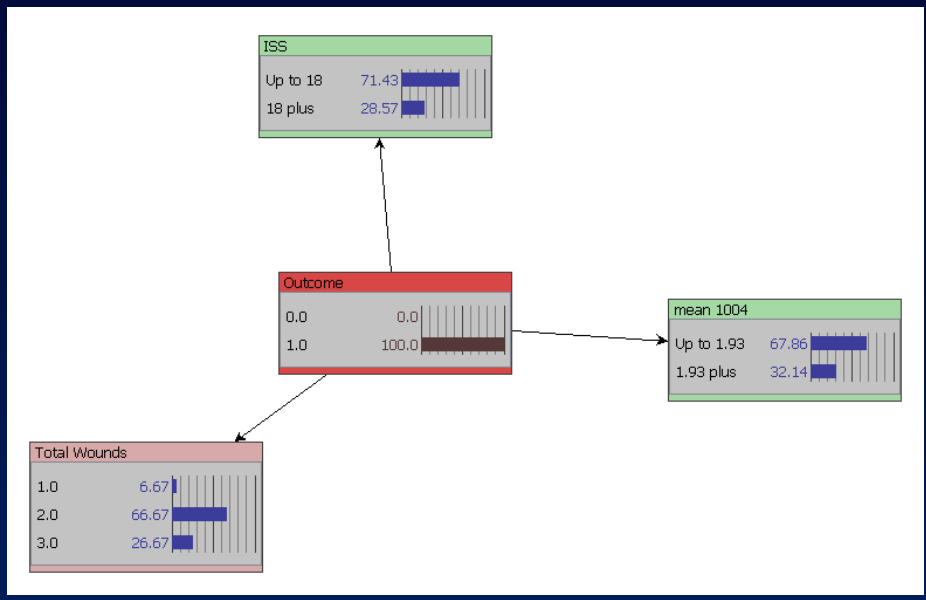

BBN Analysis of Band Areas and Clinical Data: Prediction

Here, we generated a naïve Bayes model based on a training data set of all debridements except final debridements and used it to predict the wound healing outcome for final debridements.

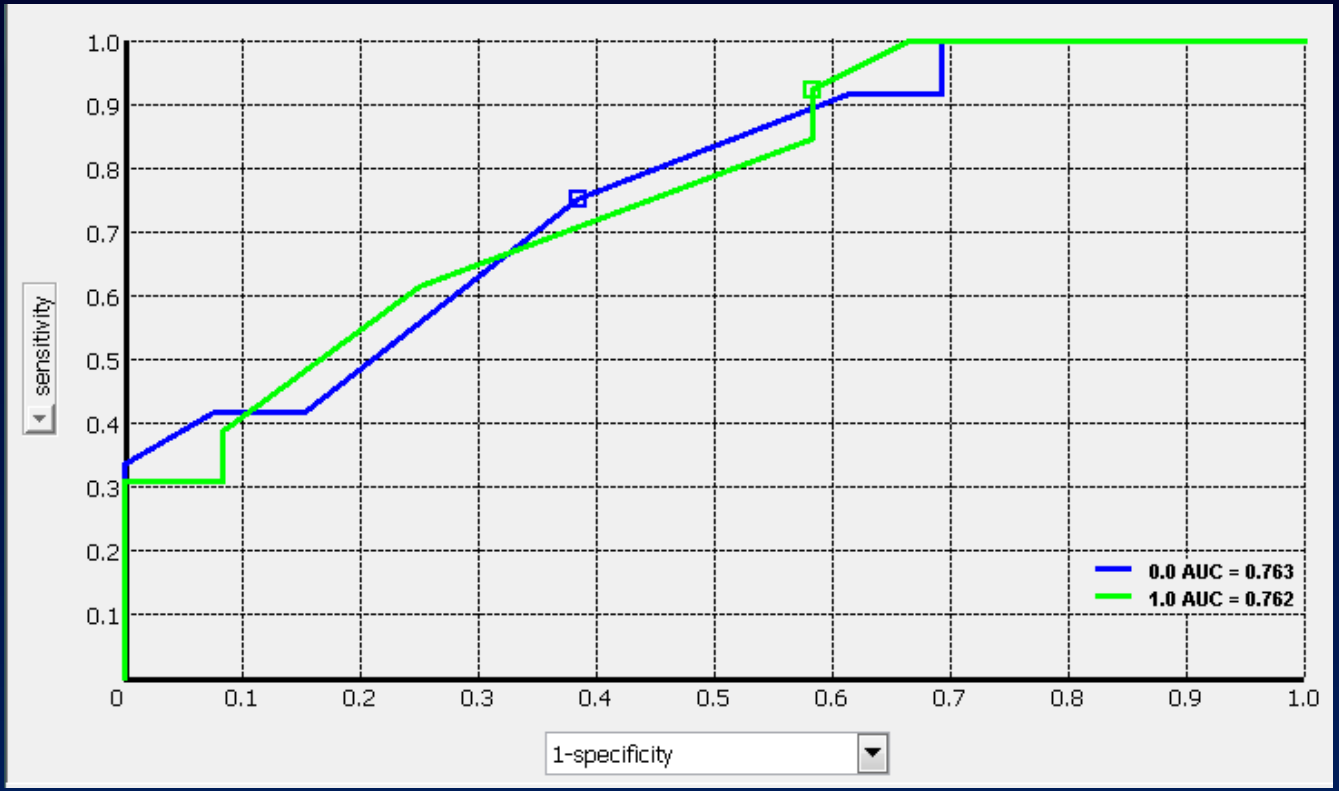

We've improved the accuracy of the prediction model - *76%* for *normal healing* wounds and *76%* for *dehisced wounds*.

Multivariate Analysis of Spectral Data Set

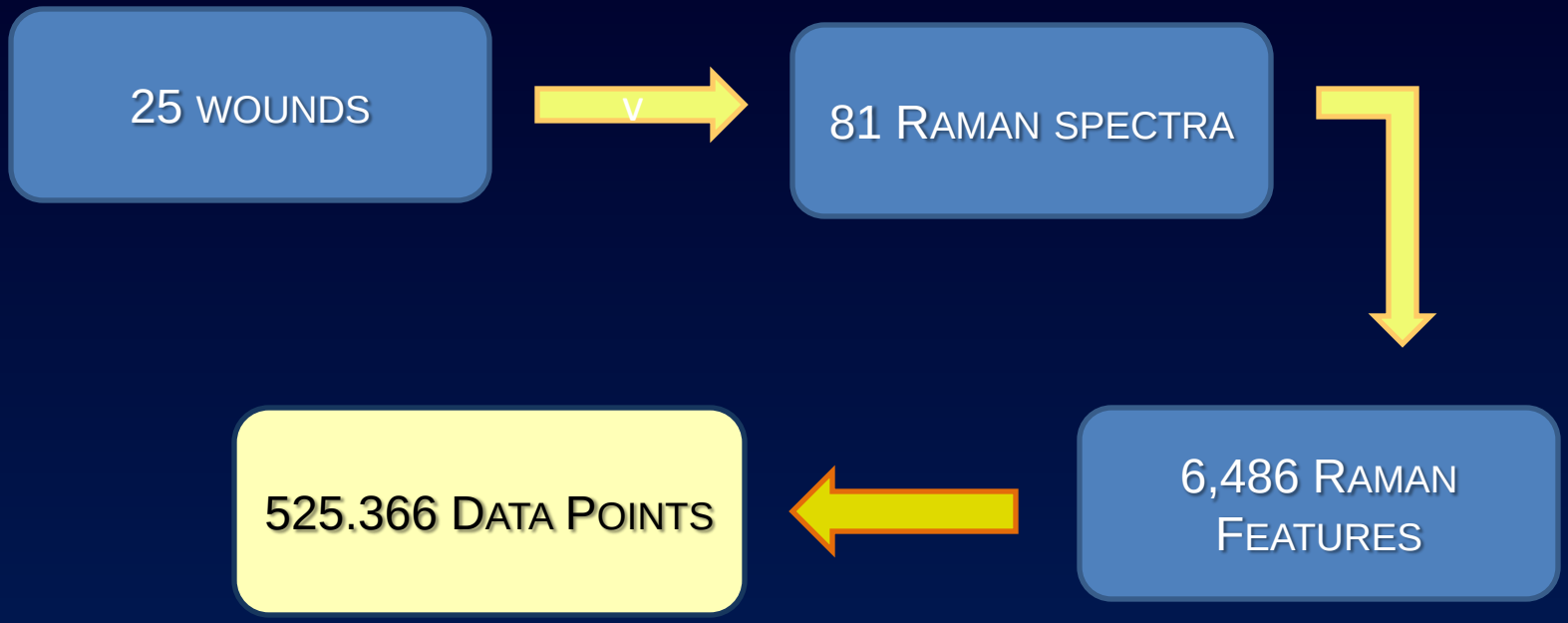

Support Vector Machine

Supervised classification method based on a non-probabailistic binary linear classifier.

- *assumes that groups are separated by a wide boundaries*
- *places samples in the two classes as far apart as possible*
- *able to handle non-linear data*
- *can be susceptible to overfitting*
- *may perform better on data sets with more examples of training and fewer labels*

Support Vector Machine

Support Vector Machine

Developed a subset of spectra for a training data set (N=61), randomly selected from the whole data set.

Used the entire spectrum with no pre-processing (derivatization, smoothing, normalization).

Actual	Predicted	
	Healed	Dehisced
Healed	36	0
Dehisced	0	25

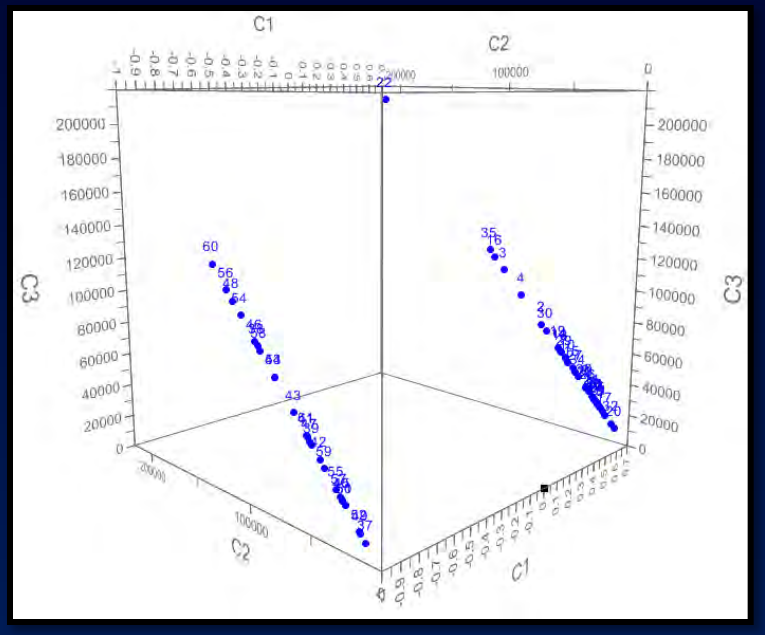

For a test data set (N=20), **80%** of the wound spectra were classified correctly as dehisced.

Linear Discriminant Analysis

Supervised classification method based on Bayes' formula.

- *assumes a normal distribution*
- *assumes that the variability between each group has the same structure*
- *uses PCA to reduce dimensionality*
- *places samples in the same class close to one another but samples not in the same class far apart*
- *may perform better than SVM in cases of many labels and little training data*

Linear Discriminant Analysis

Linear Discriminant Analysis

Developed a subset of spectra for a training data set (N=61), randomly selected from the whole data set.

Used the entire spectrum with no pre-processing (derivatization, smoothing, normalization).

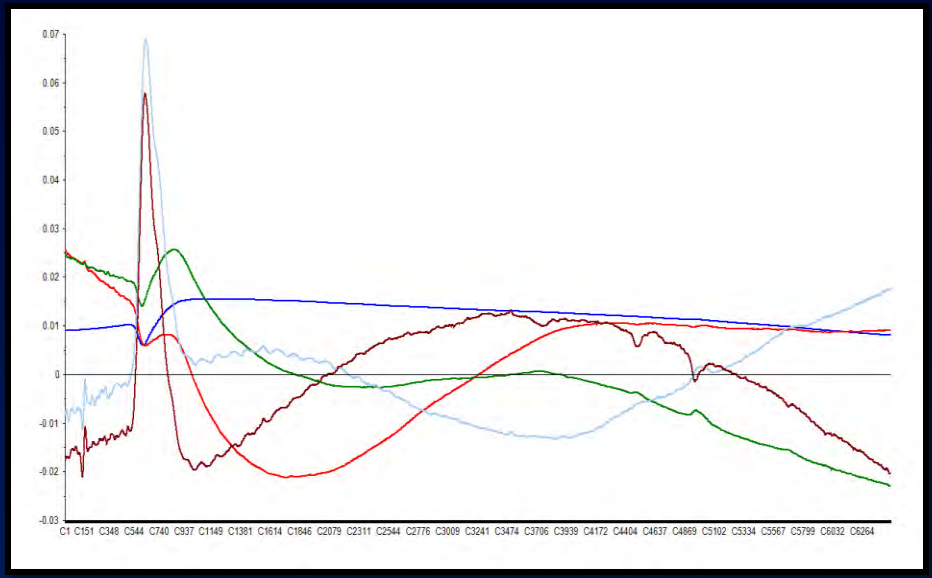

Actual	Predicted	
	Healed	Dehisced
Healed	33	2
Dehisced	3	23

For a test data set (N=20), **90%** of the spectra were classified correctly as dehisced.

Which Model to Choose?

- The models shown require significant optimization.
- We need to ensure complete data sets for training (include different acquisition parameters, multiple acquisitions, different instrument operators – i.e. build robustness into our model).
- The final evaluation of the prediction model will require both the highest sensitivity and specificity.
- Preliminary results demonstrate promise for the use of Raman spectroscopy to predict wound outcome.

Ongoing Projects

- Currently, we are continuing to build our biopsy database for Bayesian Belief Network modeling and other multivariate analysis techniques.
- We have over 250 tissue biopsies from over 50 patients, most of which we have collected spectra in triplicate (over 4 years).
- Peak fitting needs to be performed over the entire spectrum to determine which vibrational bands provide optimal sensitivity and specificity. Some regions of the spectrum require a more in depth peak fitting.
- Other aspects of the spectra, such as the fluorescence background, may also provide indications of the status of the tissue overall.

Project Goals

- The final prediction model will have to incorporate over 1.4M data points.

- Validate spectroscopic wound healing prediction models in a military and civilian population.

Acknowledgements

Naval Medical Research Center

Department of Regenerative Medicine

Dr. Jonathan Forsberg
Dr. Trevor Brown
Dr. Doug Tadaki
Tala Ghadimi
Dr. Felipe Lisboa
Stacia Moreno
Frederick Gage
Rajiv Luthra
Maricela Rodriguez

USUHS

Department of Surgery

Dr. Eric Elster

WRNMMC

General Surgery, Orthopaedics and Rehabilitation

http://www.med.navy.mil/sites/nmrc/Pages/ccc_regenmed.htm

Disclaimer

- The multidisciplinary care of these patients would not have been possible without the dedicated efforts of everyone at WRAMC and NNMC. Both civilian and military personnel have rendered skilled and compassionate care for these casualties. All of our efforts are dedicated to those who have been placed in harm's way for the good of our nation.

- The views expressed in this manuscript are those of the authors and do not reflect the official policy of the Department of the Army, Department of the Navy, the Department of Defense or the United States Government.

- This effort was supported (in part) by the U.S. Navy Bureau of Medicine and Surgery under the Medical Development (PE 0604771N) and Office of Naval Research work unit number (602115HP.3720.001.A1015), in part by Army DMRDP grant D10-I-AR-J2-501, and in part by CDMRP PRORP award OR090136.

- This study was approved by the Walter Reed National Military Medical Center Institutional Review Board in compliance with all Federal regulations governing the protection of human subjects.

Understanding Systemic Responses to Localized Limb Ischemia/Reperfusion Injury: A Yorkshire Swine Model

Maricela Rodriguez[1], Rajiv Luthra[1], Tiffani Slaughter[2], CPT Eric Elster M.D.[2,3], Dr. Nicole J. Crane Ph.D.[1,2]

[1]Department of Regenerative Medicine, Naval Medical Research Center, Silver Spring, MD; [2]Department of Surgery, Uniformed Services University of Health Sciences, Bethesda, MD, [3]Walter Reed National Military Medical Center, Bethesda, MD

ABSTRACT

In Operation Iraqi Freedom (OIF) and Operation Enduring Freedom (OEF), many blast injuries result in limbs with severe soft-tissue, bone, and vascular injuries ("mangled extremities"). These wounds are potentially mortal and often require amputation as definitive treatment. Limb salvage is confounded by the combination of devastating injuries, the drawback of current methods to provide temporary perfusion, and the inability to measure extremity perfusion. A Yorkshire swine model has been developed in which two types of extremity injuries are simulated - femoral artery occlusion simulating a direct vessel injury and limb tourniquation, simulating a crush injury. In this model, we collect traditional clinical samples to evaluate injury systemically and use novel, non-invasive monitoring via spectroscopic imaging to evaluate the limb locally. Infrared imaging shows us that limb temperature decreases during ischemia (-15.3%) while body temperature and heart rate increase (2.5% and 20.5%, respectively). Some systemic markers such as blood urea nitrogen (Day 0 (D0)=5.0 1.0, Day 1 (D1)=9.7 0.6, Day 3 (D)3=9.0 1.0, Day 7 (D7)=6.7 3.2) and albumin (D0=2.0 0.1, D1=2.3 0.1, D3=2.3 0.1, D7=2.4 0.1) increase and stay elevated post-operatively in the control ischemia group when compared to baseline values (p≤0.05), indicating possible damage to the liver and kidneys. Histopathology is also used to grade tissue damage to the limb and the end organs, such as the liver and kidney. Ultimately, this model will establish measurements for determining critical ischemia in extremities with the intent to help advance the treatment of injured war fighters.

INTRODUCTION

- Explosive blasts has affected approximately 60% of the soldiers injured in combat. **(1)**
- Our goal is to establish measurements of limb viability to improve care of combat-wounded soldiers.
- Limb salvage is limited by the combination of devastating injuries, the drawback of current methods to provide temporary perfusion, and the inability to measure extremity perfusion.

Severe leg injury (medicaretips.com, by Arun Pal Singh, July 2009).

- Effects of IRI occur across a spectrum ranging from mild injury with no lasting sequelae to a systemic response with multi-organ injury.
- Ultimately, a better understanding of IRI and identifying biomarkers that help predict tissue viability are the goals for this project.

ISCHEMIA-REPERFUSION INJURY

There are two parts to the reperfusion syndrome : the local component, resulting in increasing regional damage from ischemia, and a systemic component resulting in secondary failure of organs and tissues remote from the ischemic tissue.

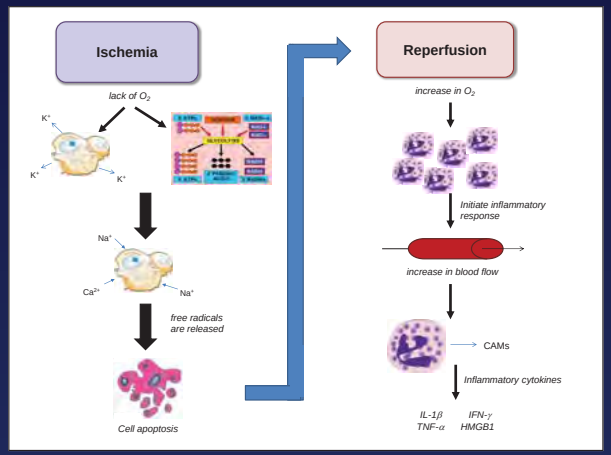

STUDY DESIGN

Experiment Arm	Group	Ischemic Time (min)	Preservation Type	n	Vessel Occlusion
A	1	0	Sham	6	N/A
B	2	120m	Control	7	Cannulation
B	3	210m	Control	5	Cannulation
C	4	120m	Control	9	Tourniquet
C	5	210m	Control	5	Tourniquet
Total number of animals:		32			

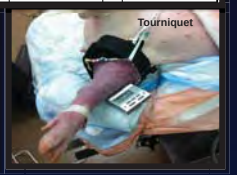

- Female Yorkshire swine of 3-4 months of age and 40-60kg in weight were used for this study.
- Samples were collected every hour during ischemia , after 30 minutes of reperfusion and at Day 1 (D1), Day 3 (D3) and Day 7 (D7).
- Heart rate, body temperature, resting respiration, end tidal CO_2 and oxygen saturation were monitored throughout the procedure.
- The animals were observed twice a day for seven days. Their behavior was rated on general clinical appearance, food and water consumption, and provoked behavior.

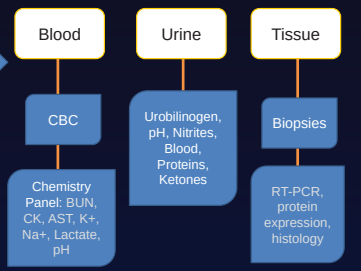

RESULTS AND DISCUSSION

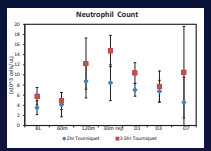

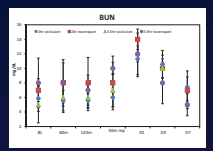

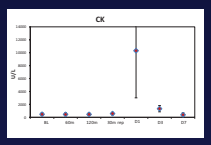

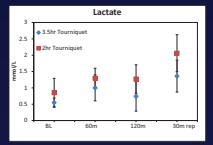

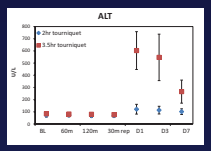

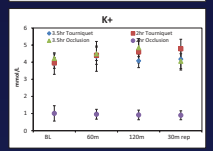

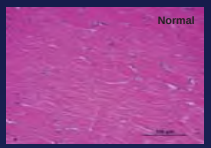

ACTUAL

Within the tourniquet groups, neutrophil count increased during reperfusion and D1 ($p<0.05$) and stay elevated through D7 compared to the occlusion groups. Prolonged periods of ischemia show a greater increase in neutrophil count.

Control groups with 2 hours of ischemia showed an increased level of CK in early stages of ischemia (60 min), during reperfusion and at D1 ($p<0.05$). The 3.5 hour tourniquet group also had a significant increase on D1 ($p<0.05$).

Serum alanine aminotransferase (ALT) and lactate were significantly higher in both tourniquet groups post-operatively and during reperfusion, respectively. Lactate had a significant increase after 30 min of reperfusion for both tourniquet groups ($p<0.05$).

Blood Urea Nitrogen (BUN) increased in all control groups. The significant time points are D1 for all groups and D3 for 2 hour control groups ($p<0.05$ when compared to baseline).

Increase in potassium levels in all control groups except 2hr occlusion. The significant time points are 120 minutes and 30 minutes after reperfusion ($p<0.05$ when compared to baseline).

Normal skeletal muscle (Left) vs. damaged skeletal muscle (Right). The double arrows indicate myocyte degeneration and necrosis with loss of cross striations and fragmentation of the sarcoplasm with mineralization.

EXPECTED

It is thought that neutrophils are the early mediator of local microvascular damage and monocytes infiltrate later extending the injury phase (2).

Creatine phosphokinase (CK) levels may be the most sensitive indicator of muscle injury and may also be predictive of development of renal failure (3).

Glantzounis et al. reported increased levels of ALT and lactate in an acute limb ischemia model in rabbits that caused liver damage (4). Lactate increase is also due to the conversion of muscle metabolism from aerobic to anaerobic (3).

Blood urea nitrogen (BUN) helps determine renal function and when elevated can denote possible kidney damage.

Increased potassium levels in systemic blood is common during ischemia and reperfusion showing possible development of rhabdomyolysis.

Longer ischemic exposure results in more severe tissue damage, specifically directly under the tourniquet placement.

CONCLUSIONS

- The differences seen between all control groups can be attributed to the length and type of ischemia.
- Tourniquet groups resulted in a stronger pathophysiological response compared to occlusion.
- It is possible that a longer period of ischemia and a modification on where the vessel is occluded is needed for the occlusion groups to show larger physiological response. This modification would help compare and evaluate the different types of vascular injury that can be sustained in combat and civilian scenarios, thus establishing a well developed large animal model for limb ischemia.
- Although variable, these results provide us with a baseline for understanding the effects of IRI, the modifications that are needed for developing a better model and help us indicate which parameters to take under consideration when evaluating limb viability.

The authors thank the surgical residents Dr. Jason Radowsky, Dr. Earl Lee and Dr. Joe Caruso for contributing to this protocol. We also thank the Department of Regenerative Medicine and the Department of Pathology at the Naval Medical Research Center and the Department of Surgery at the Uniformed Services University of Health Sciences.

REFERENCES:

[1]Linfert, D. et al.Transplant Rev, 2009; **23** (1), 1-10.
[2]Mernoff, S.T. amd Correia, S., Med and Health, 2010, **93**, 16-21
[3]Glantzounis, GK. et al. Angiology, 2009, **60** (5), 554-561.
[4]Eliason, J.L. and Wakefield, T.W., Metabolic. Semin Vasc Surg, 2009, **22**, 29-33.